Operational Modal Analysis on a Tied-Arch Railway Bridge

M. Benschop

Technische Universiteit Delft

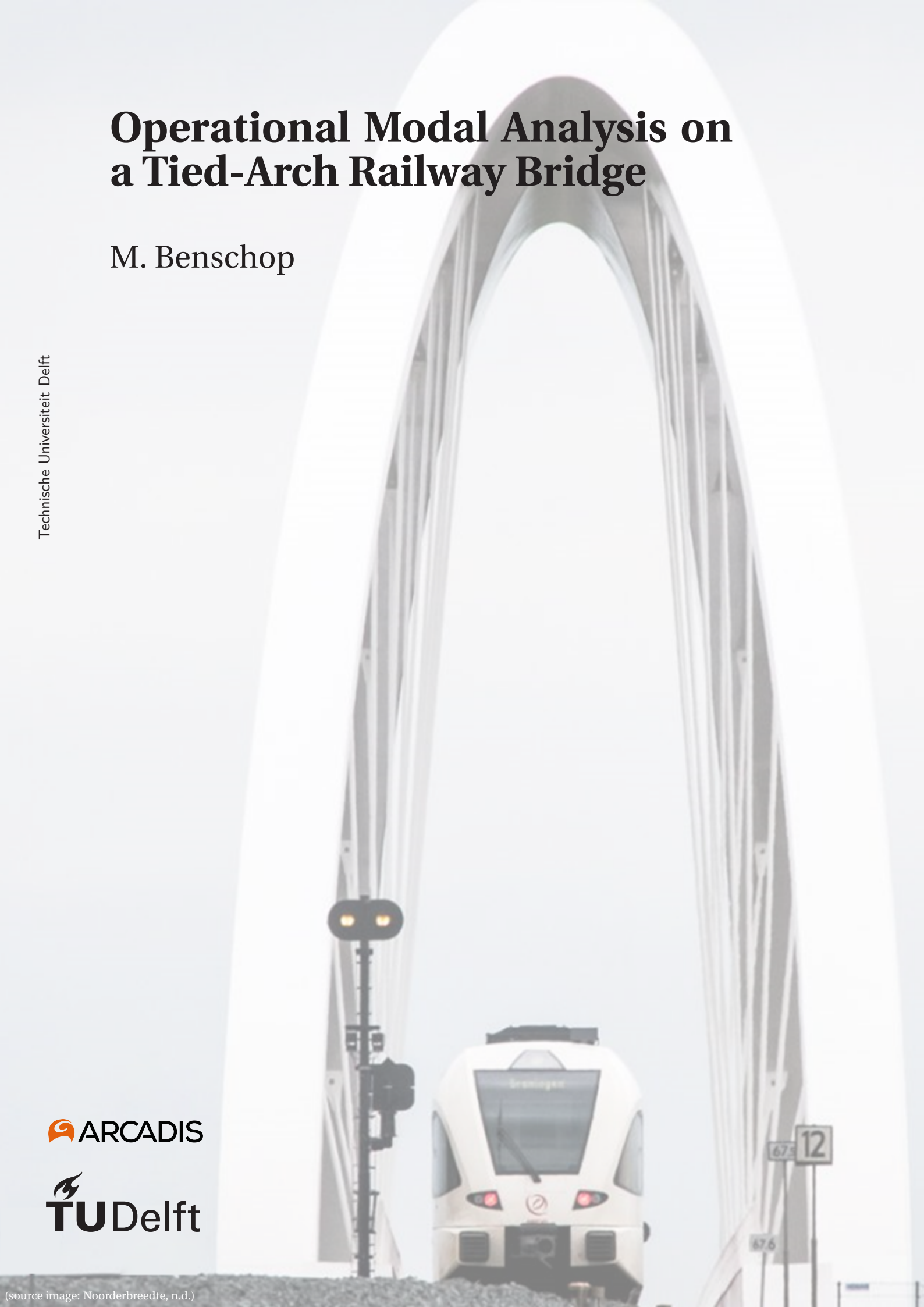

(source image: Noorderbreedte, n.d.)

Operational Modal Analysis on a Tied-Arch Railway Bridge

A case study to determine the natural frequencies and mode shapes from in-situ accelerational measurements

by

M. Benschop

to obtain the degree of Master of Science
in Civil Engineering
at the Delft University of Technology,

Student number:	4741013	
Project duration:	December 6, 2021 – September 30, 2022	
Thesis committee:	Dr. Ir. E. Lourens,	TU Delft, supervisor
	Dr. Ir. A. Cabboi,	TU Delft, supervisor
	Ir. C. van der Vliet,	Arcadis, supervisor

TU Delft

PREFACE

This research project is conducted as the final part to successively obtain the Master's degree in Structural Engineering at the faculty of Civil Engineering and Geo-sciences of the Delft University of Technology.

The field of research to assess structures on their current performance and deterioration is extremely relevant due to the increase demand for sustainable building methods, as well as structural donor elements. This project has presented me the opportunity to learn and develop my technical skills.

On behalf of Arcadis, I have investigated the possibilities to extract dynamic characteristics from an operational large scale civil engineering structure through measurements. Arcadis has given me the opportunity to explore the field of operational modal analysis. To fully comprehend the subject, it requires interdisciplinary knowledge on structural dynamics, signal processing and data science.

I would like to thank my university supervisors Dr. Ir. E.M. Lourens and Dr. Ir. A. Cabboi for the in-depth discussions, which helped me develop my technical skills and general understanding of the subjects during this research project. Also, I would like to thank my company supervisor Ir. C. van der Vliet for his extensive commitment to the project and for sharing his engineering knowledge and experience. He has encouraged me to keep improving up until the final version of this dissertation.

Finally, I would like to thank my parents, fellow students, friends and colleagues for the support and motivation. It is an amazing feeling to have such an inspiring group of people around.

M. Benschop
Rotterdam, August 2022

ABSTRACT

Due to increasingly efficient engineering of the last decades, the design process for civil structures is heading in the direction of optimal solutions. Among other things, the reduction in self-weight enhances the susceptibility to dynamic loads. As the process for the determination of realistic modal parameters from a digital model often diverges from the reality, the uncertainties should be investigated. This research aims to gain knowledge on the accuracy and stability of such modal parameter estimates.

A case study is investigated to determine modal parameters for a realized tied-arch railway bridge. The desired modal properties include the natural frequencies, mode shapes and damping parameters. The frequency domain decomposition (FDD) method is applied on a set of accelerational measurements to determine the modal parameters. Four dominant frequencies are identified and investigated, from which the most dominant operational deflection shapes are extracted. The overall response of the structure shows great similarities with the expected mode shapes for similar bridge types. The computed modes show signs of complex behaviour, due to the characteristics of the load or the structure. An effective method to reduce uncorrelated noise is the application of an autocorrelation function (ACF) to the time domain signals, before execution of the FDD. Prior to the computation of the final results related to the case study, a simplified test case is considered to validate correctness of the FDD implementation.

LIST OF ABBREVIATIONS

Abbreviation	Definition
ACF	Autocorrelation Function
ADC	Analogue-to-Digital Converter
DFT	Discrete Fourier Transform
DOF	Degree of Freedom
EFDD	Enhanced Frequency Domain Decomposition
EMA	Experimental Modal Analysis
ERA	Eigensystem Realization Algorithm
FDD	Frequency Domain Decomposition
FEM	Finite Element Method
FFT	Fast Fourier Transform
FRF	Frequency Response Function
IDOF	Infinite Degree of Freedom
IDFT	Inverse Discrete Fourier Transform
IFT	Inverse Fourier Transform
LDDE	Logarithmic Decrement Damping Estimation
LTI	Linear-time invariant
MAC	Modal Assurance Criterion
MAClim	Modal Assurance Criterion limit value
MACoh	Modal Amplitude coherence
MDOF	Multi Degrees of Freedom
MPC	Modal Phase Collinearity
MPE	Modal Parameter Estimation
MSS	Magnitude Squared Spectrum
MU	Model Updating
NPD	Non-proportional Damping
ODS	Operational Deflection Shape
OMA	Operational Modal Analysis
OMAX	Operational Modal Analysis with Exogenous inputs
PCA	Principle Component Analysis
PSD	Power Spectral Density
RQA	Recurrence Quantification Analysis
SDOF	Single Degree of Freedom
SHM	Structural Health Monitoring
SSI	Stochastic Subspace Identification
SVD	Singular Value Decomposition
SVP	Singular Values Plot

Contents

1

INTRODUCTION

STRUCTURAL vibrations are common phenomena in in civil engineering. Structural vibrations are induced by dynamic loads, such as wind-, wave- or traffic loads (ambient vibrations). In extreme cases, the excitations become harmful and can result in structural damage. Gaining insights on the dynamic behavior of structures can enable a robust validation and assist in the improvement of the digital model at hand.

The dynamic behavior of structures is becoming increasingly important, as structures are becoming lighter due to more efficient engineering (Blok et al., 2018, Craveiro et al., 2017). Slender structures with reduced self-weight are known to be more susceptible to dynamic loads (Zhang et al., 2016, Avci et al., 2022). This means that full dynamic analyses will have to be considered to design a safe structure. In order to perform a dynamic analysis, a digital model of the structure is created. The acting loads on the structure are modelled as well. By means of a dynamic simulation, the response of the structure to the ambient vibrations can be replicated. The response is dependent on the model characteristics and parameter values. The challenge in a dynamic analysis concerns accurate model assumptions for a realistic representation.

In theory, the dynamic (modal) parameters of a structure can be derived through fundamental mechanics. In practice however, the results often diverge from the initial derivation due to great uncertainty of the current mechanical properties, boundary conditions, ambient loads, interaction properties etc. which influence dynamic behavior (Soroushian, 2014, Derife et al., 2022). Feedback on the initial design, also known as model updating (MU), can be used to calibrate the model with representative parameter values (Mottershead & Friswell, 1993). This will allow structural engineers to make more accurate assumptions on the dynamic behavior of a structure (Soroushian, 2014).

Capturing the dynamic response of structures provides a starting point, to be able to assess the current performance and deterioration of a structure (Frangopol & Kim, 2022), also known as Structural Health Monitoring (SHM). Measurement data can be obtained through controlled testing or during the operational stage of the structure. When working with data from measurements, additional challenges emerge which influence the accuracy of the determination of modal parameters (Derife et al., 2022). The computed modal parameters are never equal to the actual parameters due to a variety of imperfections. Instances which cause such discrepancies are the strict fundamental assumptions on the response of the structure, continuous shortage of data and measurement noise (Gre et al., 2021). Parameters describing modal characteristics of a structure are recognized as valuable indicators for evaluating structural performance (X.-M. Yang et al., 2021). These characteristics can be determined more accurate and realistic, when data is collected on the dynamic behaviour. This research aims to determine modal parameters based on vibrational data.

A case study is performed on an operational tied-arch railway bridge, from which data is collected prior to the start of the research project. Identifying dynamic properties through vibrational data provides several challenges. This research aims to investigate these challenges, by providing an in-depth analysis of the most governing interferences when using measured signals to determine dynamic properties. The goal of the research is to provide an analysis to accurately extract reliable dynamic properties of a structure with sufficient stability and reliability from measurement data.

1.1. PROBLEM STATEMENT

In the preceding paragraph, the importance of addressing dynamic behavior of a structure is mentioned. In this section, the relevance of the analysis of dynamic behavior is elaborated on. In Section 1.1.1, concepts of structural vibrations are defined. In Section 1.1.2 the importance on the derivation of modal parameters are being discussed. Finally in Section 1.2, the research questions for this research project are presented.

It is likely that an increased amount of future structures will require a full dynamic analysis. For this dynamic analysis, accurate modal parameters should be determined, to which the digital model can be calibrated by applying MU techniques. The values to which the model will be updated should be realistic and representative, and being obtained through reliable methods.

In the introduction it is stated that in order to be able to accurately simulate the behaviour of structures, realistic model parameters are required. It was also stated that several challenges arise when using vibrational data to identify dynamic properties. Challenges such as non-compliant structural behaviour to the fundamental assumptions, computationally expensive operations to evaluate time signals of significant length, and sufficient interdisciplinary knowledge on structural behaviour, signal processing and statistics & probability to confidently apply and verify the used methods. In addition, measurement signals contaminated with artifacts such as noise or non-structural behaviour increase the complexity to accurately determine structural behaviour from measurement signals. The current research aims to define modal parameters based on vibrational data through reliable methods.

The process of modal analysis to determine structural dynamic properties can be time consuming, which is a problem in itself. Even after computing the modal parameters, an engineer should feel confident that the derived properties are accurate, to effectively design a structure. The influential parameters which are included in the analysis and reliability of the results are further investigated.

1.1.1. STRUCTURAL VIBRATIONS

Loads can be classified in three categories, being static loads, quasi-static loads and dynamic loads. In civil engineering, the majority of structures are designed to carry extreme loads in a static sense. However, as mentioned in the previous section, with the increase of use of lightweight materials, it becomes increasingly important to consider the effects of dynamic loads.

A dynamic load implies that the response of the structure is dependent on the change in magnitude of the load over time (Hwang & Nowak, 1991). How quick the magnitude of the load changes over time, influences the response of the structure. This phenomenon can be described through periodic loads and responses. Periodic loads are said to have repeated characteristics after some time length T. The amount of periods to fit in a specified period of time is described by the frequency f. When the response of the structure is characterized as periodic, the structure is vibrating. The amount of vibration over time is based on the output frequency response and the amount of damping, further explained in Chapter 2 (Literature review).

If the acting force is periodic with a frequency considerably close to any of the natural frequencies of the structure, resonance can occur. Resonance ensures amplification of the deflections during the time-period over which the periodic load is acting on the structure. The increasing amplitudes for the deflections of the structure can result in serious structural damage (Bhandary et al., 2021), and should therefore be avoided.

1.1.2. MODAL PARAMETERS

When a structure is susceptible to dynamic loading, knowledge on its natural frequencies is essential. Information on the influential parameters, concerning dynamic properties, is accounted for in the modal parameters. The circumstances at which a structure is dynamically loaded in the most unfavorable way, is when resonance can occur. Resonance can be avoided by designing a structure where the natural frequencies do not coincide with the frequencies of the acting periodic loads. Additionally, resonance can be counteracted by introducing significant damping in the structure (e.g. through the application of dampers). Damping ensures the dissipation of energy from the system, and is able limit the dynamic amplification caused by resonance.

The natural frequencies of the structure can be derived theoretically, but model uncertainties are high (Zhu & Au, 2020), meaning the chance of inaccurate results is high as well. Therefore, in practice, measurements on the modal properties should be performed supplementary to the theoretical derivation (Cawley & Adams, 1979).

After measurements have been performed, data has to be processed, to provide the correct and realistic parameter values. Issues that arise when computing accurate parameter values can be solved by deploying automated techniques (Sun et al., 2017). The automated techniques become increasingly important for seamless implementation of SHM tools (Sun et al., 2017). Therefore, this research will investigate the possibility to automate the process, which takes a set of vibrational data as input and provides the correct dynamic parameters as output.

1.2. RESEARCH QUESTIONS

To perform this research, the following research questions are formulated. The research questions will be answered after the results from the case study are presented and discussed, in the conclusions (Chapter 8).

How can the dynamic properties be obtained for an arch-railway bridge based on measurement data with appropriate stability and reliability?

1. What methods are commonly used in the analysis of vibrations?
2. How to assess the quality of the measured data?
3. What methods can be used to improve the usability of the signal?
4. Is it possible to distinguish closely spaced natural frequencies in the measured signal?

2

Literature Review

THIS chapter includes the necessary fundamental knowledge for the ability to comprehend and assess the methods that will be elaborated on. To be able to compute modal parameters, sufficient knowledge on the theory should be mastered, as modal analysis is an ongoing interdisciplinary physical issue, which requires knowledge in multiple fields (Bao et al., 2015).

First, the theory on the response (behaviour) of structures when subjected to dynamic loading, are presented. Secondly, elaborations are given on methods to describe and analyse these responses in the frequency domain. Subsequently, the literature with respect to signal processing and dealing with random signals in general is presented. This section includes fundamental concepts for a statistical representation of random signals, to prepare the reader for Chapter 4 (Methods). Finally, a short description is given on the particular response regarding arch bridges and dynamic train loading.

2.1. STRUCTURAL RESPONSE

For this case study, the dynamic response of the structure is investigated through modal analysis to be able to describe the behaviour of the structure. The equations of motion of a multi degree-of-freedom (MDOF) system is presented in Equation 2.1.

$$M\ddot{u}(t) + C\dot{u}(t) + Ku(t) = F(t) \tag{2.1}$$

TRANSFORMATIONS

The common techniques for an analysis of the dynamic behaviour of a structure can be divided in two categories, namely, frequency domain and time domain methods (Magalhães & Cunha, 2011). The most common way to gather data is, like in the case of this case study, through accelerational data in the time domain. However, this is not the best way to represent dynamic properties of a structure numerically. When considering the dynamic response, a clear depiction to represent the modal characteristics of a structure is in the frequency domain. In order to be represented in the frequency domain, the measured data will have to be transformed

2.2. FREQUENCY RESPONSE

When considering modal analysis, a linear framework is adopted to represent the response of the structure. This representation implies a linear superposition, according to Fourier's series. In Equation 2.2, A_n and B_n represent the Fourier constants, and ω_n represents the frequency.

$$u(t) = \sum_{n=-\infty}^{\infty} A_n \cos(\omega_n t) + B_n i \sin(\omega_n t) \tag{2.2}$$

When representing the signal in the frequency domain, the Fourier transform of the signal can be depicted using an alternative representation, in order to simplify the general understanding. Instead of using the Fourier constants in cosine and sine form (equation 2.2), the two terms are merged into a single cosine term with a distinct amplitude and a corresponding phase shift, and can be represented in the form:

$$u(t) = \sum_{n=-\infty}^{\infty} C_n \cos(\omega_n t + \varphi_n) \tag{2.3}$$

In the above equation, the amplitude (C_n) and phase shift (ϕ_n), derived from equation 2.2, are computed in the following way:

$$C_n = \sqrt{{A_n}^2 + {B_n}^2} \tag{2.4a}$$

$$\phi_n = \arctan\left(\frac{B_n}{A_n}\right) \tag{2.4b}$$

2.2.1. MODE SHAPES

In theory, the total behaviour of the structure can be decomposed into the superposition of all individual and orthogonal modes. The considered modes adopt standing wave characteristics, which are amplified and attenuated in the periodic behaviour, in the case of real modes.

NORMAL MODES

When describing a dynamic system, the modal behaviour can be described as the superposition of fundamental (non-dependent) modes. If the modes are independent, the modes are considered normal modes (Erlicher & Argoul, 2007).

Modal Assurance Criterion When defining mode shapes through statistical properties, the chances of determining an identical mode shape when considering a different data set is relatively low. The same holds for the dominant mode shapes corresponding to neighbouring frequencies in the system power spectrum. To quantify comparability of two modes, the Modal Assurance Criterion (MAC) can be determined. The MAC value is most sensitive to large difference and relatively insensitive to small differences in mode shapes (Pastor et al., 2012). The MAC value can be determined by taking the inner product of the two vectors which represent the mode shapes (equation 2.5). The result is a scalar value, which can vary between 0 (no correlation between the two modes) and 1 (full correlation between the two modes).

$$MAC(\phi_i, \phi_j) = \frac{(\phi_i^T \phi_j)^2}{\phi_i^T \phi_i \phi_j^T \phi_j} \tag{2.5}$$

In equation 2.5, ϕ_i and ϕ_j represent the mode shape vectors to be compared.

NOISE MODES

Noise modes are modes which do not have any substantial relation to the response of the structure. The noise modes are merely the side-product of the uncertainties in the response of the structure. "However, it is still difficult to sort out noise modes, which requires the experience and judgment to use sorting tools (such as stability diagrams) effectively" (Bao et al., 2015, p. 1). Stability diagrams are mostly used in time domain methods, such as ERA. The MAC value of two noise modes should be close to zero, as they are uncorrelated.

NON-CONSERVATIVE SYSTEMS

A free vibration is a vibration where the mass is able to vibrate freely after being subjected to an initial displacement. In this system, the initial energy is preserved (or the energy is said to be conserved). When a system is introduced to damping, this system is not able to conserve the energy, as damping in the system inherently introduces energy dissipation. When energy is dissipating from the system, the system can no longer preserve the initial energy.

DAMPED SYSTEMS

First, the linear system of equations 2.1 could only possesses normal modes if $C = 0$, $M = M^T$ and $K = K^T$, where the entries of the damping matrix are equal to zero. The first analytical model to be used to study damping for an MDOF system is proportional damping (He & Fu, 2001b). The concept of proportional damping was first introduced by Rayleigh, 1894. He presented that passive non-conservative systems can posses normal modes as well, therefore implying normal modes when $C \neq 0$. However, the damping is assumed low and the damping matrix should be proportional to the mass and stiffness matrix (Erlicher & Argoul, 2007). If the damping matrix is proportional to mass and stiffness matrix, the system possesses normal modes (Ahmadian & Inman, 1984).

COMPLEX MODE SHAPES

A structure, when excited by a load, will displace in a certain shape. If the load possesses dynamic characteristics, the response of the structure adopts dynamic behaviour as well (Spijkers et al., 2005). In common engineering practice, every DOF of the system is assumed to either move in-phase or anti-phase ($\varphi = 0$ or $\varphi = \pi$, respectively). This way, the excitations will share extreme positions at corresponding points in time. However, in more realistic cases, the relative phase angles are not completely opposite. In this case, a certain *complex* mode shape is considered. The complex mode is dependent on time and will not include of a discrete moment where all the displacements are at their extremes. A cause of a complex mode is non-proportional damping or load dependency of the observed operational deflection shape (ODS). In the latter case, the ODS can not be considered a mode.

MODE SHAPE PROPERTIES

To quantify the system and noise modes, two accuracy indicators have been developed by Juang and Pappa, 1985. The two indicators are the modal amplitude coherence (MACoh) and modal phase collinearity (MPC), which are represented by γ_j and μ_j, respectively, for mode j. Both indicators return a scalar value between 0 and 1. The MACoh value determines a distinction between a system mode (when close to 1) and a noise mode (when close to 0). Juang and Pappa, 1985 also state that further investigation is required to be able to *clearly* distinguish a system mode from a noise mode. The MPC value indicates the strength of the linear

functional relationship between the real and imaginary parts of the mode shape for each individual mode. The two indicators are developed for the eigensystem realization algorithm (ERA), which is a time domain method. However, the concepts of these indicators can be translated to fit the needs that correspond to the considered frequency domain methods. By applying such an algorithm, the quality of the data can be quantified.

$$\gamma_j = \frac{\left|\bar{\phi}_j^H \phi_j\right|}{\left(|\bar{\phi}_j^H \bar{\phi}_j||\phi_j^H \phi_j|\right)^{1/2}} \tag{2.6}$$

In equation 2.6, the symbol ϕ represents the considered mode shape vector. It is clear to see the the MACoh indicator is almost identical to the determination of the MAC value (Equation 2.5), being the dot-product of two vectors, to define a coefficient.

Modal Phase Colinearity When in the process of determining mode shapes for damped systems, the outcome can be a complex mode (Oke et al., 2019). To check if this is the case, the MPC can be computed following Gre et al., 2021, where the determination is implemented using slightly different equations w.r.t. Juang and Pappa, 1985. The MPC is a quantification method to assess the linear relation between the real and imaginary part of the mode. It is a method to determine non-linear components in Equation 2.1, which is most sensitive to large differences and relatively insensitive to small differences (Pastor et al., 2012). The MPC value ranges from 0 to 1, where 0 indicates low accuracy (therefore a noise mode or a complex mode) and 1 indicates high accuracy of the mode shape. The MPC can be derived by solving matrix S for its eigenvalues:

$$S = \begin{bmatrix} S_{xx} & S_{xy} \\ S_{yx} & S_{yy} \end{bmatrix} \in \mathbb{R}^{2x2} \tag{2.7}$$

Where input values of the matrix S are determined as described in equations 2.8a, 2.8b and 2.8c:

$$S_{xx} = \mathrm{Re}(\phi)^T \mathrm{Re}(\phi) \tag{2.8a}$$

$$S_{yy} = \mathrm{Im}(\phi)^T \mathrm{Im}(\phi) \tag{2.8b}$$

$$S_{xy} = S_{yx} = \mathrm{Re}(\phi)^T \mathrm{Im}(\phi) \tag{2.8c}$$

To compute the MPC value for a frequency:

$$MPC(\phi) \triangleq \frac{(\lambda_1^s - \lambda_2^s)^2}{(\lambda_1^s + \lambda_2^s)^2} \tag{2.9}$$

Again, the symbol ϕ represents the considered mode shape vector. The symbols λ_1^s and λ_2^s represent the eigenvalues of matrix S. The result quantifies the complexity of the considered mode shape. When the complexity increases for low MPC values, the relative phase delays in the considered mode are becoming less in-phase, therefore introducing a greater significance in time dependency. Oktav, 2020 reflects on this behaviour, being identical to a non-proportional damping (NPD) case, as he states that the out-of-phase component implies the relative phase delay, not being an integer multiple of $\pi/2$, for the DOF's of the system.

2.3. OPERATIONAL MODAL ANALYSIS

When performing modal parameter estimation (MPE), the modal parameters are determined based on a set of measured data. The modal parameters can be obtained by performing operational modal analysis (OMA) (Grocel, 2014). Unlike experimental modal analysis (EMA), which is performed in a lab-like setup, OMA can be performed on a structure during the operational stage. It is currently the most economically viable and often more appropriate method for obtaining in-situ dynamic properties for large scale civil structures (S.-K. Au et al., 2021, Reynders et al., 2012). A combined approach can also be used, where both the measured and unmeasured forces are accounted for, and yields an optimal approach: operational modal analysis with exogenous inputs (OMAX) (Reynders et al., 2012). Magalhães and Cunha, 2011 states that output-only MPE of dynamic systems are classified as time domain or frequency domain methods.

LINEAR TIME-INVARIANT SYSTEM

To be able to describe the structures' dynamic behaviour, a model (system) is required which defines fundamental principles related to the response. For this research project, a mechanical system model for the structure is adopted. The structure is represented as a linear time-invariant (LTI) system model. When the LTI model is adopted, basic computations regarding convolution and linear multiplication can be used to describe the system, due to the principle of superposition and the principle of homogeneity which inherently imply the commutative, distributive, and associative properties (Saini, n.d.). The fact that the system is considered linear, implies that if we think of the input as the sum of different input functions, then the output is equal to the sum of different output functions (Shin & Hammond, 2008).

"*Linear time-invariant systems respond to complex exponentials or eigenfunctions in a very special way: their output is the input complex exponential with its magnitude and phase changed by the response of the system*" (Chaparro & Akan, 2018, p.167).

FREQUENCY RESPONSE FUNCTION

In engineering practice, the properties of a system can be described through a so-called transfer function. The system takes an input signal and *transforms* this to an output signal. The system characteristics, which transform the input signal, are introduced through a transfer function. When expressing the transfer function in the frequency domain, it is identified as the frequency response function (FRF). For LTI systems, the definition of the FRF is best to be described by the ratio between output and input of the signal (Shin & Hammond, 2008). This provides straightforward multiplication (in the frequency domain) of the FRF with the input signal to determine the output signal.

$$\tilde{H}(\omega) = \frac{\tilde{d}(\omega)}{\tilde{p}(\omega)} \tag{2.10}$$

In Equation 2.10, $\tilde{H}(\omega)$, $\tilde{d}(\omega)$ and $\tilde{p}(\omega)$ represent the FRF, frequency output signal and frequency input signal of the system, respectively. In the frequency domain, the time-domain convolution operation becomes a product operation. The FRF is the Fourier transform of the impulse response function. Figure 2.1 depicts the definition of the FRF for different domains.

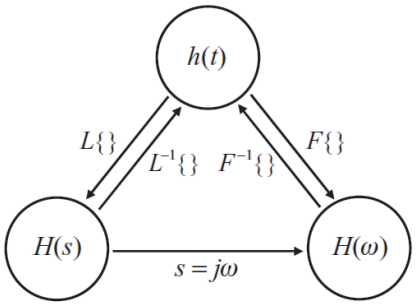

Figure 2.1: This image shows the relation between the impulse response [$h(t)$], the transfer function [$H(s)$] and the FRF [$H(\omega)$] (source: Shin and Hammond, 2008, p. 78).

Lack of input signal The relation between the input- and output signal for an LTI system are presented in Equation 2.10. If both signals are obtained, the system characteristics can be derived. However, for large scale civil structures, the acquisition of the input signal (ambient loads) can be rather challenging to acquire. Therefore, alternative methods for the derivation of the FRF will have to be investigated to resolve for the lack of input signals.

OUTPUT-ONLY SYSTEMS

OMA is an output-only method that is applied when the input signal is unknown. The structure can be modelled as an output-only system. The principles of this type of system adopt similar characteristics from the LTI system. However, additional assumptions concerning the properties of the ambient loads should be taken into account. Chapter 4 presents the methods to analyse the output signal of the structure to determine the modal parameters.

ASSUMPTIONS

The OMA method is based on various assumptions (Grocel, 2014, p. 131), which are listed below:

- Linear system
- Properties of the system are not dependent on time
- White noise characterized input load
- Measurements provide possibility for MPE

The latter assumption is rather straightforward, however originates mainly from a practical standpoint (e.g. proper sensor placement to capture the desired dynamic properties).

TIME DEPENDENCY

The fundamental assumptions of the OMA method regarding time dependency can be described through stationarity. As the input signal is unknown, the characteristics of the structure and the ambient loads are assumed to remain similar over time. Hereby, being able to compare the output signals, which then can be linked to the characteristics of the structure. In Equations 2.11 to 2.12c, $p(\ldots)$ represents the probability distribution of a random variable. If the recorded output signals do not fully comply with the stationarity, the results of the MPE will be affected.

Ergodicity Ergodicity describes the dynamic property of a system, which states that the *average* behaviour over time generally corresponds to the average behaviour over all the states the system may present itself in, over time. The mathematical definition of ergodicity, as stated in Shin and Hammond, 2008:

$$p(x,t) = p(x) \tag{2.11}$$

Stationarity With respect to ergodicity, stationarity defines three properties that should hold to ensure full stationarity, namely:

$$p(x,t) = p(x) \tag{2.12a}$$
$$p(x_1,t_1;x_2,t_2) = p(x_1,t_1+T;x_2,t_2+T) \tag{2.12b}$$
$$p(x_1,t_1;x_2,t_2;\ldots;x_k,t_k) = p(x_1,t_1+T;x_2,t_2+T;\ldots;x_k,t_k+T) \tag{2.12c}$$

Equation 2.12a implies that the mean $\mu_x(t)$ and variance $\sigma_x(t)$ are constant over time. Equation 2.12b implies that the probabilities do not change over a single time shift T. If only the first two equations are satisfied, the signal is said to be weakly stationary. If the stationarity holds over every point in time, the signal is said to be fully stationary (Shin & Hammond, 2008, p. 224). This is implied by the third equation (Equation 2.12c).

2.3.1. FREQUENCY DOMAIN DECOMPOSITION

The frequency domain decomposition (FDD) is used in modal analysis for MPE. It is a user-friendly method which decomposes a summed frequency response spectrum, and represents the contributions for the most dominant modes (Brincker et al., 2001). The method can be implemented and used to describe an MDOF model, however the accuracy of the algorithm depends on the recording and signal processing parameters (Hadianfard & Kamali, 2020).

SINGULAR VALUE DECOMPOSITION

The singular value decomposition (SVD) is an effective and practical tool to apply model dimension reduction. Besides the FDD, other OMA algorithms make use of the SVD to decompose data matrices (Magalhães & Cunha, 2011). In Chapter 4 (Methods), a comprehensive explanation is presented on the application of the FDD. The method includes a sequence of steps to be taken. The singular value decomposition is also reflected on.

ENHANCED DECOMPOSITION

The enhanced frequency domain decomposition (EFDD) is a method, which is used to determine structural damping. The EFDD incorporates a logarithmic decrement damping estimation (LDDE).

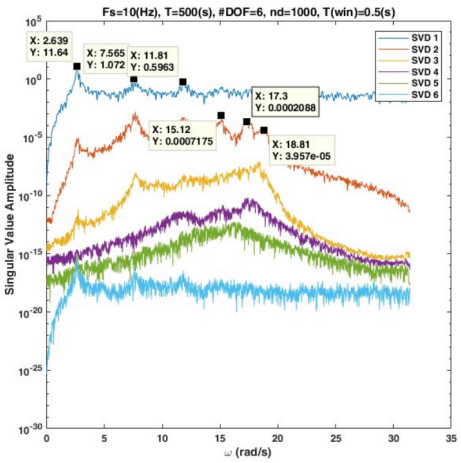

Figure 2.2: Example of singular values plot for FDD. In this plot, the contributions for the dominant modes are represented. Each colour in the spectrum contributes to a single mode, and together represent the total response of the strucutre. (source: Hadianfard and Kamali, 2020)

PEAK-PICKING

The peak-picking method is one of the most straightforward MPE methods to determine the natural frequencies of a system. This method is not preferred due to the lack of automation, and susceptibility to human errors. However, this method can be fully automated if implemented correctly (Jin et al., 2021). This is preferred in the case of highly damped systems or noisy data (Pioldi & Rizzi, 2017).

2.4. SIGNAL PROCESSING

When considering digital signals, the continuous time domain is recorded and registers a collection of discrete samples. To be able to describe continuous phenomena in the discrete domain brings forth several points of attention. In this section of the report, the concepts of the discrete domain will be briefly described. Fundamental theories regarding (digital) signal processing, described in Shin and Hammond, 2008, Smith, 2003, Parker, 2017, Brincker and Ventura, 2015 and others are presented.

DISCRETE FREQUENCIES

An Analogue-to-Digital Converter (ADC) is used to convert the continuous-time signal to the discrete-time domain. The discrete-time domain signal can be transformed to the discrete-frequency domain by the use of a discrete Fourier transform (DFT). A highly optimized implementation of the DFT is the fast Fourier transform (FFT) (Parker, 2017). Inherently, the FFT derives a discrete number of frequencies for the discrete-time domain signal. The lowest frequency in the range is identified as the fundamental frequency (f_0). Every measured frequency can be considered as an integer multiple of the fundamental frequency.

$$u[t] = \sum_{n=0}^{N/2-1} A[n]\cos(\omega_0 n t) + B[n]\sin(\omega_0 n t) \qquad \text{with} \quad \omega_0 = 2\pi f_0 \tag{2.13}$$

FREQUENCY RANGE

The frequency range is the bandwidth of the frequencies that are included in the analysis. A distinction is being made between the continuous domain and the discrete domain. From now on, the domain of the digital transform of the signal will be referred to as the discrete domain.

Sampling frequency The sampling frequency describes the frequency at which the discrete samples are taken.

Nyquist frequency The Nyquist frequency describes the highest measurable harmonic and is dependent on the sampling frequency. For a harmonic to be recognized by the FFT, the record must contain at least 2 discrete samples of that specific frequency. If a sampling frequency of $1000Hz$ is taken, then the Nyquist

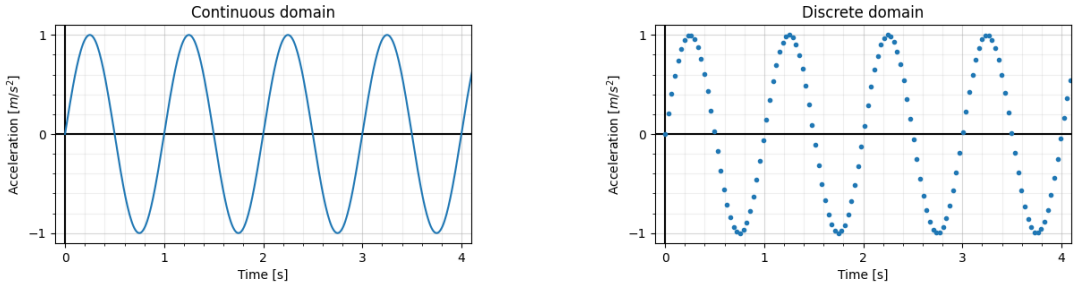

(a) Continuous domain

(b) Discrete domain

Figure 2.3: The difference in domains

frequency is at $500Hz$. This implies that the highest measurable harmonic is also $500Hz$.

$$f_{nyq} = \frac{f_s}{2} \tag{2.14}$$

Fundamental frequency The fundamental frequency is the lowest measurable frequency. This is directly related to the length of the recorded time signal.

$$f_0 = \frac{1}{T_{meas}} \tag{2.15}$$

Frequency resolution The frequency resolution describes the horizontal distance between the discrete frequencies, which are presented in the frequency spectrum.

Phase distortion When a low-, high-, or bandpass filter is being applied, the filter characteristics can produce (non-linear) phase delays. Therefore, a phase correction is recommended to ensure an undistorted phase. Phase correction can be performed by applying a forward-backward filtering. This will apply a filter twice, which will be responsible for rectification of the phase distortion.

2.4.1. MEASURE OF LINEAR RELATIONSHIP

Correlation When describing two random variables with respect to each other, the correlation is a useful parameter to present a value for both the strength and direction of a linear relationship (Shin & Hammond, 2008). The correlation presents a measure of similarity.

$$Corr(X,Y) = E[XY] = R_{XY} \tag{2.16}$$

Covariance Comparable to the correlation, the covariance is used as a tool to show the relation between two random variables. What differentiates the covariance from the correlation is that the covariance requires to subtract the corresponding mean before multiplication of the random variable.

$$Cov(X,Y) = E[(X-\mu_x)(Y-\mu_y)] \tag{2.17}$$

Correlation coefficient When two random variables are fully correlated, the correlation coefficient is equal to 1. If the two variables are uncorrelated, the computed correlation is equal to 0. The correlation coefficient includes the standard deviation of each variable, to normalize the result.

$$\rho_{XY} = \frac{Cov(X,Y)}{\sigma_X \sigma_Y} \tag{2.18}$$

AUTOCORRELATION FUNCTION

The autocorrelation function (ACF) is used in time-analysis. The main variable of the function is the time *lag* (τ). It represents the shifted time signal with respect to itself.

$$R_{xx}(\tau) = E[x(t)x(t+\tau)] = \lim_{T\to\infty} \frac{1}{T}\int_0^T x(t)x(t+\tau)d\tau \tag{2.19}$$

$$C_{xx}(\tau) = E[(x(t)-\mu_x)x((t+\tau)-\mu_x)] = \lim_{T\to\infty} \frac{1}{T}\int_0^T (x(t)-\mu_x)(x(t+\tau)-\mu_x)d\tau \tag{2.20}$$

$$C_{xx}(\tau) = R_{xx}(\tau) - \mu_x^2 \tag{2.21}$$

In equation 2.19, $R_{xx}(\tau)$ represents the ACF for time lag τ. The period over which the signal is autocorrelated is represented by the parameter T. Equation 2.20 gives the autocovariance function $C_{xx}(\tau)$, with μ_x as the mean value of the time series $x(t)$. In equation 2.21, the relation is given between the ACF and the autocovariance function. Furthermore, there is a relation between the total variance of the spectrum and the ACF. It is clear to see that the autocorrelation for lag 0 is equal to the variance of the spectrum (Equation 2.22).

$$R_{xx}(0) = E[x(t)^2] = \sigma_x^2 \tag{2.22}$$

Considering autocorrelation to be a measure of association, the maximum value of the ACF is located at time lag 0. To normalize the ACF, the variance will have to be factored out.

Random signal For general understanding, it is quite intuitively to presume that random signals are uncorrelated. When considering the ACF of a random signal, time lag 0 yields the time signal squared, therefore an autocorrelation of 1 (fully correlated). As the time lag increases, the correlation decreases. The correlation approaches 0, the greater the time lag grows. This behaviour describes the correlation of a random signal. An example of a random signal is white noise.

Periodic signal The correlation of a *random* signal decreases when the time lag increases. However, considering a *periodic* function (e.g. sinusoid): at time lag 0 the correlation is equal to 1 (fully correlated). When increasing the time lag, the correlation starts to decrease. After increasing the time lag for a certain period, the correlation will start to show an increase. Due to the periodic properties of the signal, the ACF also becomes a periodic function with respect to the time lag.

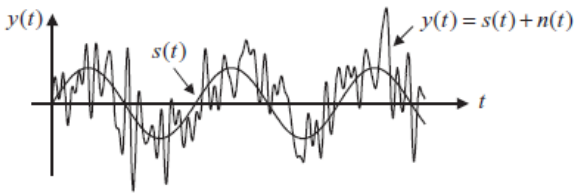

Figure 2.4: A sinusoid buried in noise (Shin & Hammond, 2008)

In Figure 2.4, a time series of a signal is presented. The total signal $y(t)$ consists of a signal $s(t)$ and noise $n(t)$. By computing the ACF, the correlation between the total signal and a lagged version of itself is presented. When the time lag increases, the noise becomes less correlated. therefore, the contribution of the noise starts to diminish for increasing values of τ. The contribution of $s(t)$ will remain in the ACF R_{yy}. The ACF is a useful tool to filter out the uncorrelated noise (Shin & Hammond, 2008).

Autocorrelation & autocovariance In Section 2.4.1, a distinction is made between the correlation and the covariance, where the dissimilarity between the two involves the mean of the signal. The correlation is described as the product of two terms premultiplied by the probability, whereas the covariance requires the mean value to be subtracted from the signal before taking the product. During this project, the signals are assumed to be *zero-mean* (due to a linear detrending computation) and therefore, the autocorrelation and autocovariance are identical.

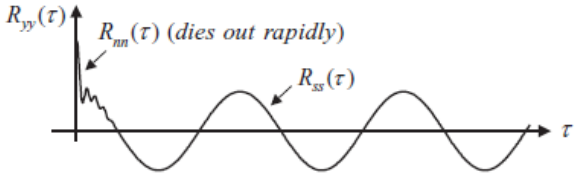

Figure 2.5: Autocorrelation function with dying noise (Shin & Hammond, 2008)

Wiener-Khinchin theorem The Wiener-Khinchin theorem states that the auto spectral density function can be computed by taking the Fourier transform of an autocorrelated time signal (James, 2011). Taking the ACF of a time series results in attenuation of the uncorrelated behaviour, whilst the periodic part remains present. By applying the Wiener-Khinchin theorem, relaxed assumptions on the stationarity and non-linearity can be assumed (Zbilut & Marwan, 2008). As described with recurrence quantification analysis, the periodic trends remain present in the computed signal. Keep in mind that the absolute magnitude of the ACF, which is used in the Fourier transform, is not directly representative when compared to results from other (linear) methods. (Zbilut & Marwan, 2008).

$$S_x(f) = \mathscr{F}\{R_{xx}(\tau)\} \tag{2.23}$$

When dealing with digital finite-length signals, the envelope of the ACF decreases for greater values of the time lag. This is presented in the correlogram of Figure 2.6. The (auto)correlation function can contain significant noise for greater time lags. Tarpø et al., 2017 addresses this phenomenon and presents methods to effectively truncate the noise tail of the correlation functions, whilst maximizing the preservation of the fundamental frequency.

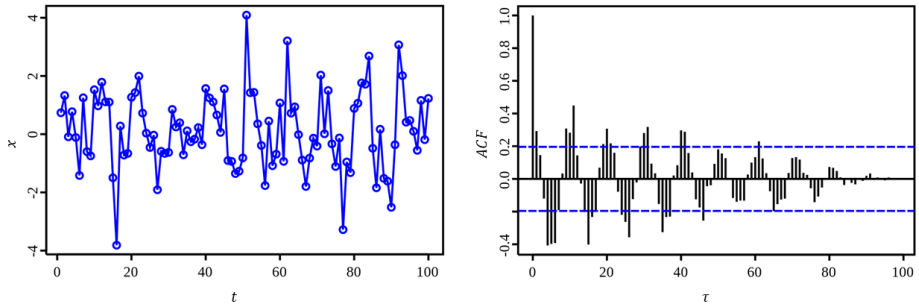

Figure 2.6: Example of a discrete signal as a function of time t (left) and a correlogram as a function of time lag τ (right) (source: Wikipedia contributors, n.d.)

2.5. DYNAMIC RESPONSE CHARACTERISTICS FOR SIMILAR BRIDGES

Arch bridges are a widely used type of bridge due to their advantages, like large span capacity and aesthetic characteristics (Pellegrino et al., 2010). Through basic mechanics, the deflections of structural elements, due to acting loads, increase significantly when considering larger spans (Chen et al., 2015). For arch bridges, this property also holds. When considering dynamic loading, the imposed deflections propose consequences in the dynamic behaviour as well (Lu et al., 2017). Therefore it is essential to determine dynamic properties for larger span arch bridges.

In this section of the report, a brief introduction to arch bridges and railway bridges is presented to give sufficient background knowledge on the dynamic behaviour of such structures, as the case study covers a similar structure. The consideration of specific loading types is well outside the scope of this research project. However, to be able to make a distinction between computation- and structural- or load-related results, a quick overview is presented on common characteristics for both arch bridges and railway bridges.

The dynamic properties of a structure, like natural frequencies, are not load dependent. That is, the natural frequencies and eigenmodes of the bridge will be determined on the characteristics of the bridge only. Besides modal parameters, the structure will most certainly adopt a dynamic response when it is subjected

to forced vibrations (Spijkers et al., 2005). This response can be described as an *operational deflection shape* (ODS). The ODSs are *not* solely determined by the dynamic properties of the bridge. By analysing the total response of the bridge for slight variations in loading during several loading periods, a distinction can be made between load- and structure-related responses. The homogeneous response is inherent to the structure and the particular response is inherent to the load. In general, train loads consist of significant axle loads with periodic motions (X.-M. Yang et al., 2021). In section 2.5.2, the characteristics of train loads will be discussed.

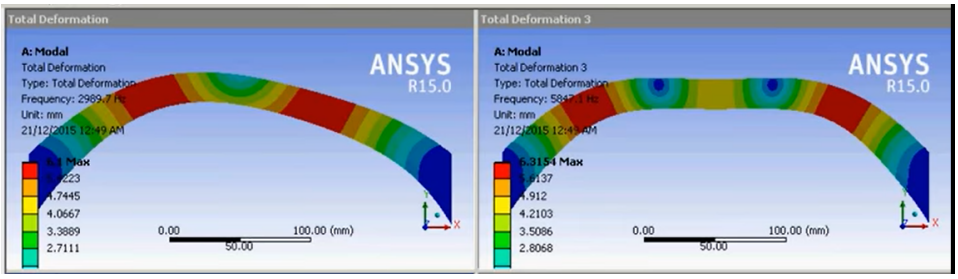

Figure 2.7: Modal analysis (FEM) of an arch element in Ansys for the first 4 modes. (source: ANSOL, 2015)

2.5.1. ARCH BRIDGES

By static analysis, the main load bearing component is the arch, which is predominantly loaded in axial pressure. The arch also experiences a bending moment and shear force. The maximum values of the bending moment and shear force are located at the middle and base of the arch, respectively. The horizontal thrust of the arch rib imposes some engineering challenges due to the great horizontal forces that are introduced at the base of the arch. When considering tied arch bridges, a possible solution to counteract the horizontal thrust is to introduce prestressing forces into the beams which thereby overcome the deficiency of traditional arch bridges (Jiang et al., 2019).

Identification of the modes in the arch bridge give various options for the *operational deflection shapes* of the arch bridge. The first vertical in plane bending mode shape, determined through FEM software (Jiang et al., 2019, Kong et al., 2006, Lonetti et al., 2016), shows the second expected bending mode for a traditional beam. This mode shows a sagging- and a hogging shape over the total span (Figure 2.8).

When considering damping, F. T. Au et al., 2001 states that the influence of damping on impact factors is significant but depends on the type of load effect considered and the location (F. T. Au et al., 2001, p. 461).

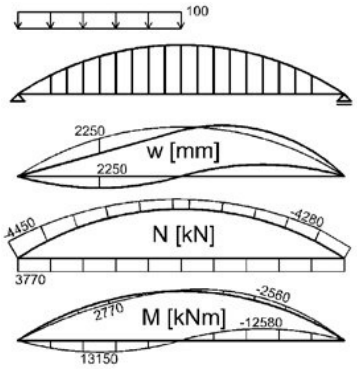

Figure 2.8: Asymmetrical loaded arch bridge for typical deflection shape (source: Zwingmann, 2010)

2.5.2. RAILWAY BRIDGES

When considering dynamic properties of a structure, the input loads are of significant importance to be able to determine (or approach) an accurate transfer function. However, when the concepts of OMA are being applied, certain assumptions are made to simplify the determination process. For most general cases of OMA techniques, assumptions to present the input load as white noise (or broadband random) are used. When this assumption is taken into account, it will inherently point out that every single amplification in the output signal is caused by the structure itself. However, the axle spacing of a train load are far from random.

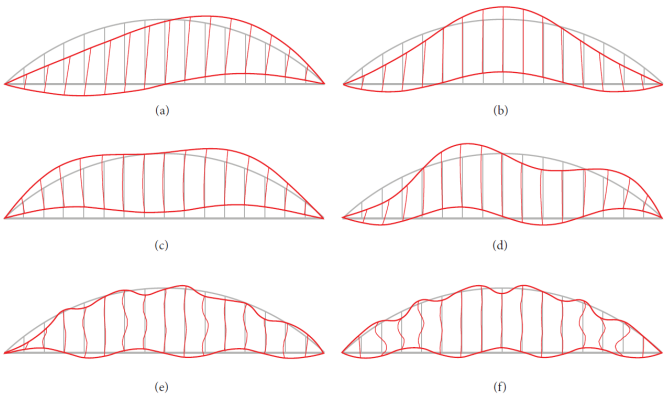

Figure 2.9: First 6 mode shapes (a → f) for a digital analysis (source: Lonetti et al., 2016)

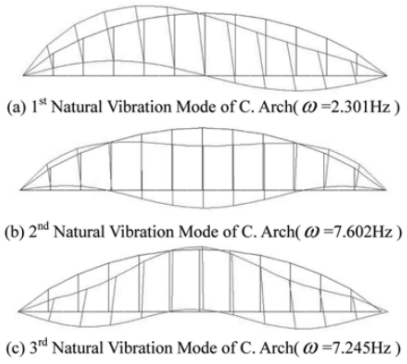

Figure 2.10: First 3 mode shapes for a digital analysis multiple arch bowstring bridge (source: Kong et al., 2006)

If the bridge is mainly excited by the train loads, modal parameters become difficult to identify due to the regularly spaced and highly energetic axle loads (X.-M. Yang et al., 2021). This is contrary to the general assumption of a white noise loading scheme. Therefore, it does not comply with this general assumption when regarding OMA. Y.-B. Yang et al., 1997 states that the moving loads can be assumed as *moving loads with regular non-uniform intervals*.

When comparing railway bridges to standard highway bridges, the heavy concrete decks are not present. This results in lesser dead load and corresponding decrease in inertial forces (Khan, 2013, pp. 230-231). Although the decrease in self weight will preserve additional capacity to support the moving loads, the structure will be more susceptible to dynamic behaviour imposed by the moving load, precisely due to its lesser inertial properties. It is observed that, in almost all cases, the impact effects of a solitary locomotive are more significant than those of an entire train (F. T. Au et al., 2001, p.461). At the tower (support), the impact effects are moderate, the cables close to the support show large impact effects, whereas the cables far away from the supports show low impact effects (F. T. Au et al., 2001, p. 461). Probably due to stiffness related appearances.

A moving train will portray specific load characteristics. These characteristics are dependent on a vast variety of parameters, like train velocity, axle spacing, gross train weight and axle weights (Wang et al., 2019, p. 263). Regarding the deflection shape, for a long span stay cable bridge the vertical response of the car body seems to be only slightly higher than the lateral response (Xia et al., 2000, p. 274). The velocity of the train plays a role in the dynamic response of the bridge. It is seen that the train responses increase significantly with the increasing train velocity (Xia et al., 2000, p. 275). From observations, the maximum impact factors are mostly concentrated around a specific velocity range where one may be led to think that such pronounced impact effects are due to the excitation of the lower vibration modes (F. T. Au et al., 2001, p. 455). Literature shows that the response of the forced steady-state vibration reaches its maximum values when the period of the moving load is equal to an equivalent period of the structure, or an integer multiple of it (Frýba, 1972). The period $T = d/v$ of the moving loads has been identified as a key parameter, where d and v represent the length of the uniform intervals between wheel bases and constant speed, respectively (Y.-B. Yang et al., 1997).

When a computer model is used during an analysis, imperfection parameters are taken into account as

well. This may lead to pseudo-dynamic behaviour which should be included in the calculation. However, this can not entirely be modelled realistically. An example of such imperfections is/are track irregularities (F. T. Au et al., 2001) and/or stiffness deviations.

Castellanos-Toro et al., 2018 states that the estimation of operational frequencies, to provide evidence on the current dynamic behaviour of bridges, is possible through OMA. However, the estimation of damping ratio's for the considered operational frequencies did not present clear relations between the geometric and/or material properties of bridges. In this study, also a railway bridge is considered.

3

Case study

FOR the derivation of the dynamic bridge properties, a case study is investigated on the Bert Swart bridge. The location of the bridge is near Zuidhorn, which is a small town in the northern part of the Netherlands. The bridge is constructed explicitly for railway traffic between the cities Leeuwarden and Groningen. The Bert Swart bridge is an arch bridge with a span length of approximately 120 meters to cross the Van Starkenborghkanaal (Figure 3.1). During the case study, only the relevant natural frequencies will be taken into account. The focus will be on the natural frequencies, located at the lower end of the frequency spectrum.

Figure 3.1: A plan view of the location of the bridge. In the figure A represents the location of the bridge, B represents the nearest station (Zuidhorn). Leeuwarden is situated to the west, Groningen to the east. (source: Google Maps)

DATA ACQUISITION

For the acquisition of the data, 5 accelerometers are utilized. The accelerometers are equally spaced along the span of the bridge deck (each about 30 meters apart). Two sensors are applied above the supports, two at a quarter and three quarters of the span and a single sensor at midspan. See Figure 3.2 for a visual representation of the bridge, the deck and the sensor locations.

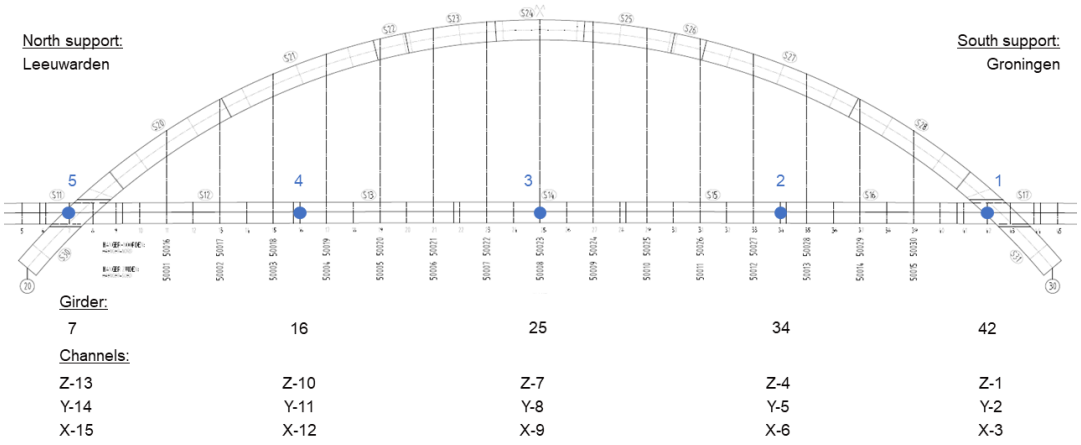

Figure 3.2: Overview of the locations of the sensors, with corresponding girder numbers

The type of accelerometer which is used during the measurements, is the PCL Model 338B35 from PCB Piezotronics (Fugro, 2021). This sensor is capable of measuring in 3 orthogonal directions. Each direction registers to a separate channel, and is connected to a collective mainframe. The mainframe registers all sensor channels for corresponding discrete time, until the 20 second time mark is reached and the accelerometers stop recording, after which the data-file is constructed and saved. A preview of such a data file is presented in Figure 3.3. The channels of the data-file correspond to the channels of the Figure 3.2.

[Data]															
Time	Chan1	Chan2	Chan3	Chan4	Chan5	Chan6	Chan7	Chan8	Chan9	Chan10	Chan11	Chan12	Chan13	Chan14	Chan15
[Sec]	[m/s2]	[m/s2]	[m/s2]	[m/s2]	[m/s2]	[m/s2]	[m/s2]	[m/s2]	[m/s2]	[m/s2]	[m/s2]	[m/s2]	[m/s2]	[m/s2]	[m/s2]
0	0.0024	-0.0073	0.0025	-0.0148	0.0049	0.0025	0	-0.0125	-0.01	0.0025	-0.0025	0.005	0	-0.0051	-0.0133
0.001	0.0024	-0.0073	0	-0.0148	0.0025	0.0025	0	-0.0125	-0.01	0.0025	-0.0025	0.0025	0	-0.0025	-0.0159
0.002	0.0024	-0.0073	0.0025	-0.0123	0.0049	0.0025	0.0025	-0.0125	-0.01	0.0025	-0.0025	0.0025	-0.0025	-0.0051	-0.0159
0.003	0.0049	-0.0049	0.0025	-0.0123	0.0025	0.0025	0	-0.0125	-0.0075	0.0025	-0.0025	0.0025	0	-0.0051	-0.0159
0.004	0.0024	-0.0073	0.0025	-0.0123	0.0049	0.0049	0	-0.0125	-0.0075	0.0025	-0.0025	0.005	0	-0.0051	-0.0159
0.005	0.0024	-0.0073	0.0025	-0.0123	0.0049	0.0025	-0.0025	-0.0125	-0.005	0	-0.0025	0.005	0.0025	-0.0051	-0.0159
0.006	0.0024	-0.0073	0.0025	-0.0123	0.0049	0.0025	0	-0.0125	-0.005	0	-0.005	0.005	0	-0.0051	-0.0133
0.007	0.0024	-0.0098	0	-0.0123	0.0049	0.0025	-0.0025	-0.0125	-0.0075	0.0025	-0.0025	0.0025	0	-0.0076	-0.0133

Figure 3.3: Preview of the data-file

Besides the accelerometers, two additional sensors are placed, to indicate a passing train, and have been used to determine the average train velocity over the bridge. Determination of the average velocities is done by registering the time length between two measurement locations, spaced approximately 500 metres apart, on each side of the bridge. The computed average velocities are presented in Figure 3.5.

During the time of the measurements, the train types and velocities have been recorded (Fugro, 2021). Only a single train type is registered to pass over the span of the bridge during the time of data acquisition. The train type to have passed is the Stadler GTW 2/8. This is determined by combining description and photographs that are included in the measurement report of Fugro, 2021. Specifications of this train type are presented in Table 3.1. An overview of the train configuration is depicted in Figure 3.4.

The acquired measurements have been performed on the 31st of August 2021 from 11:09 to 13:04. Each recording is performed with a samping frequency of 1000Hz and a total time duration of 20s.

Stadler GTW 2/8		
No. carriages	3	pc.
No. axles	8	pc.
Mass (no passengers)	91	tons
Length over coupling	55.94	m
Centered axle base	15.05	m
Vehicle width	2.95	m
Vehicle height	4.035	m
Axle arrangement	2' Bo 2' 2'	
Max. velocity	140	km/h
No. seatings	163	pc.
Suspension type	Air suspension	

Table 3.1: Specifications of Stadler GTW 2/8 (source: W. contributors, 2022)

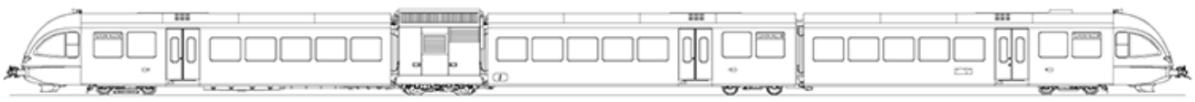

Figure 3.4: Overview of Stadler GTW 2/8 (source: R. contributors, n.d.)

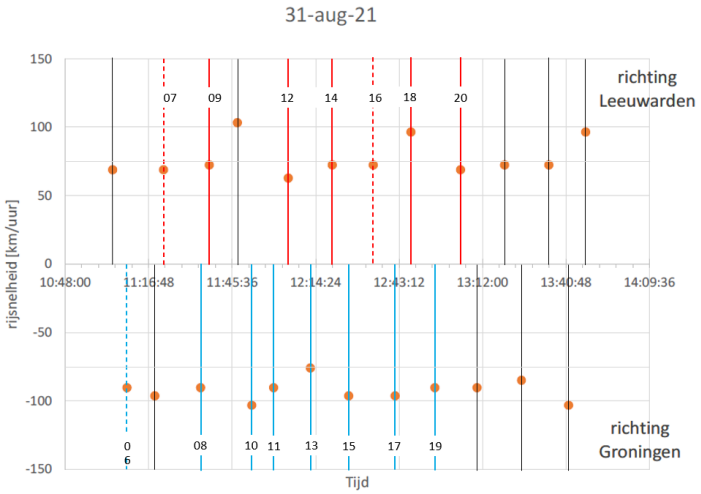

Figure 3.5: Train velocities per recording (original version from report Fugro, 2021). The numbers on the vertical lines represent the recording number, which will be used in Section 4.4.1.

3.0.1. BERT SWART BRIDGE - DIGITAL MODEL

Prior to the start of this research project, an extensive FEM model is constructed to identify modal parameters. The model is constructed by an external firm and commissioned by Arcadis. The results are presented in the report of SFF Ingenieure, 2021. It includes results which determine the first dynamic modes of the bridge. The first three mode shapes are presented in Figure 3.6.

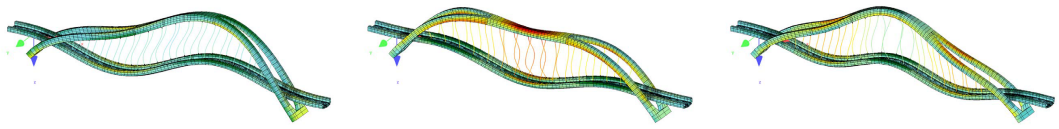

(a) First mode shape ($f_n = 1.566$) (b) Second mode shape ($f_n = 2.181$) (c) Third mode shape ($f_n = 3.712$)

Figure 3.6: First three mode shapes, determined by extensive FEM model in report (source: SSF Ingenieure, 2021, pp. 12-13)

4

Methods

THIS chapter presents an overview of the methods used to produce the desired results. First, the necessary preprocessing related subjects are being discussed. Subsequently the details regarding SVD, FDD and EFDD algorithms are presented. Finally, rounding up to present the cases, which will be used for the FDD to determine the modal parameters of the structure. The results will be presented in Chapter 6 and Appendix A, and discussed in Chapter 7.

4.1. PREPROCESSING OF THE DATA

A sequence of preprocessing computations is applied prior to the estimation of the modal parameters. The following computations are performed on the set of input data:

1. Import records
2. Detrend individual signals
3. Apply low- or band-pass filter (main focus on the natural frequencies at low end of frequency spectrum)
4. Downsample to improve on required computational effort
5. Return detrended, filtered and decimated records in data frame for corresponding time domain

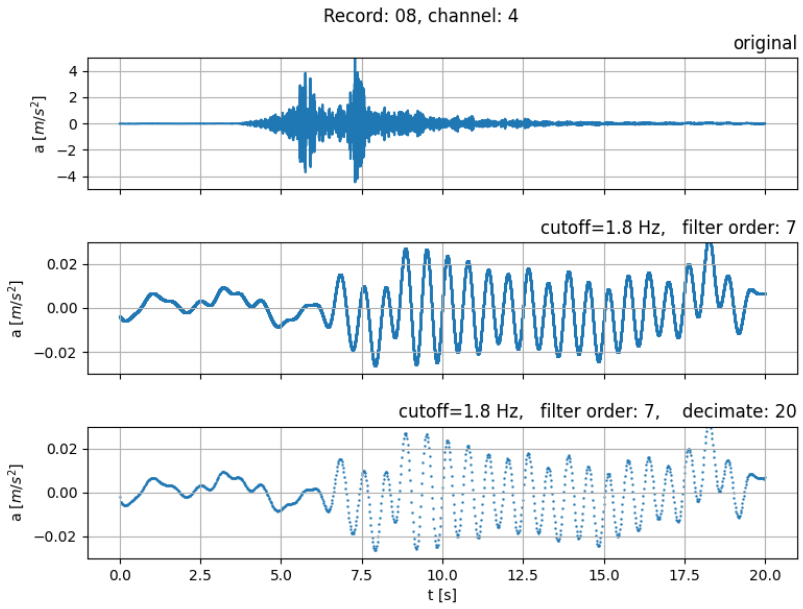

Figure 4.1: Example of the original, filtered, filtered & downsampled results. The preprocessing parameters for this example do not relate to the true preprocessing parameters for the results of the case study. The true preprocessing parameters are presented in Table 4.4.

Remark downsampling It is important to check whether the down-sampling process makes use of an *anti-aliasing filter*. If this is not the case the filter will have to be applied manually. This can be explained by an example, shown in Figure 4.2.

The graphs represent a time domain signal with varying signal-to-noise ratios. Whenever the signal-to-noise ratio is high, decimation will not necessarily be a problem. But when regarding a low signal-to-noise ratio, the chances of the discrete point taken at the wrong instance is very likely, which will produce non-acceptable results after the decimation. When first applying a low-pass filter, decimation can be performed without negative side effects.

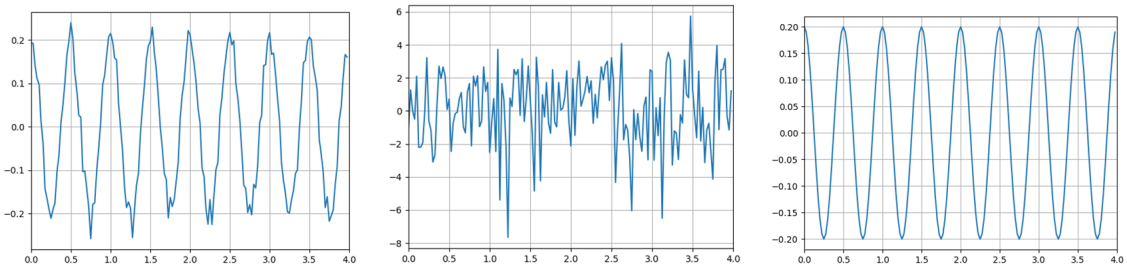

Figure 4.2: high signal-to-noise ratio (l), low signal-to-noise ratio (m), low signal-to-noise ratio with applied low-pass filter (r)

4.2. FREQUENCY DOMAIN DECOMPOSITION

To perform an FDD from a set of measurement signals, the data will be prepared by making distinct segments, transforming the segments, summing the signals in the frequency domain and computing the outer product to form a spectral matrix, finally performing an SVD. By performing the SVD, the spectral matrix is decomposed into a set of frequency domain functions, with corresponding mode shapes. This result is almost exact in the case of white noise loading, minimal damping and orthogonal mode shapes for closely spaced modes (Brincker et al., 2001). If deviations from these assumptions are present, the results will have to be interpreted accordingly. The FDD presents the contributions of a collection of dominant operational deflection shapes.

OPERATIONAL DEFLECTION SHAPES, MODE SHAPES & CLOSELY SPACED MODES

When combining the data of multiple accelerometers, an overall ODS can be determined. However, the main goal of MPE is not to identify the ODSs, but to separate the mode shapes (native to the structure), as forced vibration responses are not considered modal parameters. When a forced vibration response is measured, often multiple modes are amplified, whereas for a structural mode, only a single mode will be amplified. This behaviour is observable through the singular values plot (Figure 2.2).

A major advantage of the FDD method is the ability to identify the contributions of multiple modes, present at a discrete frequency. In theory (and practice), the response of the structure is a superposition of all the individual eigenmodes (Spijkers et al., 2005). These modes are determined through the SVD and the contribution of each mode is determined by its corresponding participation factor (singular value).

4.2.1. PRINCIPAL COMPONENT ANALYSIS

Principal component analysis (PCA) is a concept that is applied during the SVD. PCA is often used for dimension reduction of (data) matrices (Nanga et al., 2021). In the case of the FDD, it is responsible for the extraction of the mode shapes. The mathematical term for mode shape is eigenvector. The eigenvectors hold the information on the relative amplitude and phase angle between the DOFs of the system. The eigenvectors of a symmetric matrix are orthogonal vectors, which implies that they are linearly independent. The number of eigenvectors determines the amount of required modes to construct all the structural behaviour, included in the data matrix. PCA determines the eigenvectors through an eigenvalue decomposition.

4.2.2. SINGULAR VALUE DECOMPOSITION

The SVD makes use of PCA to determine the mode shapes. However, these parameters will remain estimates, due to the contribution of noise and the lack of system input signals, as discussed before in subsection 2.3. The original eigenvalue decomposition can only be performed on square matrices. However, the SVD can also be performed on non-square matrices, which makes it a powerful tool (Chengwang, 2010). In short, the SVD takes a single data matrix (spectral matrix) as input and, after decomposition, returns three matrices (U, Σ and V), which represent the left singular vectors-, singular values- and right singular vectors matrix, respectively. In the case of a Hermitian data matrix, the returned left and right singular vector matrices are also each Hermitian transform. These matrices contain the eigenvectors (mode shapes) of the structure. The Σ matrix contains the eigenvalues (singular values). The eigenvalues represent the scalar value to which the corresponding eigenvectors can be linearly scaled and can hereby be represented as a 'participation factor'. It presents how much the corresponding mode contributes to the total response. Further elaboration on the properties of the SVD is presented in the following paragraphs, together with some fundamental concepts to cover the application of the SVD.

Norm of a vector The norm (or length) of a vector ϕ is a scalar value and is evaluated by the following formula:

$$\|\phi\| = \sqrt{\sum_{n=0}^{k} \phi_n \bar{\phi}_n} \tag{4.1}$$

Equation 4.1 is used to determine the norm of a complex vector. The bar symbol represents the complex conjugate of the vector. When dividing a vector by its norm, the vector will have a length equal to unity. If the norm for every eigenvector in the set of orthogonal vectors is equal to one, the collection of vectors span an orthonormal basis, which can be grouped to form an orthonormal matrix.

Decomposition When considering the complex data matrix A: the eigenvectors of AA^H constitute U, and the eigenvalues of it constitute $\Sigma^H\Sigma$. Additionally, the eigenvectors of A^HA constitute V, and the eigenvalues of it constitute $\Sigma\Sigma^H$. Because the matrix Σ is a diagonal matrix, the product of matrices $\Sigma^H\Sigma$ is identical to the product of the matrices $\Sigma\Sigma^H$ (He & Fu, 2001a). In this notation, the superscript ^{H} represents the hermitian transform. Decomposition of the matrix A can be represented by Equation 4.2. Although the matrices U and V are complex, the singular values matrix Σ contains only real values.

$$A = U\Sigma V^H \tag{4.2}$$

Rank The rank of A is equal to the amount of non-zero singular values, which is therefore also the rank of the matrix Σ (He & Fu, 2001a). Due to computational properties, residual values remain present in the Σ matrix. To disregard these residuals, a threshold value is taken into account which sets the residual values to zero (Figure 6.1).

"*If the information about the uncertainties of the measurement is minimum, the rank of the system, which is determined by the SVD, becomes larger than the number of excited and observed system modes. Hereby forcing the algorithm to describe the presence of noises in modal space*" (Juang & Pappa, 1985, p. 622).

In this sentence, Juang and Pappa, 1985 describe the presence of non-existent modes in the form of additional singular values to account for the noise in the signal. The noise can be filtered out if the information on the uncertainties is completely known.

Sorting After performing the SVD, the data is returned in an ordered fashion. As described in the subsection regarding PCA, the derived eigenvectors represent the orthogonal mode shapes of the structure. The accelerations for dominant modes are greater than for non-dominant modes. Therefore, the norm of the dominant eigenvectors is also greater. However, the returned eigenvectors of the SVD are normalized. The magnitude, or participation factor, is therefore directly related to the singular value. Which are collected in the real valued, diagonal Σ matrix.

The singular values are sequentially ordered ($\lambda_1 > \lambda_2 > \ldots > \lambda_n$), sorted from largest to smallest, positioned on the diagonal of the Σ matrix. The left and right singular vectors are positioned accordingly, based on the position of the corresponding singular values, for the U and V matrices respectively.

$$\begin{bmatrix} u_{11} & u_{21} & u_{31} \\ u_{12} & u_{22} & u_{32} \\ u_{13} & u_{23} & u_{33} \end{bmatrix} \quad \begin{bmatrix} \lambda_1 & 0 & 0 \\ 0 & \lambda_2 & 0 \\ 0 & 0 & \lambda_3 \end{bmatrix} \quad \begin{bmatrix} \bar{v}_{11} & \bar{v}_{12} & \bar{v}_{13} \\ \bar{v}_{21} & \bar{v}_{22} & \bar{v}_{23} \\ \bar{v}_{31} & \bar{v}_{32} & \bar{v}_{33} \end{bmatrix}$$

In the depiction above, the matrices U, Σ and V^H are presented, respectively (for matrix size 3x3). The colours in the matrices show the relation between the singular values and corresponding singular vectors. The bar symbol represents the complex conjugate of the matrix values. The singular values will be sorted from largest to smallest (significant contribution to admissible contribution). The amount of non-zero singular values indicate how many orthogonal components are contributing to the total response at a certain frequency. The singular vectors indicate the amount of contribution each DOF has w.r.t. the total mode.

4.2.3. STEPS

As mentioned at the beginning of this section, the FDD consists of several steps to prepare the data for a linear decomposition in the frequency domain, followed by the SVD. This subsection presents a compact analytical description on the sequence of steps to execute the FDD method.

The raw data matrix is compiled after the preprocessing sequence. After compiling, it can be represented in the form of Table 4.1 (comparable to Figure 3.3). The input values a_{ijk} are the discrete recorded accelerations, where i, j and k represent the segment number, channel number and time position respectively.

	r_1			
Time	c_1	c_2	$\cdots$	c_n
0	a_{111}	a_{121}	$\cdots$	a_{1n1}
t_s	a_{112}	a_{122}	$\cdots$	a_{1n2}
$2t_s$	a_{113}	a_{123}	$\cdots$	a_{1n3}
$\vdots$	$\vdots$	$\vdots$		$\vdots$
$(m-1)t_s$	a_{11m}	a_{12m}	$\cdots$	a_{1nm}

Table 4.1: Raw data matrix overview

ANALYTICAL FORM

1. **Split data record into discrete segments** to form **c**-vector. Each column with a header c in table Table 4.1, is split up into separate time segments of equal length. For the current example, the number of segments is taken equal to 2. The amount of segments should be taken at least equal to the amount of modes to be identified in the system. The maximum rank of the Σ matrix after decomposition is equal to the number of segments, due to the number of expected linear dependencies. Please note that the length of the segment, will determine the fundamental frequency (f_0).

$$\mathbf{c_1}(t) = \begin{pmatrix} c_{11}(t) \\ c_{12}(t) \end{pmatrix} \quad \mathbf{c_2}(t) = \begin{pmatrix} c_{21}(t) \\ c_{22}(t) \end{pmatrix} \quad \mathbf{c_3}(t) = \begin{pmatrix} c_{31}(t) \\ c_{32}(t) \end{pmatrix} \tag{4.3}$$

2. **Restructure for corresponding time** to ensure corresponding time between the collection of channels in the $\mathbf{d_i}$ vector. This vector holds the time domain functions of all channels for segment i.

$$\mathbf{d_i}(t) = \begin{pmatrix} c_{1i}(t) \\ c_{2i}(t) \\ c_{3i}(t) \end{pmatrix} \tag{4.4}$$

3. **Compute Fourier transform** for each individual segment and form frequency-domain vector. The tilde symbol represents the signal in the frequency domain. By transforming the signal to the frequency domain, the result can become complex, meaning the transform of the signal can consist of a real part and an imaginary part.

$$\tilde{c}_{1i}(\omega) = \mathscr{F}\{c_{1i}(t)\} \tag{4.5a}$$
$$\tilde{c}_{2i}(\omega) = \mathscr{F}\{c_{2i}(t)\} \tag{4.5b}$$
$$\tilde{c}_{3i}(\omega) = \mathscr{F}\{c_{3i}(t)\} \tag{4.5c}$$

$$\tilde{\mathbf{d}}_\mathbf{i}(\omega) = \begin{pmatrix} \tilde{c}_{1i}(\omega) \\ \tilde{c}_{2i}(\omega) \\ \tilde{c}_{3i}(\omega) \end{pmatrix} \tag{4.6}$$

4. **Compute Hermitian transform** of the $\mathbf{d_i}$-vector in the frequency-domain. By computing the Hermitian transform of the vector, the complex conjugate is taken and the vector is transposed from a column-vector to a row-vector. In equation 4.7, the bar symbol represents the complex conjugate.

$$\tilde{\mathbf{d}}_\mathbf{i}(\omega)^H = \begin{pmatrix} \bar{\tilde{c}}_{1i}(\omega) & \bar{\tilde{c}}_{2i}(\omega) & \bar{\tilde{c}}_{3i}(\omega) \end{pmatrix} \tag{4.7}$$

5. **Construct spectral matrix** by taking the summed multiplication as presented in equation 4.8. The product of the frequency-domain vector $\mathbf{d_i}$ with its conjugate transpose, is a cross-spectral matrix. This is a Hermitian matrix, meaning the real part of the matrix is symmetric and the imaginary part of the matrix is anti-sign symmetric ($a_{ij} = \bar{a}_{ji}$). By transforming a complex number to its conjugate, and

taking the product with a different complex number, will yield a magnitude and relative phase angle. The relative phase angle is an important property when describing (complex) mode shapes. The phase delay indicates the delay of a single DOF w.r.t. the other DOFs in that mode. For real modes, the phase is close to π or an integer multiple of it, whereas for complex modes this can be any value between 0 and 2π.

$$\tilde{S}_{dd}(\omega) = \sum_{i=1}^{N_s} \tilde{\mathbf{d}}_\mathbf{i}(\omega)\tilde{\mathbf{d}}_\mathbf{i}(\omega)^H \tag{4.8}$$

The $\tilde{S}_{dd}$ matrix contains every auto- and cross-spectrum for each of the data segments with corresponding time. The doubled letters represent the auto- and cross spectrum of the matrix. Parameter N_s is an integer and represents the total number of segments. By using the sum operator, a linear dependency can be formed. As N_s is responsible for the number of summations, the maximum amount of identified linear combinations can never be greater than this value.

6. **Perform SVD**. The first step of the SVD is to compute the matrices containing the left- and right singular vectors (U and V matrices respectively). These vectors are orthogonal to each other because the matrix from which they are derived is symmetric. Steps 4 & 5 ensure that the matrix is (square Hermitian) symmetric.

SPECTRAL MATRIX

In Figure 4.3a, the compiled spectral matrix in presented. The spectral matrix is constructed by columns, where a single column of this 3D matrix represents one auto- or cross spectrum. Over the height of this matrix, the discrete frequencies are represented. The auto- and cross- spectra share identical discrete frequencies, which are represented as *slices*.

In this example, a 3 DOF system is considered. The slices depict a 3x3 matrix, with data points $s_i s_j[f_k]$, which represents the frequency domain multiplication of DOF i with DOF j at discrete frequency k (see Figure 4.3b). This is where the information regarding the amplitude and relative phase between two DOFs for various frequency domain signals is stored.

During the SVD, the spectral matrix is solved for every discrete frequency. The singular values and singular vectors for that specific frequency are determined. The results are stored in three new slices which subsequently compose the U, Σ and V matrices (3D matrices). The dimensions of the three computed matrices are similar to the dimensions of the S_{dd} matrix.

4.3. ENHANCED FREQUENCY DOMAIN DECOMPOSITION

The enhanced frequency domain decomposition (EFDD) method is an addition to the original FDD method. The original FDD can present dominant frequencies and is able to identify multiple modes, or even distinguish an apparent harmonic from a structural mode. The EFDD method takes the current results and elaborates further on these results. This method provides an option to identify structural damping through an inverse Fourier transform (IFT) and logarithmic decrement. This computation is known as the logarithmic decrement damping estimation (LDDE).

When the natural frequencies of the system are identified, the corresponding mode shape is taken into account. The MAC value is determined for the mode shape of neighbouring frequency w.r.t. the mode shape at the location of the natural frequency (dot product of two eigenvectors). If the two modes are similar, the MAC value will be close to 1. If the two mode shapes are dissimilar, the MAC value will be considerably lower. If the determined MAC value is greater than the predefined MAC limit value (MAClim), the next MAC value (for second neighbouring frequency with corresponding mode shape) will be evaluated. This process is continued for neighbouring frequencies (left and right) until the computed MAC value is lower than the MAClim value. The total set of collected neighboring frequencies will be transformed to the time domain using inverse discrete Fourier transform (IDFT). A visual representation of the damping according to the EFDD method is presented in Figure 4.4.

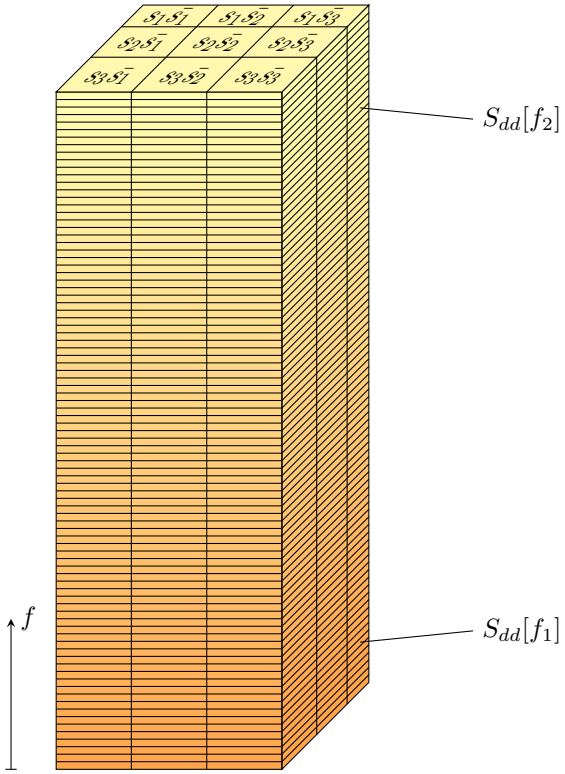

(a) Spectral matrix S_{dd}

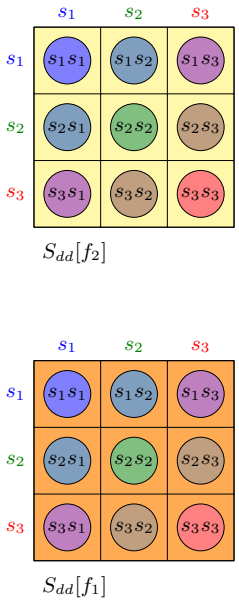

(b) Two slices of the spectral matrix at discrete frequency f_1 and f_2

Figure 4.3: Overall representation of the spectral matrix

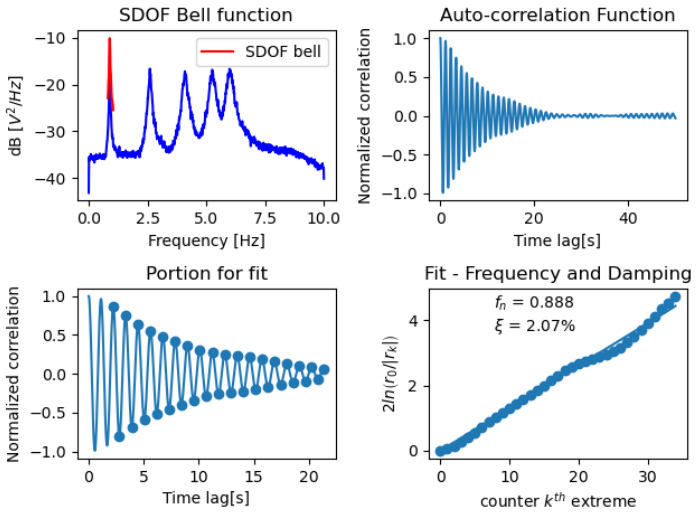

Figure 4.4: Determination of damping trough LDDE (this image is taken from the explanatory web page of the PyOMA package. This package includes methods to process OMA algorithms using Python, source: “PyOMA”, n.d.)

4.4. SETUP RESULT CASES

For the MPE of the Bert Swart bridge, various cases are considered to maximize the effectiveness for the determination of modal parameters. For this research project, discrete measurement recordings are acquired. Each recording can be considered a segment. Generally, the response of a structure is continuously monitored, which results in a single extensive measurement recording. The long signal should be segmented to be able to identify linear dependencies whilst simultaneously making the MPE process less computationally expensive. However, for this research project the data is already segmented during the acquisition process. Therefore, the data will not require any additional segmentation. Keep in mind that the segmentation process will inherently affect the fundamental frequency (f_0), due to shortening of the time signal. Figure 4.5 presents the time domain recordings from the data acquisition. The various colors in the plots represent different measurement channels (Figure 3.2)

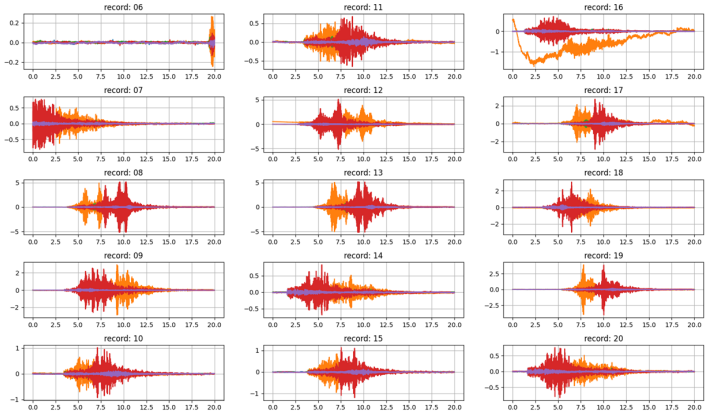

Figure 4.5: Overview of data segments, where each train passing represents a segment due to the data acquisition method $\left(T_{measure} = T_{segment} = 20s = \frac{1}{f_0}\right)$.

4.4.1. TRAIN DIRECTION

For the current case study, the acceleration recordings are previously segmented. Therefore, additional segmentation of the data will not have to be applied. The train directions can be divided into the two main directions. Dependent on the direction, input signals can be included in the MPE process. The train directions are derived from Figure 3.5, which display the train velocities. Table 4.2 presents the included recordings for each train direction.

Direction	**Included records**	**Amount**
Leeuwarden	09, 12, 14, 16, 18, 20	6
Groningen	08, 10, 11, 13, 15, 17, 19	7
Both	06, 07, 08, 09, 10, 11, 12, 13, 14, 15, 16, 17, 18, 19, 20	15

Table 4.2: Overview train directions

Records '06' and '07' are not included in the set of input signals for any single direction analysis, due to its poor measurement properties. When both train directions are included, the total set of recordings is used in the MPE process. By doing so, the quality of the results can be investigated when all recordings are included. This is scenario is most interesting as it does not require any prior knowledge on the quality of the data-set. However, it may not produce the most promising results.

4.4.2. SENSOR DIRECTION

As depicted in Figure 3.2, the data is collected through various channels, on which the accelerations are registered. Each channel represents a unique combination of sensor location and acceleration direction. The exact location of each sensor is presented in Figure 3.2. The channels for each acceleration direction are presented in Table 4.3.

Direction	Description	Channels
X	Parallel to the longitudinal bridge axis	3, 6, 9, 12, 15
Y	Perpendicular to the longitudinal bridge axis (horizontal)	2, 5, 8, 11, 14
Z	Perpendicular to the longitudinal bridge axis (vertical)	1, 4, 7, 10, 13

Table 4.3: Sensor directions with corresponding channels

4.4.3. CASES

For the determination of the natural frequencies, two main preprocessing methods are considered:

1. **Original**
   The unprocessed time signals are used for the computation, no preprocessing is applied.

2. **Autocorrelated**
   First, the time domain signals are preprocessed according to the characteristics in Table 4.4, and subsequently an ACF is applied.

Two separate cases are considered. The goal is to gain a better understanding on the influential parameters and to be able to quantify the benefits of the preprocessing techniques. The ACF will attenuate uncorrelated noise and preserve the periodic trends in the measured signals, preparing the input signals for the Fourier transform.

Case	f_s	q	f_{cutoff}	n_{seg}	n_{fft}
	$[Hz]$	$[-]$	$[Hz]$	$[-]$	$[-]$
Original	1000	1	[-, -]	1	20,000
Autocorrelated	50	20	[0, 10]	1	20,000

Table 4.4: Case specifications for MPC values

When in the process of determining the *mode shapes*, the ACF is not applied for case 2 does due to the amplitude- and phase distorting properties. The computed modes will not be representative due to the distorted phase delays. The remaining preprocessing techniques will be applied to the data. The values of the preprocessing parameters are displayed in Table 4.4. In this table; f_s and q represent the sampling frequency and downsampling factor respectively. f_{cutoff} gives the boundaries of the cutoff frequency where an attenuation of $-3dB$ is achieved. n_{seg} and n_{fft} represent number of segments from a single recording and number of output points (for zero-padding), respectively.

4.4.4. DETERMINATION NATURAL FREQUENCIES AND MODE SHAPES

For the determination of natural frequencies and mode shapes, identical preprocessing techniques cannot be applied due to the phase distorting properties of the ACF. A distinction is made in the identification for the natural frequencies (part 1) and the mode shapes (part 2). For part 2, the FDD will be performed slightly different for the autocorrelated case. Namely, with application of the preprocessing techniques, except for application of the ACF.

After the dominant frequencies in the singular values plots are identified, a selection on relevant mode shapes, with corresponding case specifications, can be made. Defining the selection of mode shapes to investigate prior to the identification of dominant frequencies is not practical due to the large amount of possibilities (combination of train directions, acceleration directions, discrete frequencies and order singular vector).

The determination process is split in two parts, where the results from the first part affect the results of the second part. Additionally, the cases which produce the most clear results can be used, whereas the cases where the results are of no use, can be left out of the inspection.

No.	Train direction	Acceleration direction	Autocorrelated
1.1.1	Leeuwarden	Z	No
1.1.2	Groningen	Z	No
1.1.3	Both	Z	No
1.2.1	Leeuwarden	Y	No
1.2.2	Groningen	Y	No
1.2.3	Both	Y	No
1.3.1	Leeuwarden	Y Z	No
1.3.2	Groningen	Y Z	No
1.3.3	Both	Y Z	No
2.1.1	Leeuwarden	Z	Yes
2.1.2	Groningen	Z	Yes
2.1.3	Both	Z	Yes
2.2.1	Leeuwarden	Y	Yes
2.2.2	Groningen	Y	Yes
2.2.3	Both	Y	Yes
2.3.1	Leeuwarden	Y Z	Yes
2.3.2	Groningen	Y Z	Yes
2.3.3	Both	Y Z	Yes

Table 4.5: Overview input signals included for determination of natural frequencies through FDD

5

VALIDATION DIGITAL MODEL

To be able to verify the reliability of the results, a validation case is considered. First the natural frequencies and mode shapes of the validation case are determined through analytical derivation. Subsequently, the dynamic properties of the system are computed through FDD, taking the registered output response of the system to a forced vibration.

5.1. ENGINEERING MODEL

For this case, an undamped 3 DOF beam model is designed (Figure 5.1). The span is divided into four parts of equal length. Both ends are supported through hinged supports. At a quarter, halfway and three quarters of the span, masses are located which can displace in a single direction (3-DOF system). In this model, the gravity force is not taken into account.

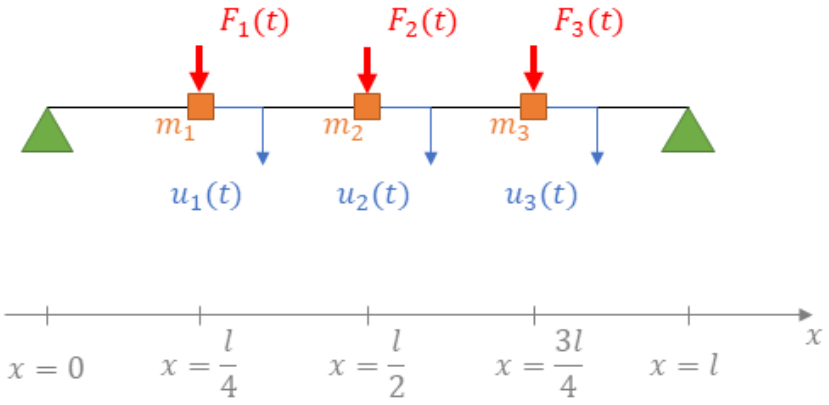

Figure 5.1: Overview 3DOF model

The undamped beam element is modelled as a collection of masses, which are connected through a series of springs (Figure 5.2).

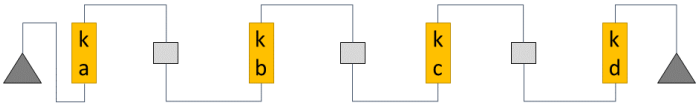

Figure 5.2: Representation of the system spring configuration

SYSTEM MATRICES

The mass, damping and stiffness matrices for the validation case are derived after determination of the equations of motion:

$$M = \begin{bmatrix} m_1 + \frac{m_2}{2} & 0 & 0 \\ 0 & m_2 & 0 \\ 0 & 0 & \frac{m_2}{2} + m_3 \end{bmatrix} \quad C = \begin{bmatrix} 0 \end{bmatrix} \quad K = \begin{bmatrix} k_a + k_b & -k_b & 0 \\ -k_b & k_b + k_c & -k_c \\ 0 & -k_c & k_c + k_d \end{bmatrix}$$

System parameter values To numerically determine the natural frequencies and mode shapes of the validation case, the following parameter values are taken into account:

$$m_1 = m_2 = m_3 = 1kg \tag{5.1}$$

$$k_a = k_b = k_c = k_d = 1000N/mm \tag{5.2}$$

5.2. ANALYTICAL SOLUTION

To determine the dynamic properties of the system, the solution to the free vibration case is required (Equation 2.1). By solving for the eigenvalues and eigenvectors of the system, the natural frequencies and corresponding mode shapes can be determined. The values for the determined natural frequencies are:

$$f_1 = 3.43Hz \tag{5.3}$$
$$f_2 = 5.81Hz \tag{5.4}$$
$$f_3 = 8.52Hz \tag{5.5}$$

The analytically determined mode shapes are presented in Figure 5.3.

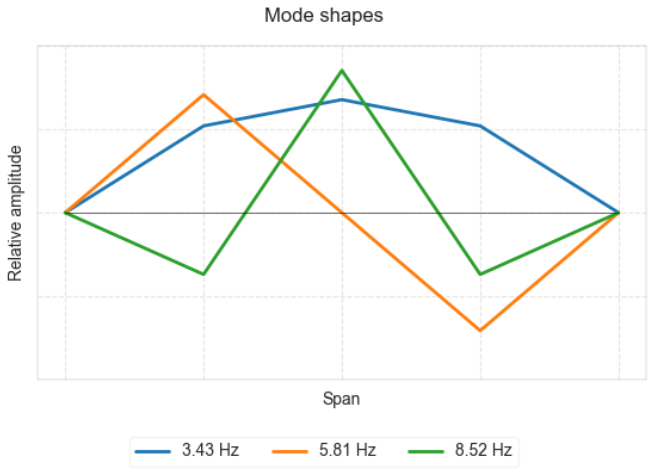

Figure 5.3: Mode shapes determined through the analytical derivation

5.3. FDD SOLUTION

To be able to determine the dynamic properties of the system, the structure is subjected to a Gaussian white noise load at each DOF:

$$F_1(t) \sim N(0,1) \tag{5.6}$$
$$F_2(t) \sim N(0,1) \tag{5.7}$$
$$F_3(t) \sim N(0,1) \tag{5.8}$$

POWER SPECTRUM

A simulation is performed on the validation case with the random loads, applied to each DOF. The output response of the system during the simulation is registered and subsequently used as input signals for the FDD. In Figures 5.4 and 5.5 the results from the FDD case are presented. The peaks in the singular values plots for both cases show sufficient local increase to be able to manually identify the natural frequencies of the system.

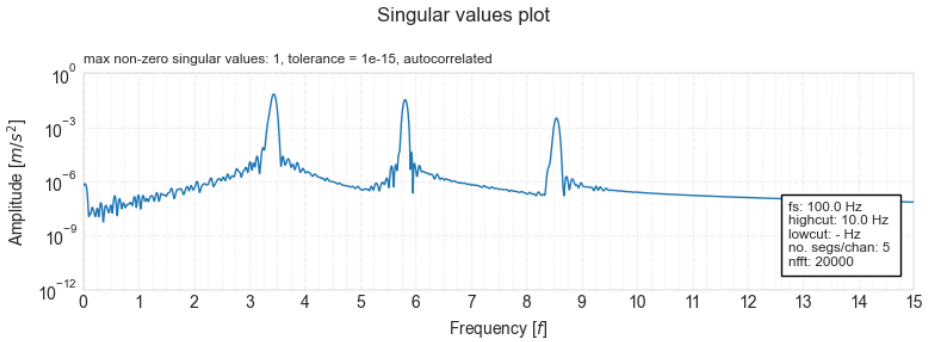

Figure 5.5: Power spectrum for displacements validation case (autocorrelated)

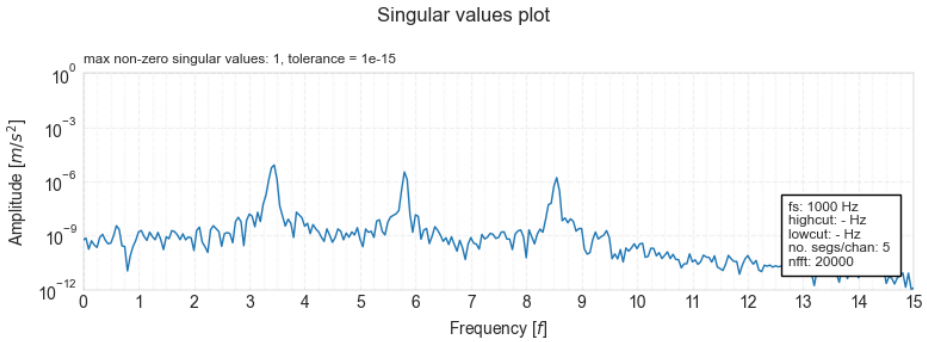

Figure 5.4: Power spectrum for displacements validation case (original)

MODE SHAPES

The mode shapes are evaluated at the locations of the identified natural frequencies. Figure 5.6a displays the first classical in-phase bending mode, whereas Figure 5.6b shows the second classical anti-symmetric bending mode. Figure 5.7a displays the anti-phase third bending mode. All computed modes are real, due to the MPC value being approximately 1.

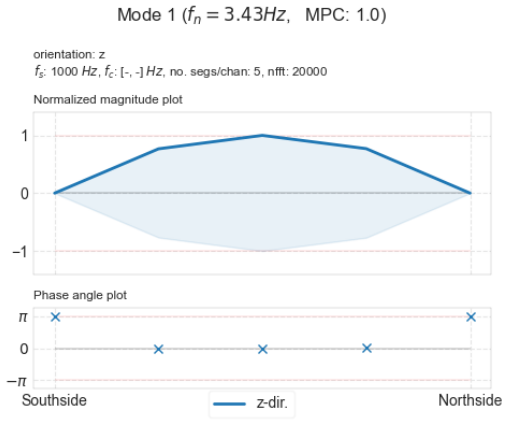

(a) Mode plot for validation case, natural frequency f_1

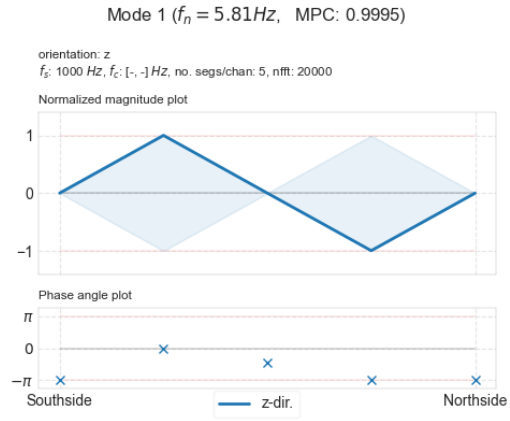

(b) Mode plot for validation case, natural frequency f_2

Figure 5.6: Mode plots for the validation case (1/2)

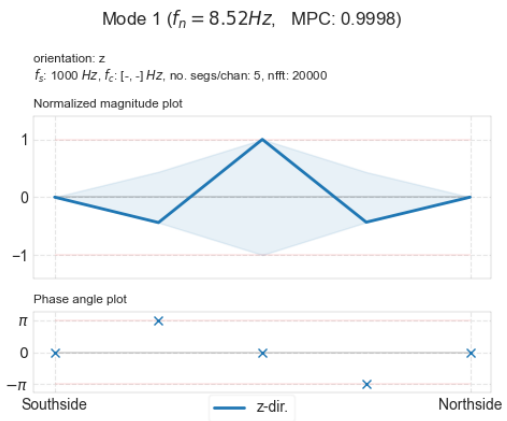

(a) Mode plot for validation case, natural frequency f_3

Figure 5.7: Mode plots for the validation case (2/2)

5.4. COMPARISON

The natural frequencies and mode shapes, computed through FDD are compared to the natural frequencies and mode shapes, obtained from the analytical solution. The results from the FDD correspond to the determined modes from the analytical solution. Therefore, correct implementation of the FDD is confirmed.

6

Results

IN this chapter, the results of the FDD method are presented. The goal of the research is to be able to determine modal parameters with significant accuracy and stability. The results are presented in a collection of figures, tables and additional descriptions throughout this chapter and Chapter 7. In the latter, an interpretation on the presented results is discussed.

First the natural frequencies of the structure are considered through a series of singular values plots. The characteristics of these plots show close similarities with estimated power spectral density (PSD) plots. Secondly the results regarding mode shapes are considered, which are obtained from the left singular vectors matrix. As the right singular vectors matrix is merely the hermitian transpose in the case of FDD, identical modal behaviour is stored both the singular vectors matrices. Finally, the computed singular vectors are investigated to determine the mode complexity (MPC value). The MPC values are presented by means of two tables, which can be used to determine the complexity of the deflection shapes.

6.1. POWER SPECTRA

The FDD is able to identify recurring patterns in the measured data. However, when the amount of input signals (included in the computation) increases, the result will not necessarily present convergence in the results. Dependent on the level of correspondence between the input signals, the computed results can either become clearer, or the desired results can be attenuated. To be able to identify corresponding behaviour, the train direction over the bridge, as well as the accelerations in 3 euclidean orthogonal directions (X, Y and Z) at the locations of each sensor are registered. The results are depicted accordingly.

6.1.1. SINGULAR VALUES PLOTS

To represent the estimated power spectrum, use is made of singular values plots. As mentioned in Section 4.2, the various lines in the singular values plots show the contributions of the dominant ODSs in the total response of the structure. On the horizontal axis, the frequency domain is presented. The vertical axis depicts the magnitude of the singular values. This is a real value, and can be regarded as a proportional scaling factor for the corresponding singular vector. The total response of the structure, at a specific frequency, is obtained when taking the superposition of each contributing singular vector, scaled by its corresponding singular value. Remember that the *total* response of the structure is indirectly equivalent (proportional) to the superposition of each individual transformed measurement signal (before decomposition).

The main goal of this project is to determine *relevant* modal parameters. These are oriented in the lower end of the frequency spectrum. Therefore, the lower end of the frequency spectrum will be investigated.

The results for the identification of the natural frequencies for the original- and autocorrelated cases are presented using the singular values plots. For each set of cases, the results are presented whilst varying in sensor orientation and train direction. The set of included input signals for each case are varied to gain a valid understanding of the characteristics of the data. The results are presented in sets of 3, as described in Table 4.5.

In each singular values plot (SVP), the included channels (orientation), records, preprocess details, max singular values (together with tolerance threshold) are presented. The records describe the train passing, which can be used to retrace the corresponding train velocity (Figure 3.5), and/or other characteristics of the regarded train passing. A visual representation of the explanation is presented in Figure 6.1. The FDD is computed for 2 distinct cases which are:

Original No computations to the input time signals are applied.

Autocorrelated The autocorrelated case makes use of preprocessing techniques. The preprocessing parameters are defined in Table 4.4 (autocorrelated case). After preprocessing, the time signal is autocorrelated for *positive time lags only*. By applying the ACF, the most dominant and periodic behaviour is amplified, whilst uncorrelated noise is reduced. The absolute amplitude after application of the ACF is not relevant and/or should not be directly compared to the results of the original case, due to the magnitude distorting properties. However, the relative amplitudes show local increase in power when comparing it to neighbouring frequencies of that same case.

ORDER SINGULAR VALUES PLOT

The singular identities (singular values with corresponding singular vectors) are sorted from highest to lowest magnitude of the singular value, due to the properties of the SVD. Throughout the following chapters, the

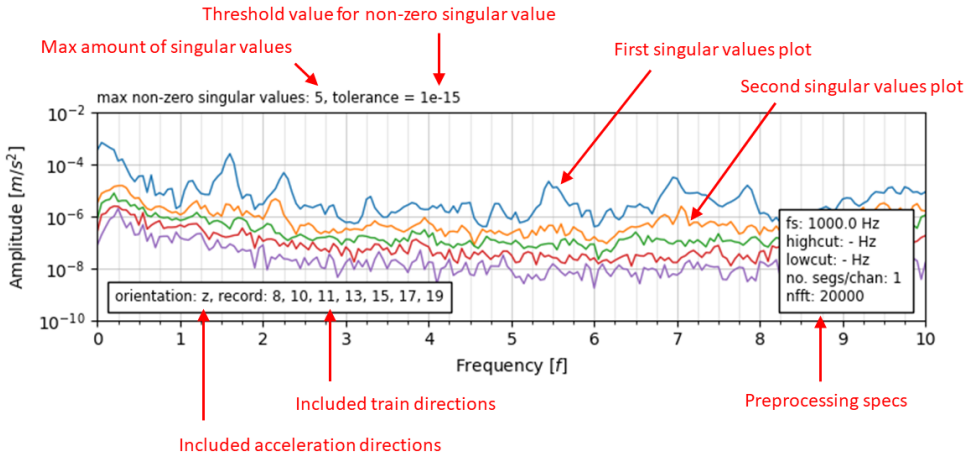

Figure 6.1: Explanation of singular values plot

order of the singular identities is mentioned. The order defines the *position* it holds within the sequence of singular identities. That is, the first order singular identity corresponds to the singular value with the highest absolute magnitude. The second order singular identity corresponds to the singular value with the second largest absolute magnitude. This sequence repeats all the way down to the last singular value.

The order of the singular identities is not to be confused with the matrix order (rank), which is also determined during the SVD. The order of the matrix describes the total amount of singular identities, whereas the order of the singular identity describes the location in the sequence of singular identities.

The SVPs are presented, where each order is displayed in its own colour. In chapter 7, a reflection is given regarding the SVPs up to the fourth order. Table 6.1 presents the order and the colour of the corresponding SVP.

Order	Name	Colour
1	First singular values plot	Blue
2	Second singular values plot	Yellow
3	Third singular values plot	Green
4	Fourth singular values plot	Red

Table 6.1: Description singular values plots

6.2. MODE SHAPES

The mode shapes, which are computed through the FDD, are presented in this section of the report. As the definition clearly states, only the mode shapes should be considered, whereas non-mode shapes (such as forced vibrations) should be omitted. This task introduces supplementary assessments, therefore, a distinction in deflection shapes can not be presented yet. The computed plots will be presented as mode plots, after which an elaboration on the distinction of deflection types will be presented in Section 7.2.

The challenge to distinguish mode shapes from operational deflection shapes arises when the data does not fully comply with the prerequisite assumptions of OMA. Keep in mind that this might be the case for some of the presented mode shapes.

The computation of the results for the mode shapes take two cases into account (original and preprocessed), as described in Table 4.4 (Chapter 4). The results for the autocorrelated case are not considered during elaboration of the mode shapes, due to the properties of the ACF which affect the phase delay, thereby making the results unrepresentative.

6.2.1. MODE PLOTS

For the computation of the mode plots, only the recordings for the train direction towards Groningen is included. This choice is made due to the fact that the results from the power spectra estimations are most clear for this case. When considering the computed SVPs, the majority of the cases showed a significant increase in the first SVP, and little to none increase for the remaining orders of the SVPs. The relevance of these remaining SVPs is not significant and is therefore not included in the report. The total collection of significant modes are presented in Appendix A, using two columns to describe the original case (left) and the preprocessed case (right). Remarkable results are discussed in Section 7.2. An explanation for the mode plots is presented in Figure 6.2.

The computed mode shapes are presented in the mode plots, consisting of two subplots that visually represent the dynamic behaviour of the singular vector. The mode plots are computed through the FDD and represent a certain mode at a specific frequency, which indicates a proportional contribution to the total response of the structure. The title of the mode plot includes mode number (order of the singular vector), regarded frequency and MPC value. Additional information which describes included acceleration directions, recordings and preprocessing parameters are also included in the figure. The graphs show a normalized mode shape plot and a phase angle plot. For both plots, a shared horizontal axis depicts the longitudinal axis of the bridge deck. As mentioned in Chapter 3, the accelerometers are equally spaced over the span of the bridge.

The mode plot depicts the normalized amplitudes and relative phase delays of the accelerations. The former includes the obtained ODS (solid line) and the DOF extremes (envelope). Equation 6.1 represents the response of each DOF. In this equation, A_i and φ_i represent the maximum amplitude and phase angle for DOF i. If the DOFs with non-zero magnitude posses relative phase angles in the phase angle plot the are not approximately spaced by π (or an integer multiple of it), the mode shape will show signs of complexity. Complex modes do not possess a single point in time, where all DOFs are simultaneously in their extreme positions. The depicted mode shape represents a realistic ODS for a specific point in time. The considered point in time corresponds to the DOF with greatest absolute magnitude, in its extreme position. The envelope is based on the maximum amplitude for each DOF, and mirrored over of the horizontal axis.

$$a_i = A_i \cos(2\pi f_n t + \varphi_i) \tag{6.1}$$

As a 3 dimensional plot does not provide a clear and comprehensive understanding of the mode shapes in this report, a 2 dimensional representation is used for the mode plots. For every acceleration direction, a graph is included in the plot areas to account for a 3 dimensional representation. The normalized mode shape plot takes the total mode shape into account, therefore normalizes over the maximum value of the total singular vector. Possible relative differences in horizontal versus vertical modal amplitudes can be observed. The phase plots are also considered to be relative to each other, when considering more than one acceleration direction. The MPC value is also computed over the total mode shape.

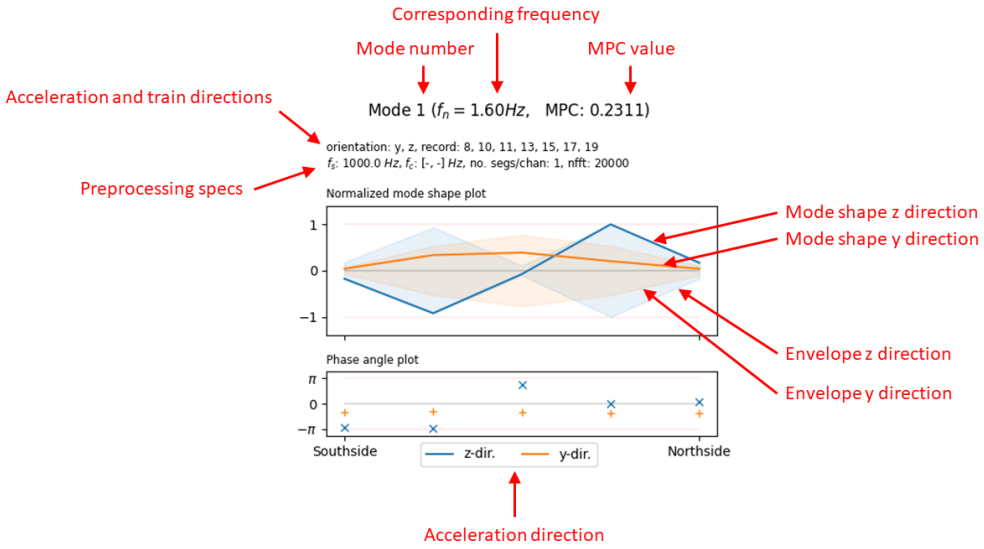

Figure 6.2: Explanation of mode plots

The computed mode shapes represent the accelerations at the locations of the sensors, not the displacements. In theory, a scaled double integration of a sinusoidal function transforms the recorded accelerations to displacements. However, in practice, this simple computation presents a variety of inaccuracies, due to the non-stationary tendencies and presence of noise. Also the initial conditions are not included in the available data, and can therefore not be used to accurately determine the displacements of the bridge deck.

COMPLEXITY OF MODE SHAPE

The tables regarding the MPC values are presented in Section 7.2, where Table 7.6 presents the MPC values for the original case, and Table 7.7 for the preprocessed case. The tabulated values correspond to the MPC values, which are mentioned in the title of the mode plots (Appendix A). The tabulated values describe the mode complexity for the considered singular vector. In the tables, MPC_i represents the modal phase colinearity for the i^{th} order singular vector. For the MPC close to 1, the identified mode is considered real, where for low MPC values, the mode is considered to be complex.

VISUALIZING (COMPLEX) MODES

In some cases a 2 dimensional static representation, such as presented in Appendix A, is not sufficient to clearly and accurately describe the computed mode shape. Therefore, a tool is developed to visually present the dynamic behaviour of the structure. Besides a 3 dimensional representation of the mode shape, the singular vectors are also represented in an animation to display the behaviour of the computed mode. This gives greater visual assistance to comprehend the presence of complex modes in a structure. A screen snap of this tool is presented in Figure 6.3. The SVPs and mode plots, as presented in this chapter, are realised using this mode visualization tool.

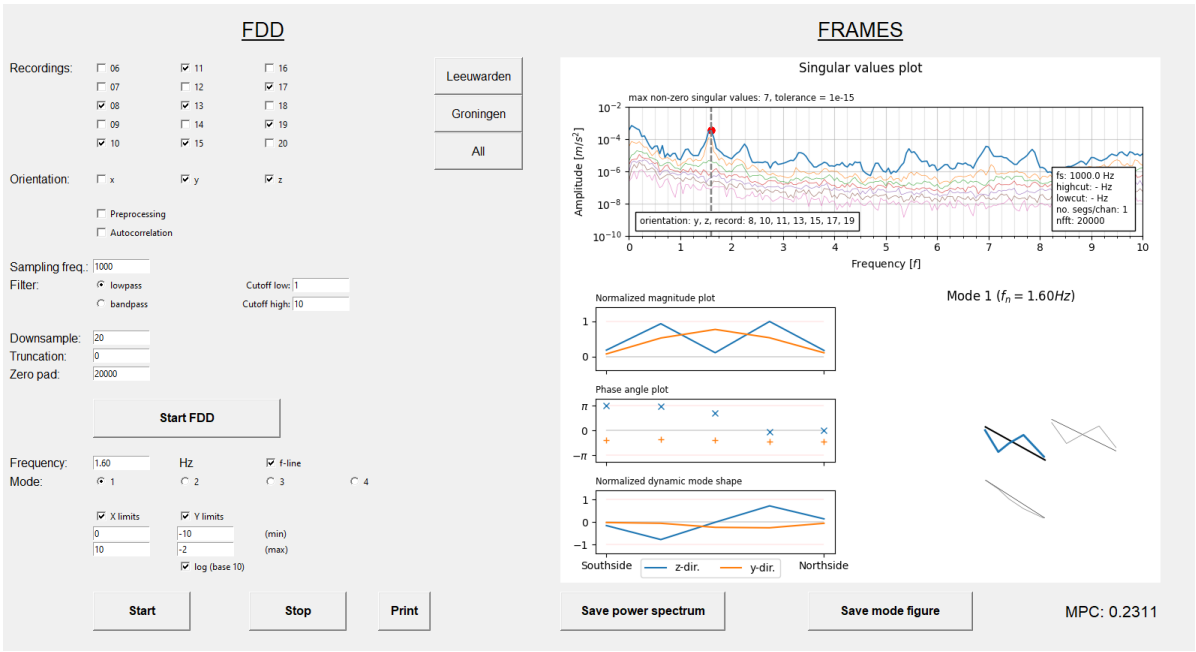

Figure 6.3: Mode visualization tool

6.3. RECORDS INCLUDED AND PREPROCESSING TECHNIQUES

For the determination of dominant frequencies, the singular values plots are computed for the entire data set, as described in Section 4.4. Due to the properties of the ACF, the results for the mode plots for this case do not present representative results. Therefore, after determination of the dominant frequencies through the SVPs, the results for the autocorrelated case will be computed again, only this time without application of the ACF, which will be referred to as the *preprocessed* case.

As will be mentioned in the chapter 7, the measurements show great correspondence in the overall dynamic behaviour of the bridge, between the various cases for train directions, but with better distinction in

the results for the train directions towards Groningen. Therefore, only the recordings for the train directions towards Groningen will be presented in the mode plots. This subcase presented the most clear results.

Figure 6.4 presents an overview of the records which are included, as well as the preprocessing techniques for the determination process of the natural frequencies and mode shapes.

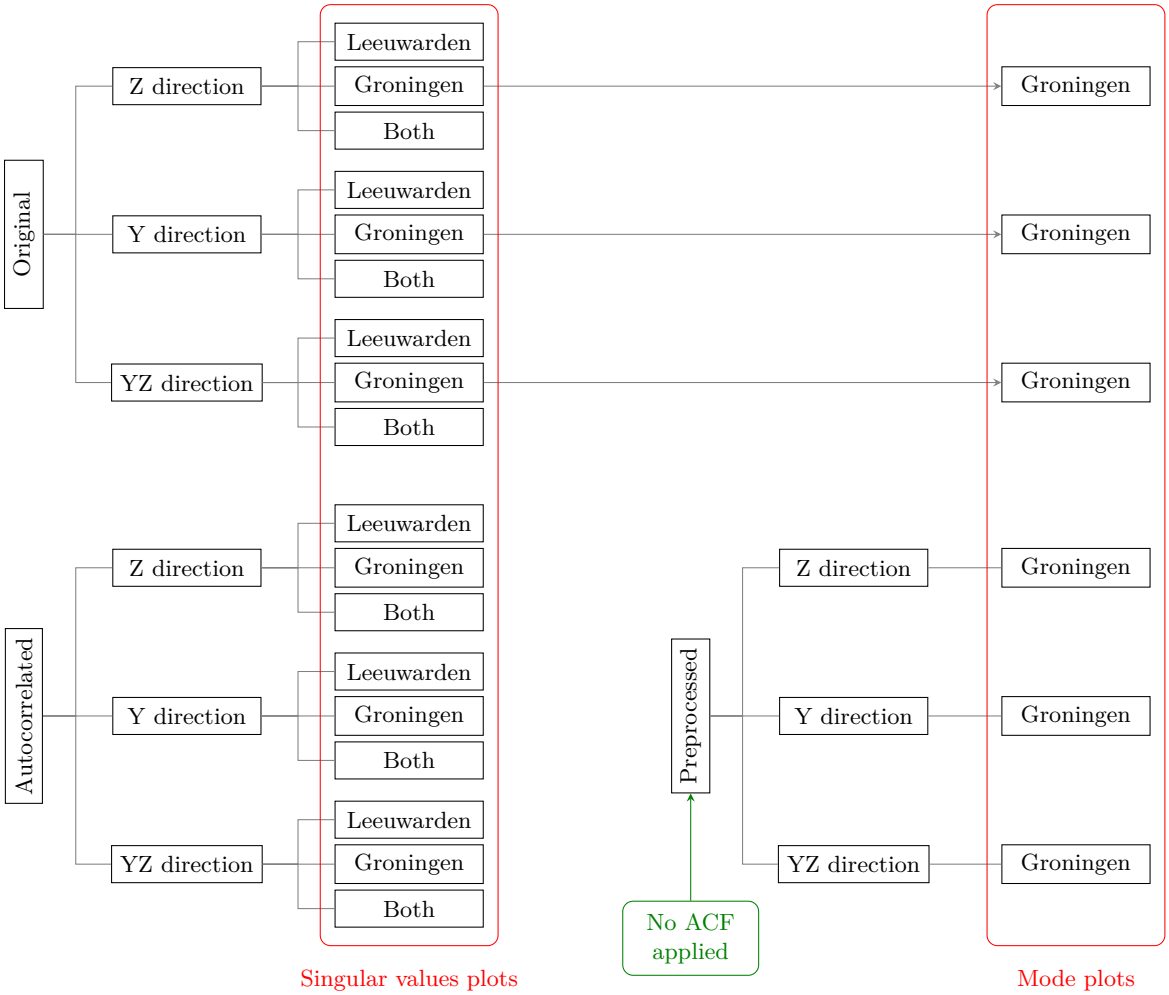

Figure 6.4: Overview results

7

Discussion

In this chapter the results from the FDD are discussed and reflected on. The aim is to present a clear interpretation of the results, based on substantiated arguments. First the power spectrum estimates for identified orthonormal modes will be discussed, after which the mode shapes with corresponding natural frequencies are determined, through the results from the mode plots. Finally, the interpretation of the MPC values to consider complexity of the modes are discussed.

7.1. POWER SPECTRUM ESTIMATES

After observation of Figures 7.1 to 7.18, the 4 dominant frequencies are identified in the lower end of the frequency spectrum. The identified dominant frequencies are ranked from f_1 to f_4, sorted on frequency (from lowest to highest). The power spectra do show similarities for frequencies higher than f_4, however, the scope excludes the necessity to investigate these higher frequencies. Table 7.1 presents the dominant frequencies with the corresponding value.

The collective subcases (acceleration direction Y, Z and YZ) are each presented in sets of three figures. Each individual figure in the subcase represents the SVPs for different train directions (Leeuwarden, Groningen and both). The SVPs of these three discrete train directions will be investigated to identify potential correspondence and deviations in the overall response w.r.t. the different train directions. As the realistic loading scheme is different for the moment where the train is present on the bridge versus when it has left the bridge. So is the train direction towards Leeuwarden a different loading scheme from the train direction towards Groningen. By investigating the response of the bridge for different train directions, the total response of the bridge can be determined more accurately. If the different train directions show significant correspondence in the response, but a single train direction presents more clear results. Then this specific train direction can be considered representative for the total data-set, but with increased accuracy. Later on, the identification process in the response of the bridge for different train directions will lead to a narrow selection of the total collection of cases to accurately determine the mode shapes.

In the ideal case, the bridge displays identical results for each train direction. However, this expectation is not entirely realistic, as shown in Chapter 6. Sections 7.1.1 and 7.1.2 reflect on the different cases, as a preparation to Section 7.2, where the corresponding mode shapes to the dominant frequencies are discussed.

First the results per subcase will be considered, after which a brief reflection is given on the subcases with respect to each other. This is presented for the original case and the autocorrelated case. Finally the results from the original and autocorrelated case will be compared to each other. Remarkable results and described.

	f_1	f_2	f_3	f_4	
Frequency	1.60	2.25	3.30	5.45	$[Hz]$

Table 7.1: Dominant frequencies

LOCAL INCREASE

Through visual inspection, any significant local increase in the SVPs (for each subcase) is registered and presented in a table. The local increase of the SVP indicates an increase in energy at that specific frequency. The local increase is identified by use of the SVD, and implies an amplified ODS. The response of the structure to the load is amplified due to the presence of an alleged natural frequency (fundamental assumptions of OMA, Section 2.3), in the case of white-noise loading.

The interpretation of the results for the estimation of the power spectra and its dominant frequencies, for the original and autocorrelated cases, are presented in Tables 7.2 and 7.3, respectively. For both cases the first 4 SVPs are considered. The first column of these tables correspond to the scenarios from Table 4.5. The second column refers to the order of the SVP. In columns 3 to 6, the identified dominant frequencies are presented. Each value in the table indicates a local increase at the specified location of the decomposed power spectrum. 'Y' indicates an identified local increase, whereas an 'N' represents no observation of any significant local increase. Table 7.2 also includes '-', which indicates a possible faulty result, on which further elaboration is presented in Section 7.1.1.

7.1.1. ORIGINAL CASE

Z ACCELERATIONS

The results for the considered subset are presented in Figures 7.1, 7.2 and 7.3, respectively.

- **Case 1.1.1** displays no significant behaviour in the first SVP. The second SVP shows an increase at f_1, f_2 and f_4. The remaining SVPs also show no local increase in the response of the structure. The most dominant structural response of the bridge does not correspond to any spectral features. The distinguishable increase in the second SVP implies a modal response of a magnitude, not as dominant, but still present when compared to the random behaviour of the first SVP.

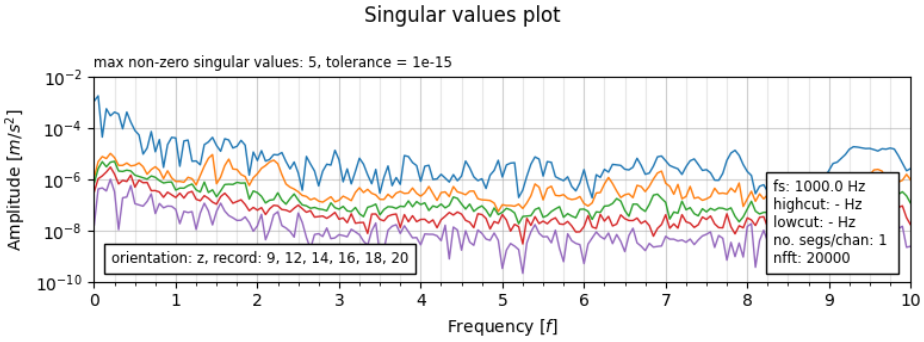

Figure 7.1: Case 1.1.1 - Power spectrum for z accelerations with trains towards Leeuwarden

- **Case 1.1.2** shows distinctive peaks at f_1 and f_2, and even local increase at dominant frequencies f_3 and f_4 for the first SVP. The second SVP shows a single peak at f_2, which implies the presence of a second mode, although it is not as dominantly present as the first SVP. The rest of the plots do not show any local amplification.

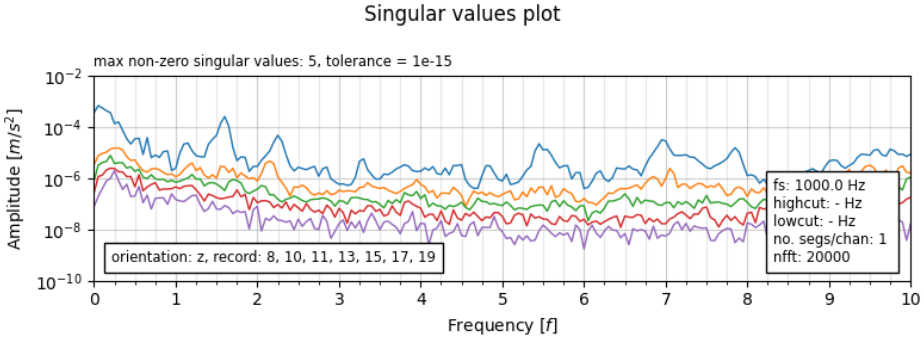

Figure 7.2: Case 1.1.2 - Power spectrum for z accelerations with trains towards Groningen

- **Case 1.1.3** represents the combined case where both train directions are included in the computation. In these plots, both the first and second SVPs show an increase at the locations f_1, f_2 and f_4. The third and fourth SVPs do not show any local increase.

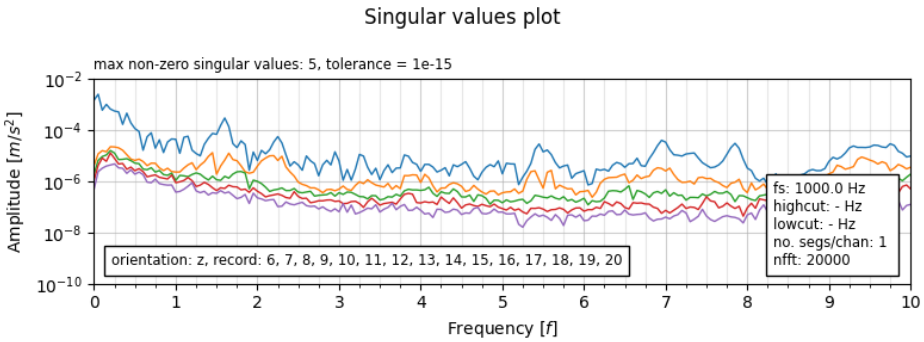

Figure 7.3: Case 1.1.3 - Power spectrum for z accelerations with trains in both directions

The results from Cases 1.1.1 to 1.1.3 present corresponding amplification for accelerations in Z direction around frequencies f_1 and f_2, although, the local increases are not convincingly clear. The case which presents the most distinctive results is for the train directions to Groningen (Case 1.1.2), the case where the train velocity is relatively higher, which could excite the structure more than in the case of the train direction to Leeuwarden, or both train directions due to the apparent averaging properties.

Y ACCELERATIONS

The results for the considered subset are presented in Figures 7.4, 7.5 and 7.6, respectively.

- **Case 1.2.1** shows an indistinguishable first SVP. An explanation for this behaviour could be a noise mode, which implies non-representative data is included in the computation. Table 7.2 does not consider local amplifications for this order of the singular identity (hence '-' for corresponding row). It is observable that the first SVP shows a noticeable decrease in the signal nearby frequency f_1. It seems that the singular value at this frequency approaches a value, which is close to the value of the second SVP. The second SVP however, shows expected modal behaviour, in the form of local increases at the dominant frequencies f_1, f_3 and f_4. The remaining SVPs do not show any local increase.

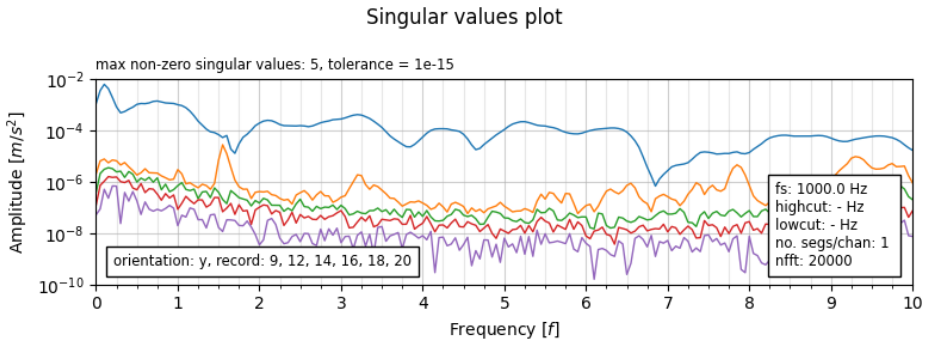

Figure 7.4: Case 1.2.1 - Power spectrum for y accelerations with trains towards Leeuwarden

- **Case 1.2.2** displays local increases for the first SVPs at f_1, f_3 and f_4. The second SVP also shows a significant local increase at f_1. Even in the lower SVP 3, the decomposed spectrum shows an local increase around frequency f_2. SVP 4 does not present any significant local increase close to dominant frequencies f_1 to f_4.

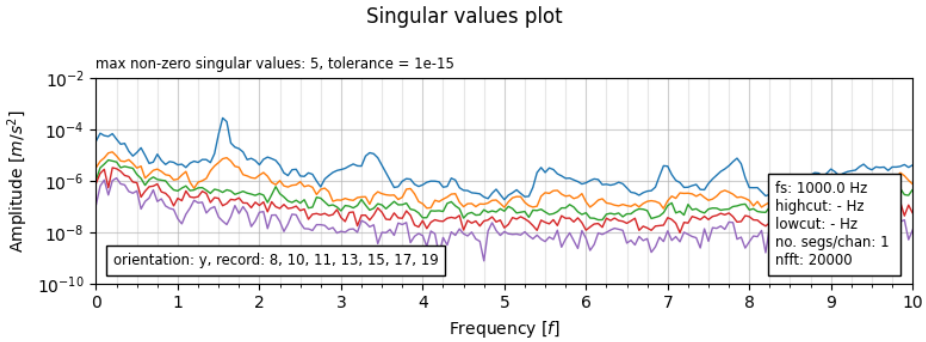

Figure 7.5: Case 1.2.2 - Power spectrum for y accelerations with trains towards Groningen

- **Case 1.2.3** combines the Y accelerations for both train directions. The noisy mode from Case 1.2.1 is easily identifiable. Although there is a local peak present in the first SVP at f_1, the reliability of the signal does not seem to be sufficient to take the results from the computation for the first SVP into account (even though the plot seems to comply around frequency f_1). Again the second SVP displays the increase around f_1 and f_3. Plots 3 and 4 do not show significant local increase around any of the dominant frequencies.

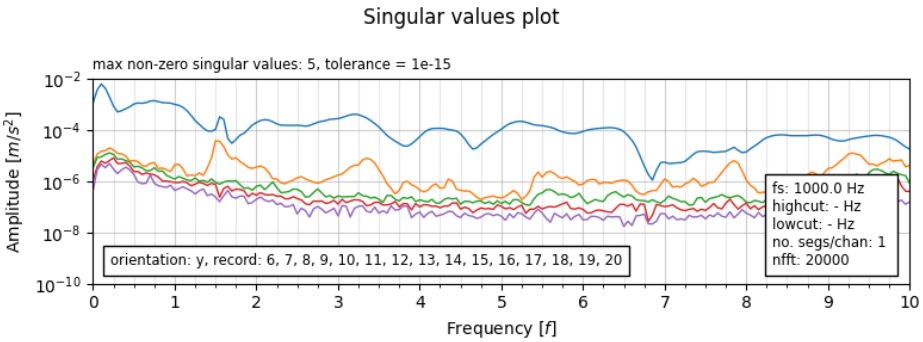

Figure 7.6: Case 1.2.3 - Power spectrum for y accelerations with trains in both directions

Figures 7.4 to 7.6 show an amplification at dominant frequencies f_1 and f_3. These figures represent the accelerations in Y direction.

The presence of an accurate modal peak within the noisy signal (Case 1.2.1) could be explained by a dominant mode presenting itself near this frequency. If this is the case, the signal-to-noise ratio can change significantly and shape the SVP near this frequency. However, this can only be speculation, and the computed data is acquired during field tests (operational data), which in itself can experience all kinds of faulty measurements. Independent of the explanation, this behaviour shall not be included in the manual analysis for the mode shape determination, as it shows no compliant behaviour to what is expected over the remaining part of the decomposed power spectrum estimate. The noisy signal can also be identified in the combined case (Case 1.2.3), as it includes all recordings for both train directions. The corresponding signal is included in the computation, as it is consecutively summed (due to the superposition principle of the FDD) in the total frequency response.

The first SVP for the train directions to Leeuwarden (Figure 7.4) shows a general non-distinctive white-noise-like behaviour. This behaviour is also identifiable in Figures 7.6, 7.7 and 7.9. This behaviour does not correspond with the behaviour as identified in the spectra regarding the results from computations for the train directions for Groningen only. Therefore, it can be assumed the behaviour is mainly induced by train traffic towards Leeuwarden. This behaviour should be attenuated, however, this is not the case due to the limitations of the FDD method, as it makes use of an unsophisticated method where the individually computed frequency spectra are summed without scaling or normalization before decomposition.

YZ ACCELERATIONS

The results for the considered subset are presented in Figures 7.7, 7.8 and 7.9, respectively.

- **Case 1.3.1** displays identical noisy behaviour for the first SVP, due to the inclusion of the same alleged faulty measurement signal (Case 1.2.1). The second SVP shows strong similarities with the indistinctive first SVP from Case 1.1.1. The third SVP shows the modal properties as expected from the structure with spectral content present at dominant frequencies f_1, f_2, f_3 and f_4. For this order singular values, all dominant frequencies are present, as both Y and Z accelerations of Cases 1.1.1 and 1.2.1 are included in the computation. The result is the superposition of both cases. The singular vectors include the mode shapes (as eigenvectors), which will now include data from both acceleration directions.

- **Case 1.3.2** shows clear peaks for f_1, f_2, f_3 and f_4 in the first SVP. The second SVP shows local increase of the signal for frequency f_1. The third SVP again shows a peak at dominant frequency f_2. However, this mode will be scaled by a negligible value (singular values), where no other dominant frequencies present, therefore it can be considered non-existent. The fourth SVP shows shows no significant local increase to consider distinct frequency content at any dominant frequency.

- **Case 1.3.3** shows the combined behaviour between Case 1.3.1 and 1.3.2. The first SVP will not be considered, due to the noisy signal. The second SVP shows a combination between the indistinctive first SVP from Case 1.1.1 and the clear first SVP from Case 1.1.2. The third SVP begins to show frequency content, from the third SVP of Case 1.3.1 and the third SVP of Case 1.3.2. The third SVP is not a great result due to the attenuation of the most significant portion of the trains towards Groningen. The information is already lost in the first two SVPs of the train directions towards Leeuwarden.

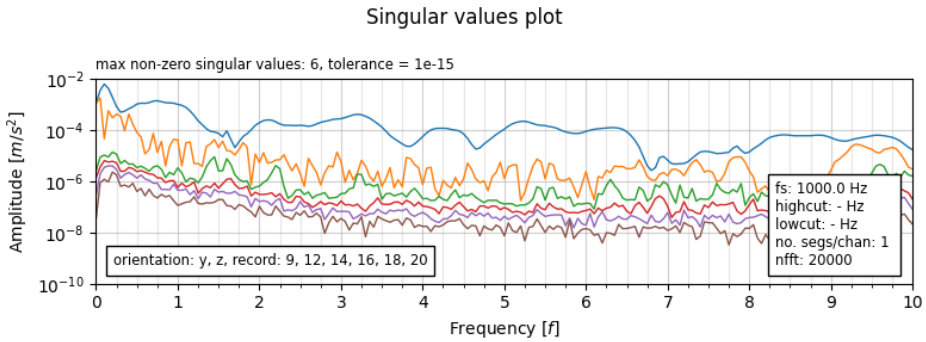

Figure 7.7: Case 1.3.1 - Power spectrum for yz accelerations with trains towards Leeuwarden

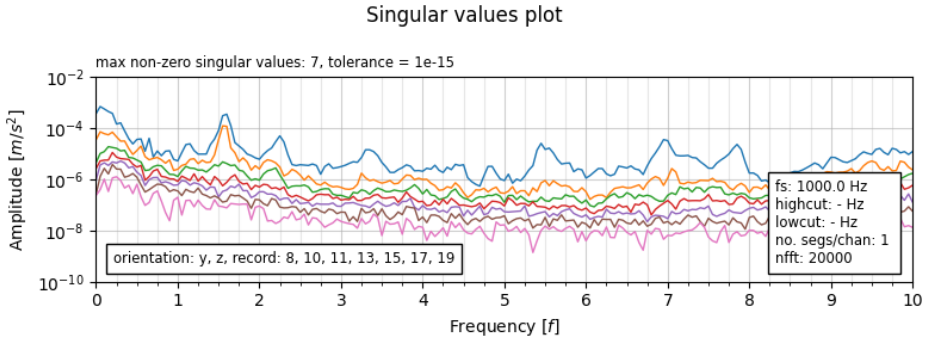

Figure 7.8: Case 1.3.2 - Power spectrum for yz accelerations with trains towards Groningen

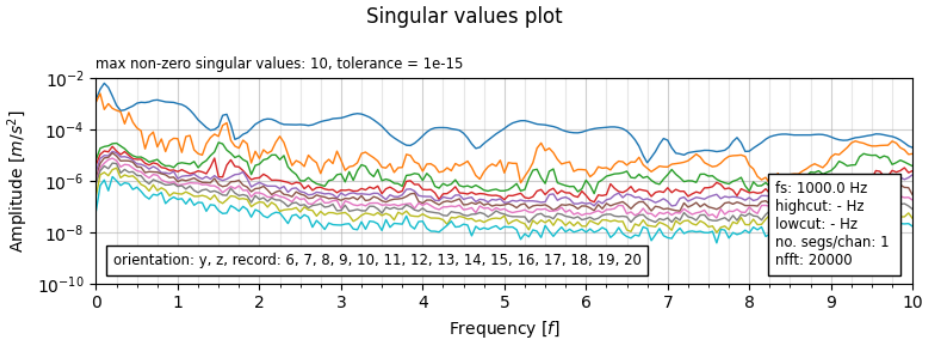

Figure 7.9: Case 1.3.3 - Power spectrum for yz accelerations with trains in both directions

Figures 7.7 to 7.9 show an amplification at 1.60Hz, 2.25Hz and 3.30Hz. This corresponds with the findings of the individual analyses (Case 1.1.1 to 1.1.3 and Case 1.2.1 to 1.2.3), where the two acceleration directions are investigated in discrete cases. However, the YZ power spectra can be considered as a summation of the two individual cases. The goal is to identify a corresponding dominant frequency in both individual cases. The frequency of 1.60Hz is a recurring frequency in both directions. This would imply a mode shape worth consideration.

REMARKS ORIGINAL CASE

- The results do not show large corresponding behaviour. The variation in train direction mainly shows more distinctive peaks for the train directions towards Groningen and less distinctive peaks for the train directions towards Leeuwarden. The cases where both train directions are included in the computations show an averaged result between the more clear peaks for direction Groningen and less clear peaks for direction Leeuwarden.

- Case 1.3.1 and 1.3.3 depict the deficiency of the FDD method. It relies strongly on the magnitudes of the individual frequency spectra. If 1 or 2 signals show great absolute magnitude during the superposition of the composed frequency spectra, the decomposition will predominantly pick up the signals with great absolute value and combine these into the primary SVP(s).

RESULTS SVP - ORIGINAL CASE

No.	Order	f_1	f_2	f_3	f_4
1.1.1	1	N	N	N	N
	2	Y	Y	N	Y
	3	N	N	N	N
	4	N	N	N	N
1.1.2	1	Y	Y	Y	Y
	2	N	Y	N	N
	3	N	N	N	N
	4	N	N	N	N
1.1.3	1	Y	Y	Y	Y
	2	N	Y	N	Y
	3	N	N	N	N
	4	N	N	N	N
1.2.1	1	-	-	-	-
	2	Y	N	Y	Y
	3	N	N	N	N
	4	N	N	N	N
1.2.2	1	Y	N	Y	Y
	2	Y	N	N	N
	3	N	Y	N	N
	4	N	N	N	N
1.2.3	1	-	-	-	-
	2	Y	N	Y	N
	3	N	N	N	N
	4	N	N	N	N
1.3.1	1	-	-	-	-
	2	N	N	N	N
	3	Y	Y	Y	Y
	4	N	N	N	N
1.3.2	1	Y	Y	Y	Y
	2	Y	N	N	N
	3	N	N	N	N
	4	N	N	N	N
1.3.3	1	-	-	-	-
	2	Y	Y	N	Y
	3	Y	Y	Y	Y
	4	N	N	N	N

Table 7.2: Local increase of singular values plots for the original case

7.1.2. AUTOCORRELATED CASE

Additional attention is required when reflecting on the autocorrelated cases, as the singular vectors on which the SVPs are determined, are not fully representative, due to the phase distortion properties and the uncorrelated noise attenuation.

Z ACCELERATIONS

The results for the considered subset are presented in Figures 7.10, 7.11 and 7.12, respectively.

- **Case 2.1.1** shows the frequency spectrum for the Z accelerations with train direction to Leeuwarden, for the autocorrelated case. Here, the first SVP folds around the dominant frequencies f_1, f_2 and f_4. Dominant frequency f_3 does not show any local increase.

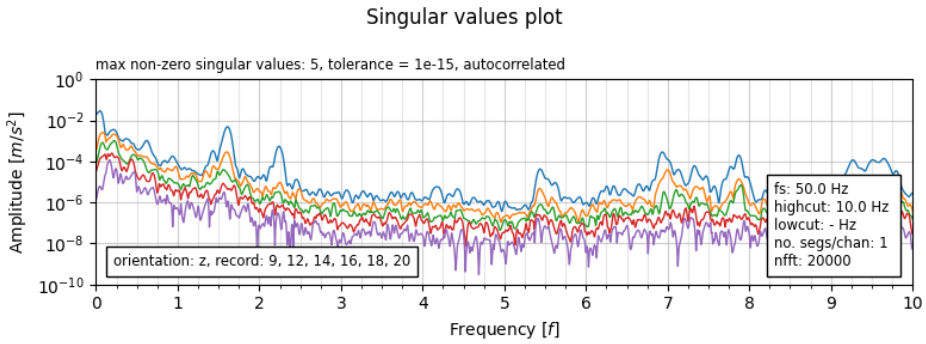

Figure 7.10: Case 2.1.1 - Power spectrum for z accelerations with trains towards Leeuwarden, from an autocorrelated time signal

- **Case 2.1.2** presents significant frequency content around f_1, f_2 and f_4 for the first SVP. The second and third SVPs show local increase around f_1, however, around the dominant frequency f_2, no signs of a local increase are present and only a slight local increase around f_4, so around these frequencies a structural mode can be considered. The slight increase of the second SVP for dominant frequency f_4 can be caused by increased frequency response due to the general amplification, so an alleged mode can not be ruled out.

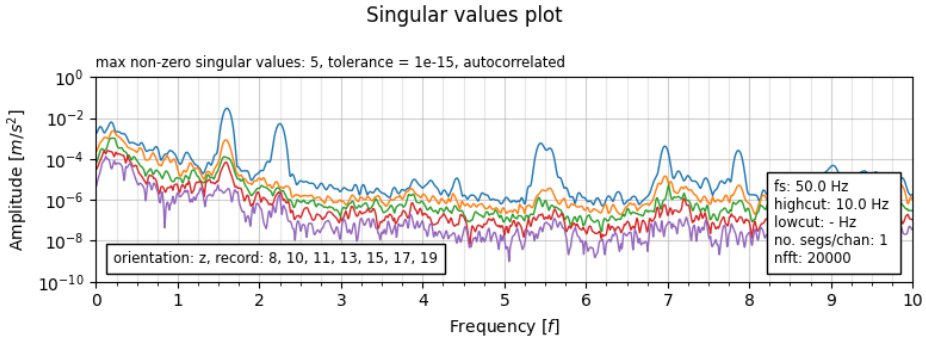

Figure 7.11: Case 2.1.2 - Power spectrum for z accelerations with trains towards Groningen, from an autocorrelated time signal

- **Case 2.1.3** suggests a single mode at frequency f_2, and the contribution of multiple modes at f_1 and f_4.

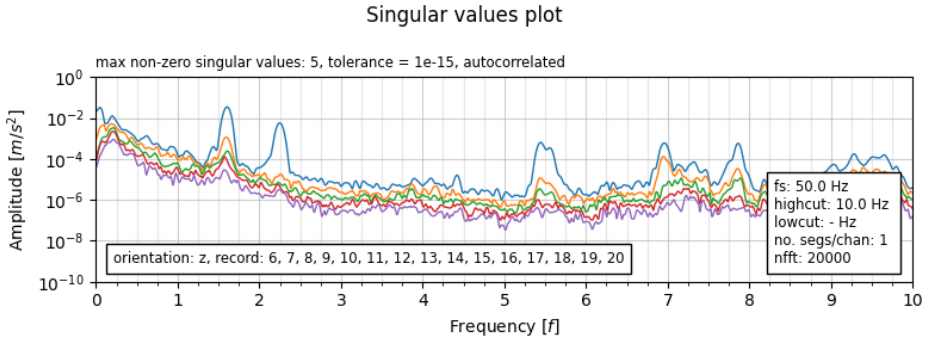

Figure 7.12: Case 2.1.3 - Power spectrum for z accelerations with trains in both directions, from an autocorrelated time signal

The SVPs for the different cases in train directions show great similarities. The three cases all show the presence of multiple modes for frequencies f_1, and considerable single modes around f_2 and f_4.

Y ACCELERATIONS

The results for the considered subset are presented in Figures 7.13, 7.14 and 7.15, respectively.

- **Case 2.2.1** shows a clear peak in the SVP for dominant frequency f_1, and small local increases for frequencies f_3 and f_4. Each identified peak is accompanied by multiple orders of the singular values, which implies the lack of a discrete structural mode.

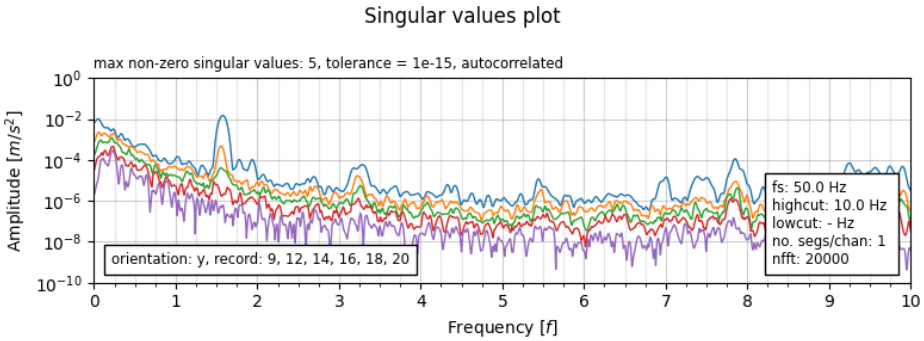

Figure 7.13: Case 2.2.1 - Power spectrum for y accelerations with trains towards Leeuwarden, from an autocorrelated time signal

- **Case 2.2.2** presents a peak at f_1, an apparent double peak at f_3 and increased frequency content at frequency f_4. The differences between the various orders of singular values for corresponding frequencies separate more distinctively when compared to Case 2.2.1.

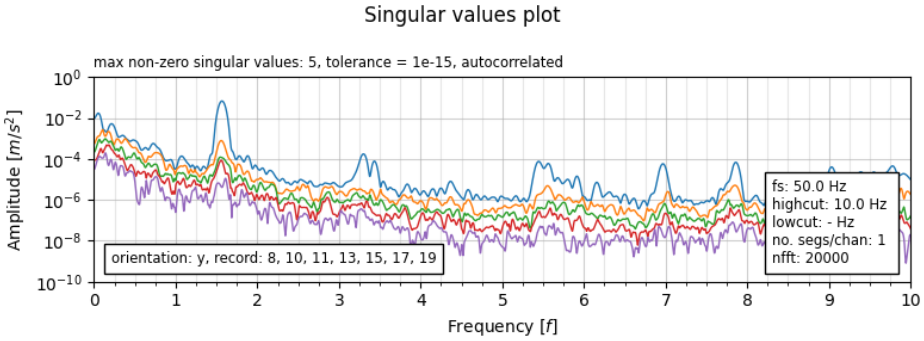

Figure 7.14: Case 2.2.2 - Power spectrum for y accelerations with trains towards Groningen, from an autocorrelated time signal

- **Case 2.2.3** describes the combined case, for train directions both ways. The spectrum shows an averaged result betweeen Case 2.2.1 and 2.2.2, where the closely spaced peaks around f_3 for the latter remain present, but are accompanied by a greater contribution of multiple modes.

When closely inspecting the SVPs of Case 2.2.1 and 2.2.2, the identified peak around f_2 is shifted slightly to the higher end of the spectrum for Case 2.2.2. This could imply a double mode. Although, the presence of a closely spaced mode around this frequency should be visible through the local increase of a different order SVP.

Dominant frequency f_3 is only present when the Y accelerations are included in the FDD, which implies a dominant horizontal mode. The presence is not clearly identifiable in the original case. Furthermore, the peaks in the spectrum at dominant frequencies f_1 and f_4 are also clearly identifiable, and correspond to the identified peaks of the cases in the Z direction. Therefore, the first and fourth dominant frequency most certainly correspond to a dominant ODS in both the Y and Z accelerations.

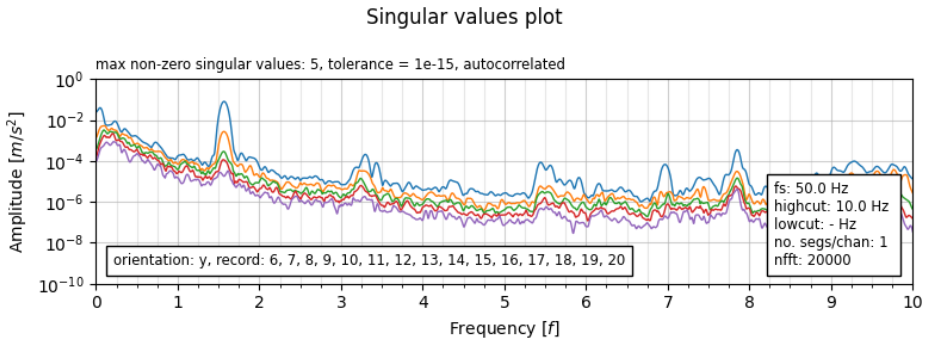

Figure 7.15: Case 2.2.3 - Power spectrum for y accelerations with trains in both directions, from an autocorrelated time signal

YZ ACCELERATIONS

The results for the considered subset are presented in Figures 7.16, 7.17 and 7.18, respectively.

- **Case 2.3.1** combines the Y and Z accelerations into a single case. The previously distinguished eigenmodes are not as distinct in the current case.

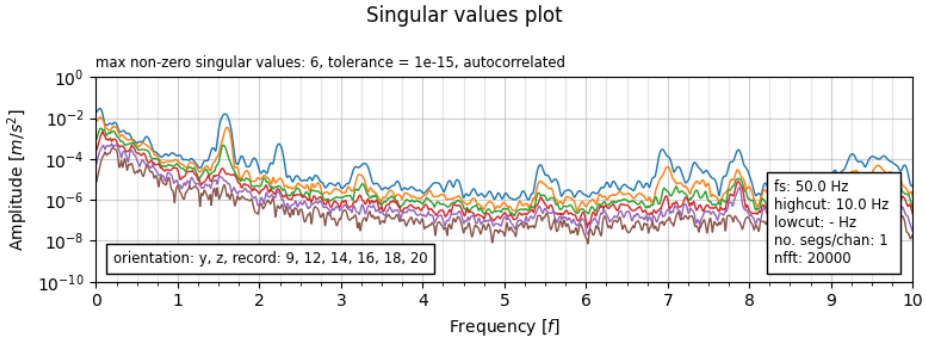

Figure 7.16: Case 2.3.1 - Power spectrum for yz accelerations with trains towards Leeuwarden, from an autocorrelated time signal

- **Case 2.3.2** presents clear distinctions of a single mode at frequencies f_2, f_3 and f_4. Frequency f_1 displays a local increase for all the SVPs.

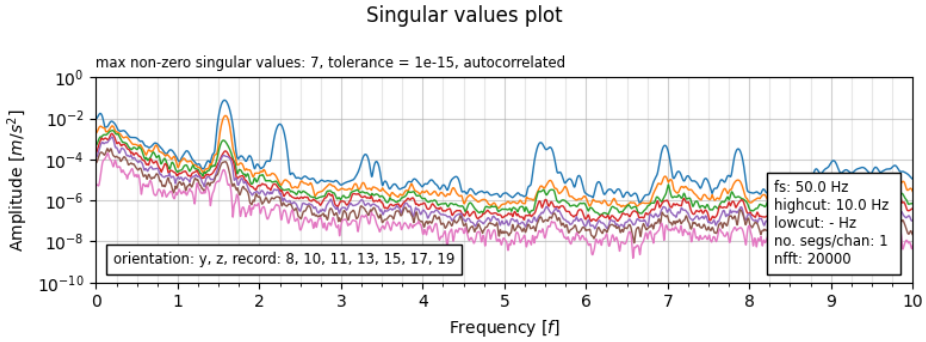

Figure 7.17: Case 2.3.2 - Power spectrum for yz accelerations with trains towards Groningen, from an autocorrelated time signal

- **Case 2.3.3** presents a great amount of SVPs to show local increase around dominant frequencies f_1 and f_3, whilst dominant frequencies f_2 and f_4 only show local increase for the first SVP.

The singular values cases for train directions to Leeuwarden present less high local peaks, and distinction of the first SVP w.r.t. the higher order SVPs, when compared to the results of the train directions to Gronin-

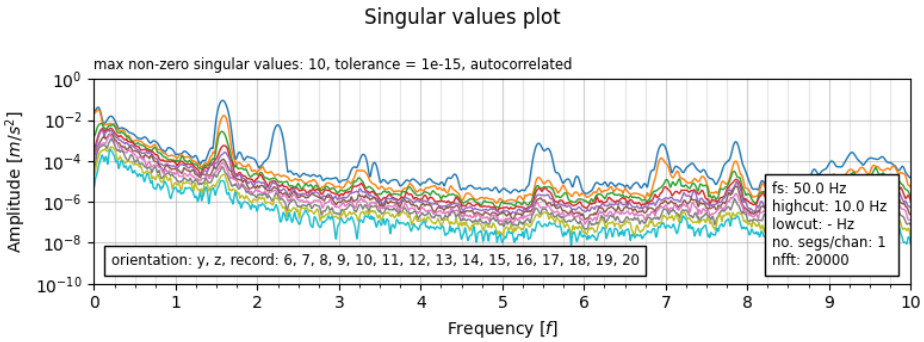

Figure 7.18: Case 2.3.3 - Power spectrum for yz accelerations with trains in both directions, from an autocorrelated time signal

gen, just like in the original case. Significant contribution of another mode is only visible around dominant frequency f_1.

The case where train directions to Groningen are included separately present the greatest difference between the first and following orders for the SVPs. As if the increased train velocity amplifies the dynamic response of the bridge significantly, and corresponds to greater magnitudes for the modal behaviour. When velocity of the train is lower, the bridge seems to not present any significant modal characteristics.

The last case combines the responses which again results in averaged SVPs. Therefore, the most clear distinctions are made for Case 2.3.2.

REMARKS AUTOCORRELATED CASES

- The autocorrelated SVPs show, in comparison to their non-autocorrelated equivalents, much clearer peaks at the dominant frequencies. Also separation of the SVPs become more significant for the autocorrelated case. The distinction in dominant acceleration directions become identifiable as well (without inspection of the mode shape plots), when comparing the peaks in the SVPs for the different acceleration directions (peak at f_2 for Z direction and peak at f_3 for Y direction).
- The majority of the identified dominant frequencies show corresponding local increases across the various orders of the SVPs. The only dominant frequency in the SVPs for the autocorrelated case which does not show a combined local increase in the SVP is dominant frequency f_2. In the general sense, this would be identified as the only structural mode to the structures' natural frequencies. The dominant mode originates from the recordings that include the Z accelerations. This implies a predominance in the Z directions for the identified mode.
- The first dominant frequency f_1, shows a great peak in most of the frequency response spectra, for all orders of the SVPs. This behaviour indicates a harmonic which does not originate from the modal characteristics of the bridge, but seems to have significant relations to the input load, for Y and Z acceleration directions. However, due to the distorting properties of the ACF, the computed modes might not be representative. Therefore, from this information only, the distinction between forced vibration and structural mode can not be made with sufficient confidence.
- Dominant frequency f_3 is mainly present in cases where the Y accelerations are included in the computations. This implies a dominant presence in the Y plane at this specific frequency.
- The dominant frequency f_4 shows great separation from the higher order SVPs in Case 2.1.2 and identifiable separation in Case 2.2.2, which implies a structural mode shape, predominantly in the Z plane, but also slightly present in the Y plane.
- Because the identified peaks for the train directions to Leeuwarden and Groningen (individually and combined) show correspondence, it is safe to assume the ODS is loading and/or structure dependent (and not random). The location of these amplified frequencies also correspond to the results from the original cases.
- The global indistinctive behaviour, as identified in the original case when including the Y accelerations (Cases 1.2.1, 1.2.3, 1.3.1 and 1.3.3) is not present in the signal, when incorporating an autocorrelation function before performing the FDD. This implies low correlation for the indistinctive behaviour.

RESULTS SVP - AUTOCORRELATED CASE

No.	Order	f_1	f_2	f_3	f_4
2.1.1	1	Y	Y	N	Y
	2	Y	N	N	Y
	3	Y	N	N	Y
	4	Y	N	N	Y
2.1.2	1	Y	Y	N	Y
	2	Y	N	N	Y
	3	Y	N	N	Y
	4	Y	N	N	Y
2.1.3	1	Y	Y	N	Y
	2	Y	N	N	Y
	3	Y	N	N	Y
	4	Y	N	N	N
2.2.1	1	Y	N	Y	Y
	2	Y	N	Y	Y
	3	Y	N	Y	N
	4	N	N	N	N
2.2.2	1	Y	N	Y	Y
	2	Y	N	N	Y
	3	Y	N	N	N
	4	Y	N	N	N
2.2.3	1	Y	N	Y	Y
	2	Y	N	Y	Y
	3	Y	N	Y	Y
	4	Y	N	Y	Y
2.3.1	1	Y	Y	Y	Y
	2	Y	N	Y	Y
	3	Y	N	Y	Y
	4	Y	N	N	Y
2.3.2	1	Y	Y	Y	Y
	2	Y	N	N	Y
	3	Y	N	N	Y
	4	Y	N	N	Y
2.3.3	1	Y	Y	Y	Y
	2	Y	N	Y	Y
	3	Y	N	Y	Y
	4	Y	N	N	Y

Table 7.3: Local increase of singular values plots for the autocorrelated case

7.1.3. SUMMARY SVPS

Table 7.4 shows a summary of possible natural frequencies, identified through the FDD for the original- and the autocorrelated case. The sensor direction describes per case, which of the acceleration directions are included in the computation. The dominant modes are presented in the header of the table, from which the mode shape can be determined.

For f_1 and f_4, the acceleration directions of the ODS will most likely be in both Y and Z directions. For frequency f_2 the mode will predominantly be in-plane for the Z direction, and the accelerations for the frequency f_3 will predominantly be in-plane for the Y direction (for the autocorrelated case). The results for

Case	Sensor direction	f_1	f_2	f_3	f_4
Original	Z	Y	Y	Y	Y
	Y	Y	N	Y	Y
	YZ	Y	Y	Y	Y
Autocorrelated	Z	Y	Y	N	Y
	Y	Y	N	Y	Y
	YZ	Y	Y	Y	Y

Table 7.4: Identification operational deflection shapes for the original- and the autocorrelated case. 'Y' represents a possible identified natural frequency, whereas 'N' represents no possible identified natural frequency.

both cases show a single discrepancy regarding dominant frequency f_3 which will be investigated further.

When carefully observing dominant frequency f_3 for the various SVPs, the original case presents a peak at this dominant frequency for the Z accelerations (Case 1.1.2), whereas the autocorrelated cases do not pick up this frequency content for the Z accelerations (Case 2.1.2), but does pick up frequency content for the Y accelerations (Case 2.2.2). The autocorrelated case also presents a distinctive double peak around dominant frequency f_3 (Case 2.2.2 and 2.3.2), which could imply closely spaced modes. Investigation of the mode plots around dominant frequency f_3 can give additional information on the response characteristics.

Further investigation is performed to accurately identify the type of mode (shape) in Section 7.2. The cases are considered where the results are clearly identifiable, which is predominantly present for the train direction towards Groningen.

7.2. MODE SHAPES

In this section, the results of the mode plots are discussed. During derivation of the mode shapes, only the measurements for the train directions towards Groningen are included, as these measurements showed greatest signs of convergence for the SVPs. The SVPs showed significant variation for the different cases of acceleration directions. Therefore, this section will elaborate on the computed mode shapes for the discrete and combined cases of acceleration directions. For the determination process of mode shapes, two different preprocessing cases are considered, namely, the original (unprocessed) case and the autocorrelated case (Table 4.4). However, by applying the ACF, the results are affected by its magnitude- and phase distorting properties. This results in the computation of non-representative modes. Therefore, the ACF will *not* be applied in the determination process of the mode shapes. From now on, the autocorrelated case will be referred to as the preprocessed case, as the preprocessing parameters are still applied without the ACF, in order to investigate the influence of such preprocessing computations.

As mentioned before, the FDD presents the ability to identify closely spaced modes. During the determination process, for a second mode to be considered, the first and second order SVPs will both have to display a local increase (Tables 7.2 and 7.3). If this is the case, the mode plot for the first and second singular vector will be presented. The mode plots which are not relevant will not be reflected on.

Corresponding to the results of the power spectrum estimates, the relevant mode plots are computed. The relevant mode plots which will be considered are presented in Table 7.5.

Acceleration direction	f_1	f_2	f_3	f_4
Z	1	1	1	1
Y	1	-	1	1
YZ	1, 2	1	1*	1

Table 7.5: Considered cases for the mode plots. The tabulated values represent the order of the singular vectors which are included in the consideration for the mode shapes. The '*' symbol represents elaborate investigation due to the discrepancies, which are identified during the derivation of the relevant frequencies.

For most cases, only the first singular vector is considered. The dominant frequency f_1 shows local increases for the first and second SVPs in the YZ accelerations (Case 1.3.2). For Y accelerations, dominant frequency f_2 is not taken into account. At f_3, the first SVP of the YZ accelerations presents a double peak at $3.30Hz$ and $3.40Hz$, so both singular vectors are presented.

7.2.1. ORIGINAL VS. PREPROCESSED CASE

Due to the magnitude- and phase distorting properties of the ACF, only the preprocessing computations, as described in Table 4.4, are applied when considering mode shapes. When comparing the results from the original case, to the results of the preprocessed case no significant differences can be identified (Figure 7.19). This relation holds for the majority of the results.

Due to the nearly identical results between the two preprocessing techniques, only the results of the original case will be discussed. The comments on the mode shapes are close to identical for the preprocessed case w.r.t. the original case.

The total collection of computed mode shapes, which include all mode plots from the original- and preprocessed case are presented in Appendix A.

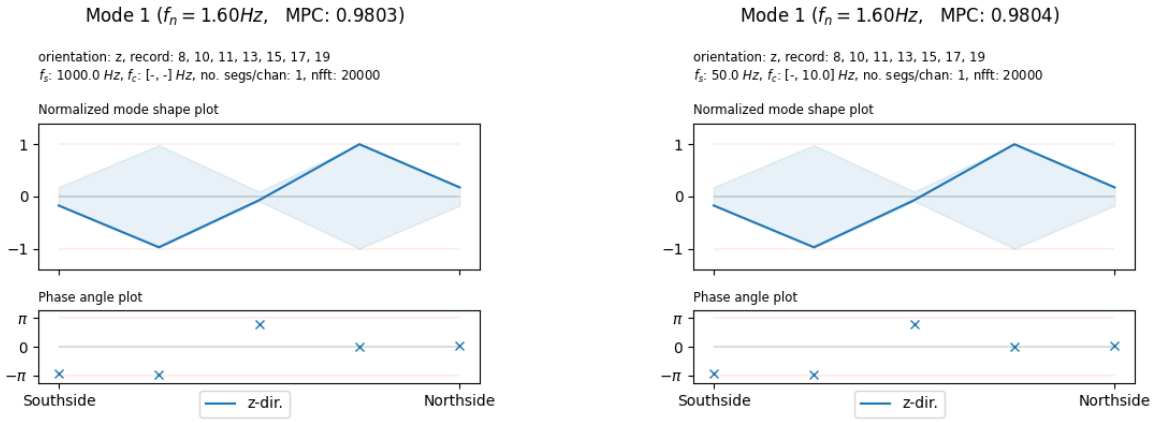

(a) Original case

(b) Preprocessed case

Figure 7.19: Sensor direction Z, dominant frequency f_1

7.2.2. RESULTS ORIGINAL CASE

Z ACCELERATIONS

The ODS accelerations in Z directions for the original case are displayed in Figures 7.20a to 7.20d.

- **f_1 = 1.60Hz - Mode 1** The mode plot of the first dominant frequency displays an anti-symmetric shape, due to the relative phase delay (of π) between a quarter and three quarters of the span. The non-integer multiple of π for the phase angle of the point at midspan does not add significant complexity due to the negligible amplitude.

- **f_2 = 2.25Hz - Mode 1** The mode plot of the second dominant frequency displays considerable accelerations at midspan and anti-phase accelerations at a quarter and three quarters of the span.

- **f_3 = 3.30Hz - Mode 1** The mode plot of the third dominant frequency displays the largest accelerations at a quarter of the span, from the southside. The point at three quarters of the span does not show significant accelerations.

- **f_4 = 5.45Hz - Mode 1** The mode plot of the fourth dominant frequency displays an overall in-phase acceleration over the unsupported points along the span. Keep in mind that at this frequency, the identified mode is dominant in both the Y and Z direction for the accelerations.

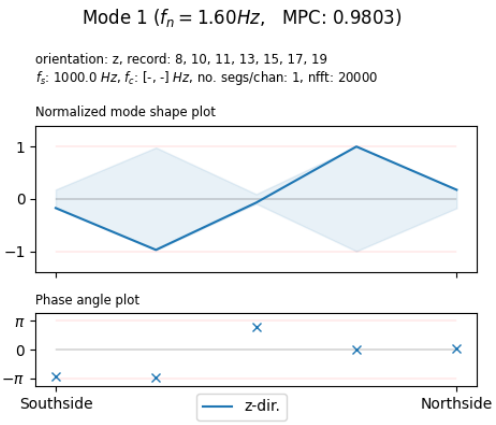

(a) Dominant frequency f_1

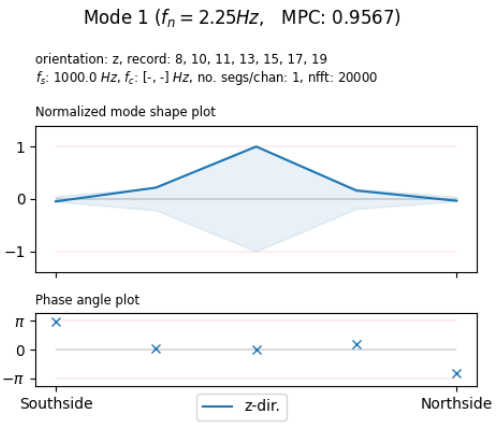

(b) Dominant frequency f_2

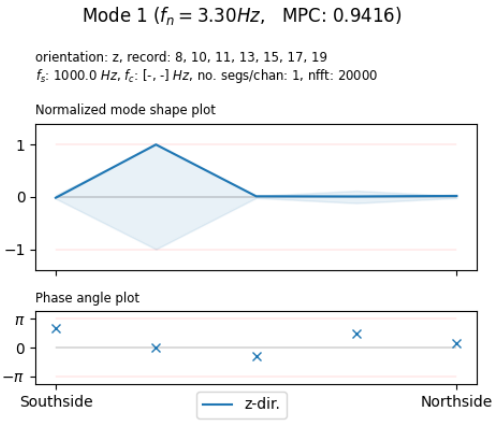

(c) Dominant frequency f_3

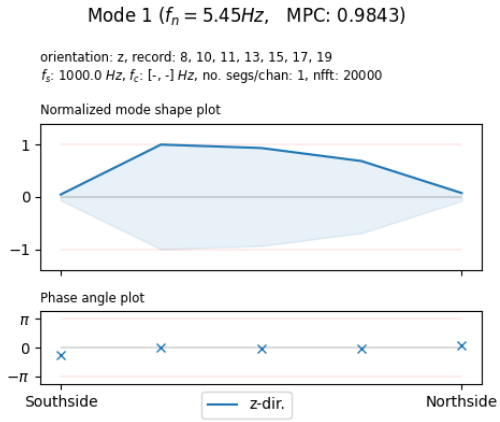

(d) Dominant frequency f_4

Figure 7.20: Mode plots for the original case, sensor direction Z

Y ACCELERATIONS

The ODS accelerations in Y directions for the original case are displayed in Figures 7.21a to 7.21c.

- **f_1 = 1.60Hz - Mode 1** The first mode plot of the first dominant frequency displays an in-phase response where for every point along the span, the unsupported points are accelerating horizontally. This ODS shows great comparison with the first classical bending mode of a simply supported beam.
- **f_3 = 3.30Hz - Mode 1** The first mode plot of the third dominant frequency displays an anti-symmetric ODS with extremes at a quarter and three quarters along the span. The accelerations for the point at midspan remain low.
- **f_4 = 5.45Hz - Mode 1** The first mode plot of the fourth dominant frequency displays in-phase behaviour, comparable to the identified ODS for the first dominant frequency for the Y directions, however, for this mode the point at midspan does not display the largest accelerations.

YZ ACCELERATIONS

The YZ accelerations give clear insights on the relative amplitudes between the vertical and horizontal components in the identified mode shape. The ODS accelerations in YZ directions for the original case are displayed in Figures 7.22a to 7.24b.

- **f_1 = 1.60Hz - Mode 1 & 2** The first and second mode plots of the first dominant frequency display comparable absolute extreme accelerations for the Y and Z directions. The vertical direction shows the first classical bending mode for an *arch bridge*, and is combined with a horizontal direction first

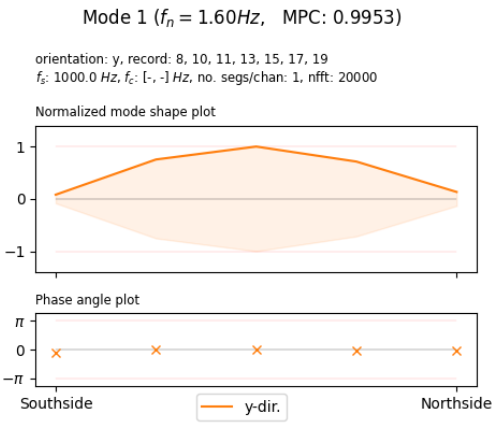

(a) Dominant frequency f_1

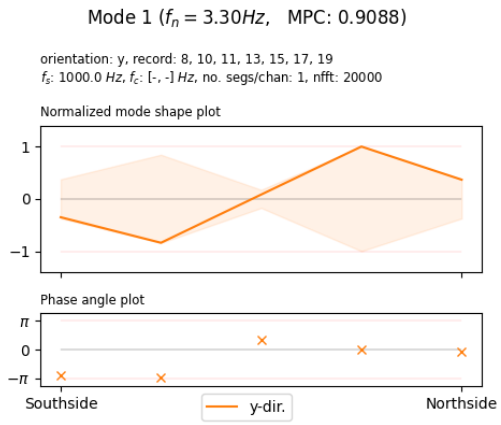

(b) Dominant frequency f_3

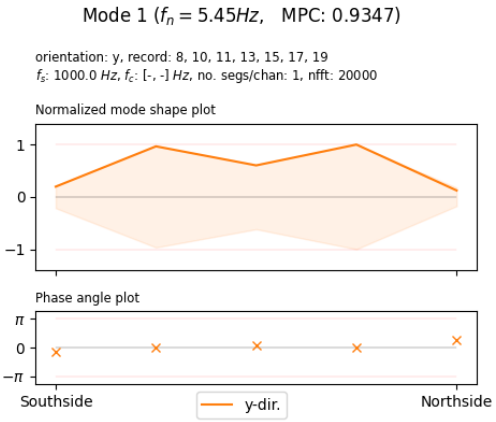

(c) Dominant frequency f_4

Figure 7.21: Mode plots for the original case, sensor direction Y

classical bending mode for a *simply supported beam*. These modes are also identified in the discrete cases for Y and Z accelerations. This combined mode however, displays significant complexity due to the relative phase delay between the Y and Z accelerations with respect to their individual cases.

The mode plots for mode 1 and mode 2 are closely related, however, the relative phase angle for the Z direction is shifted by π for the second mode w.r.t. the first mode. This implies a corkscrew motion, where the direction of motion is inverted for mode 2 w.r.t. mode 1. As the shape of both ODSs is identical, and only the direction of motion varies, the two identified ODSs can be considered as a single dominant ODS.

- **f_2 = 2.25Hz - Mode 1** The first mode plot for the second dominant frequency displays an in-phase ODS with governing Z accelerations with extremes at midspan. The horizontal component at this dominant frequency is negligible.

- **f_3 = 3.30Hz - Mode 1** At this frequency, the SVP (Case 2.3.2) displays double peaks at $3.30Hz$ ($f_{3.1}$) and $3.40Hz$ ($f_{3.2}$). The former amplifies the structure in both acceleration directions, whereas the latter displays dominant behaviour in the Y directions. $f_{3.1}$ shows increased complexity w.r.t $f_{3.2}$, as the MPC value is lower at the former frequency. The vertical motion is predominantly present for $f_{3.1}$, located at a quarter of the span from the southside support. The accelerations in Z direction at three quarters of the span are negligible. The horizontal motion is predominantly present at $f_{3.2}$ and displays an anti-symmetric bending mode. The horizontal accelerations at the supports are also greatly present, when compared to other ODSs.

- **f_4 = 5.45Hz - Mode 1** The last dominant frequency displays in-phase symmetric behaviour with dom-

inance in Z accelerations at the unsupported locations along the span. The Y accelerations again show non-negligible amplitudes at the locations of the supports.

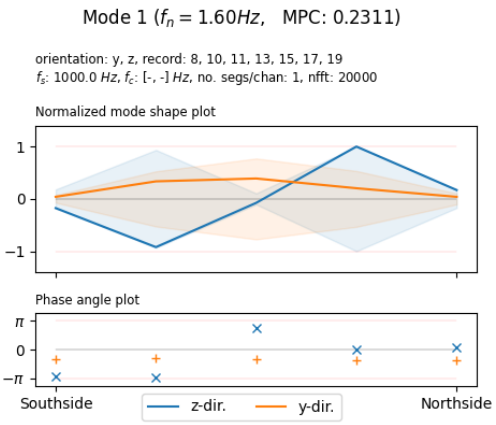

(a) Dominant frequency f_1, first mode plot

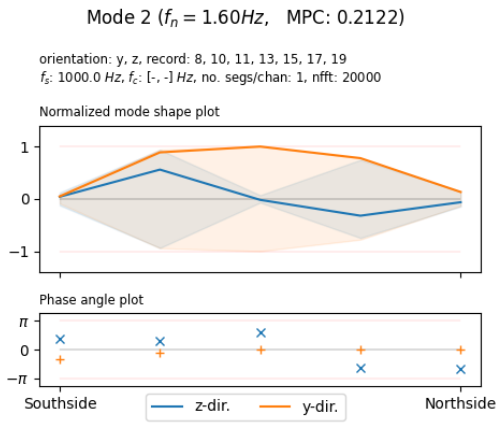

(b) Dominant frequency f_1, second mode plot

Figure 7.22: Mode plots for the original case, sensor direction YZ (1/3)

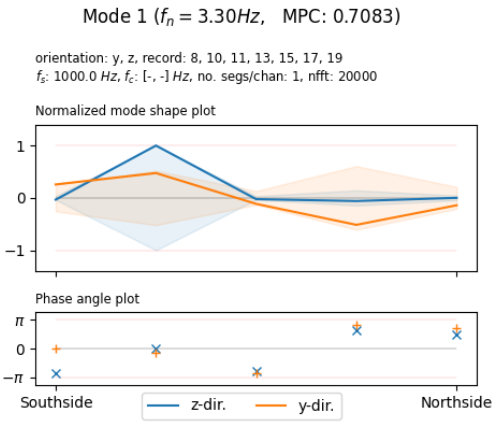

(a) Dominant frequency $f_{3.1}$

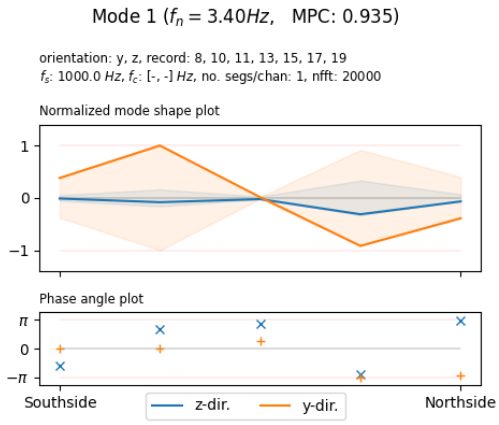

(b) Dominant frequency $f_{3.2}$

Figure 7.23: Mode plots for the original case, sensor direction YZ (2/3)

REMARKS MODE PLOTS

- The majority of the maximum accelerations are present along the span of the bridge. The maximum absolute value for the accelerations are considerably lower at the locations of the supports.
- The mode shapes for separate Y and Z cases show identical behaviour in the combined YZ cases, over corresponding frequencies.
- The mode shapes show significant correspondence to the expected mode shapes from literature and the digital model (Sections 2.5 and 3.0.1, respectively).
- The double peak at dominant frequency f_3 is investigated in Figures 7.23a and 7.23b. The former describes a significant acceleration around a quarter of the span in the Z directions, and a lesser anti-symmetric behaviour in the Y direction. The latter peak describes a dominant anti-symmetric mode in the Y direction. This corresponds to the expected second mode for a classical simply supported beam.
- Separate acceleration directions show negligible complexity, however, combining orthogonal acceleration directions for a single mode can result in a constant shift in phase delay (e.g. $\pi/2$, for a single acceleration direction), making the mode shape significantly complex. An example is the corkscrew behaviour (mode 1, f_1).

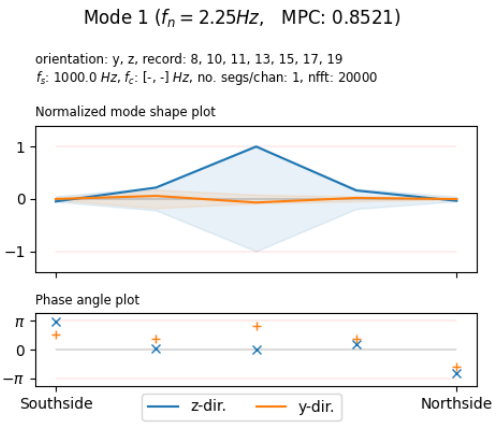

(a) Dominant frequency f_2

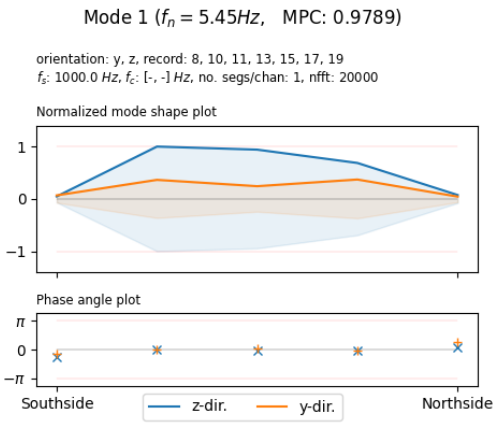

(b) Original case, sensor direction YZ, dominant frequency f_4

Figure 7.24: Mode plots for the original case, sensor direction YZ (3/3)

7.2.3. COMPLEXITY THROUGH MPC

The complexity of the derived mode shape is determined through the MPC and presented in tables 7.6 and 7.7 for the original- and preprocessed case, respectively. The mode complexity is low for MPC values close to 1, and high for values close to 0. A low MPC value indicates significant damping for that specific mode, or forced vibrations induced in the structure.

Frequency	Sensor direction	Train direction	MPC_1	MPC_2	MPC_3	MPC_4
1.60	Z	Leeuwarden	0.9695	0.9756	0.9105	0.7909
		Groningen	0.9803	0.8882	0.3121	0.7068
		Both	0.9894	0.9538	0.6877	0.5912
	Y	Leeuwarden	0.9823	0.9674	0.1200	0.4022
		Groningen	0.9953	0.9108	0.3806	0.4385
		Both	0.9981	0.9802	0.5489	0.5365
	Y Z	Leeuwarden	0.4426	0.3438	0.1489	0.4946
		Groningen	0.2311	0.2122	0.8323	0.5453
		Both	0.5198	0.4826	0.7963	0.9298
2.25	Z	Leeuwarden	0.8724	0.8452	0.6864	0.3295
		Groningen	0.9567	0.9479	0.5862	0.3043
		Both	0.9626	0.9447	0.5380	0.8819
	Y	Leeuwarden	0.9979	0.4243	0.5752	0.5152
		Groningen	0.8729	0.6749	0.3682	0.6037
		Both	0.9985	0.6377	0.2052	0.2164
	Y Z	Leeuwarden	0.9595	0.7521	0.7406	0.2015
		Groningen	0.8521	0.6220	0.0822	0.1207
		Both	0.9750	0.9284	0.8677	0.3188
3.30	Z	Leeuwarden	0.9691	0.4839	0.6913	0.6289
		Groningen	0.9416	0.3762	0.2106	0.3569
		Both	0.9918	0.4645	0.6717	0.2063
	Y	Leeuwarden	0.9752	0.9503	0.9125	0.7486
		Groningen	0.9088	0.2889	0.0619	0.0174
		Both	0.9752	0.9428	0.2985	0.0633
	Y Z	Leeuwarden	0.9712	0.9202	0.8449	0.1486
		Groningen	0.7083	0.4912	0.3717	0.0175
		Both	0.9708	0.9381	0.8610	0.4498
5.45	Z	Leeuwarden	0.9928	0.8635	0.9031	0.8856
		Groningen	0.9843	0.4953	0.0201	0.0296
		Both	0.9914	0.9008	0.6614	0.7335
	Y	Leeuwarden	0.9978	0.7225	0.4486	0.3187
		Groningen	0.9347	0.6107	0.1776	0.0048
		Both	0.9979	0.8962	0.9048	0.7918
	Y Z	Leeuwarden	0.9780	0.9487	0.7067	0.1819
		Groningen	0.9789	0.1485	0.0558	0.1665
		Both	0.9687	0.9546	0.8268	0.0482

Table 7.6: MPC values of the dominant frequencies for the original case

Frequency	Sensor direction	Train direction	MPC_1	MPC_2	MPC_3	MPC_4
1.60	Z	Leeuwarden	0.9696	0.9760	0.9133	0.7906
		Groningen	0.9804	0.8892	0.3046	0.6852
		Both	0.9894	0.9545	0.6864	0.5864
	Y	Leeuwarden	0.9821	0.9674	0.1066	0.3933
		Groningen	0.9953	0.9111	0.3844	0.4410
		Both	0.9980	0.9803	0.5476	0.5364
	Y Z	Leeuwarden	0.4426	0.3384	0.1450	0.4943
		Groningen	0.2294	0.2106	0.8322	0.5381
		Both	0.5183	0.4812	0.7959	0.9299
2.25	Z	Leeuwarden	0.8688	0.8419	0.6938	0.3241
		Groningen	0.9568	0.9472	0.5606	0.3065
		Both	0.9627	0.9452	0.5394	0.8817
	Y	Leeuwarden	0.9979	0.4188	0.5774	0.5127
		Groningen	0.8724	0.6765	0.3713	0.6079
		Both	0.9985	0.6367	0.1993	0.2118
	Y Z	Leeuwarden	0.9597	0.7504	0.7393	0.2021
		Groningen	0.8520	0.6322	0.0898	0.1194
		Both	0.9752	0.9286	0.8693	0.3225
3.30	Z	Leeuwarden	0.9239	0.7048	0.0696	0.5698
		Groningen	0.9894	0.4251	0.5810	0.7809
		Both	0.9946	0.7098	0.9651	0.8096
	Y	Leeuwarden	0.9851	0.9100	0.5042	0.5547
		Groningen	0.9815	0.1739	0.4881	0.4727
		Both	0.9849	0.9680	0.5635	0.2117
	Y Z	Leeuwarden	0.9824	0.7792	0.7542	0.2422
		Groningen	0.6916	0.4890	0.2733	0.3758
		Both	0.9810	0.6956	0.6816	0.0494
5.45	Z	Leeuwarden	0.9934	0.8594	0.9016	0.8804
		Groningen	0.9846	0.4817	0.0180	0.0350
		Both	0.9914	0.8949	0.6600	0.7471
	Y	Leeuwarden	0.9978	0.7211	0.4490	0.3204
		Groningen	0.9352	0.6165	0.1833	0.0058
		Both	0.9978	0.8967	0.9063	0.8003
	Y Z	Leeuwarden	0.9782	0.9495	0.7033	0.1732
		Groningen	0.9792	0.1452	0.0551	0.1668
		Both	0.9690	0.9549	0.8162	0.0520

Table 7.7: MPC values of dominant frequencies for the preprocessed case.

When investigating the result tables, it is visible that the MPC values for the first singular vector (MPC_1) is relatively high. The MPC value decreases for higher order singular vectors (MPC_2 to MPC_4). This implies that complexity mainly appears in the less dominant modes (corresponding to a lower singular value) for that specific frequency.

If the MPC values are low, the expectations to accurately determine structural damping through the EFDD can not be satisfied, due to chances of high structural damping, or describing a non-structural mode. In the former case, the results do not comply with the assumption of proportional damping. If the certainty of the results can not be confirmed, the damping coefficients can not be considered as accurate, and therefore, representative.

Table 7.8 summarizes the MPC values for the mode plots, which are considered in the section above. The separate Y and Z cases show greater MPC values, when compared to their equivalent combined YZ cases.

Acceleration direction	**Dominant frequency**	MPC_1	MPC_2
Z	f_1	0.9803	-
	f_2	0.9567	-
	f_3	0.9416	-
	f_4	0.9843	-
Y	f_1	0.9953	-
	f_2	-	-
	f_3	0.9088	-
	f_4	0.9347	-
YZ	f_1	0.2311	0.2122
	f_2	0.8521	-
	$f_{3.1}$	0.7083	-
	$f_{3.2}$	0.9350	-
	f_4	0.9789	-

Table 7.8: Considered relevant mode shapes with corresponding MPC_i values, where i represents the order of the singular vector.

The determined MPC values describe low complexity for the separate acceleration direction cases. However, when including both acceleration directions in the computation of the FDD, the complexity of the determined mode shape increases.

The mode visualization tool (Figure 6.3) includes a 3 dimensional animation plot, to intuitively represent the dynamic behaviour of a specific mode shape over time. This provides the user with a better interpretation of the dynamic modes, in particular for the complex modes.

REMARKS DETERMINATION MODE SHAPES

- The results from the original case w.r.t. preprocessed case are close to identical. This implies that certain preprocessing will not influence the results for the considered cases.

- Only for dominant frequency f_3, the results between the original and preprocessed case diverge slightly in the Z acceleration direction (Figures 7.20c in the report or A.3a and A.3b in the appendix). The discrepancy between the original and autocorrelated case is also identified in Table 7.4. The main contrast is identifiable in the relative phase delay, however, due to the negligible amplitude for the regarded ODS in Z direction, the discrepancy can be considered non-relevant.

- The normalized magnitude plots are represented as a continuous line through the locations of the DOFs. However, the realistic modes can deviate from the suggested mode shape, due to deficient spatial density of the sensors.

- Due to the low number of available measurement recordings, chances to converge to accurate and realistic mode shapes are debatable.

- When the characteristics of the load play a significant role in the dynamic response of the bridge, the behaviour will not necessarily converge to a certain structural mode, but tends to converge to the modal characteristics of the input load (the train).

7.2.4. APPARENT MODES

During the evaluation of the mode shapes, a small collection of apparent mode types are identified which require some additional explanations.

Noise modes For Cases 1.2.1, 1.2.3, 1.3.1 and 1.3.3 the result of the most dominant mode (first order), seems to be an indistinctive frequency domain plot, highly contaminated with noise. Around frequency f_1, where a higher signal-to-noise ratio is expected, the noise mode seems to be attenuated. However, the singular value of a another plot does not have significant magnitude to become the first order mode. The noise mode behaviour does not seem to be as present in the power spectrum of the same recording channels for the train direction to Groningen (Figure 7.5). The high noise mode is surely a contribution from the records for the train directions towards Leeuwarden.

The FDD is being used to determine the modal properties of the bridge. Due to the prerequisite assumptions of OMA methods, some boundary conditions, with respect to the input load must be taken into account. As mentioned in Section 2.5.2, the train loads are far from random. The loads also show significant impact, as the computed power spectra vary greatly when including different input signals in the computation.

Forced vibrations When the response of the structure is dominantly governed by the characteristics of the input load, the computed mode might show signs of complexity. The amount of complexity is determined through the MPC value. This parameter can assist during the determination between a structural mode of a forced vibration.

Corkscrew mode In Figures 7.22a and 7.22b, two separate modes are identified by the FDD. After inspection, the modes seem to describe the same mode shape, however for the opposite direction of motion, therefore, making it dependent on the point in time. Due to the time dependency, the complexity increases, even though the separate Y and Z cases (Figures 7.20a and 7.21a) show negligible complexity. The determination of a structural mode is still plausible, as the two acceleration directions (Y and Z) are spatially orthogonal, and both showing insignificant complexity for their discrete cases (embodying standing wave characteristics). By orthogonality, each acceleration direction can be investigated separately. Theoretically the one acceleration direction will not influence the other (no linear dependency). When investigating the discrete Y and Z mode plots, a mode shape at dominant frequency f_1 would be determined for both directions. If at this frequency, a single mode is identified in the Y direction and a single mode is identified in the Z direction, with both discrete modes showing almost no complexity, then the mode for the combined case will also represent a mode, independent of the combined significant complexity.

8

Conclusion

THE conclusions, which are based on the results of the FDD for the considered case study are presented in this chapter. Subsequently, the conclusions regarding the research cases and remarkable properties are determined. Finally, to conclude the research on the analysis of signals to determine modal parameters, the answers to the research questions are presented.

8.1. CASE RESULTS

For the research project, a case study is investigated to determine the natural frequencies and corresponding mode shapes of an arch railway bridge.

First the dominant frequencies are determined through the peaks of the SVPs. The ODSs are determined from the left singular vectors matrix to their corresponding singular value, at the location of the dominant frequency. An attempt is made to make a distinction between the structural modes and the forced vibrations by elaborate examination of the results.

As reliability of the results is preferred during this research project, the choice is made to include only a subset of the available data, which tend to show convergence during the computations. During evaluation of the locations of the natural frequencies, a vast amount of combinations for the input signals, together with preprocessing techniques is considered to assess the quality and characteristics of the measurements. The cases that showed the greatest convergence included the train directions towards Groningen. Therefore, only these signals are included during determination of the mode shapes. The remaining cases showed corresponding behaviour, only less clear. Therefore, tese results are not included during the determination process of the mode shapes.

The computed mode shapes showed signs of complexity, when the MPC value of the regarded mode shape is lower than 1. Physically, a complex mode can represent a forced vibration with complex characteristics, or implies significant structural damping. This does not correspond with the prerequisite assumptions of the OMA techniques, for the determination of reliable results.

8.1.1. NATURAL FREQUENCIES & CORRESPONDING MODE SHAPES

After investigating the singular values plots (Section 7.1) and mode plots (Section 7.2), the Table 8.1 is computed. This table concludes the analysis of the computed mode shapes. For the identified dominant frequencies, the mode type with corresponding mode shape and MPC value is presented.

Dominant frequency	Frequency	Mode type	Shape	Dominant direction	MPC
f_1	$1.60 Hz$	Structural mode	Horizontal symmetric Vertical anti-symmetric	Y Z YZ	0.99 0.98 0.23
f_2	$2.25 Hz$	Structural mode	Vertical symmetric	Z	0.96
$f_{3.1}$	$3.30 Hz$	Forced vibration	Horizontal anti-symmetric Vertical non-symmetric	Y Z YZ	0.91 0.94 0.71
$f_{3.2}$	$3.40 Hz$	Structural mode	Horizontal anti-symmetric	Y	0.93
f_4	$5.45 Hz$	Structural mode	Vertical symmetric Horizontal symmetric	Y Z YZ	0.98 0.93 0.97

Table 8.1: Mode types for dominant frequencies

In Table 8.1, the identified mode shapes and forced vibrations are presented. In the last 2 columns, the acceleration directions are presented together with their MPC values. For the mode shapes that do not dominate a single acceleration direction, the MPC values are presented for the discrete acceleration directions and the combined case.

Dominant frequency f_1 displays a corkscrew-like mode shape (Section 7.2.4), which is not classified as a complex mode due to the expected in- and anti-phase behaviour and MPC values close to 1, for the discrete

acceleration directions. At dominant frequency $f_{3.1}$ a forced vibration is identified, due to the non-symmetric mode shape, together with the low MPC values for the combined case. For dominant frequency f_4, the in-phase accelerations describe an off-axis structural mode, which is slightly more dominant in the vertical direction (Figure 7.24b).

8.2. CONCLUSIONS RESEARCH

Inclusion of data records For the determination of the natural frequencies, three cases are considered. Each case represents the inclusion of the recordings for the train directions towards Leeuwarden, Groningen and both. The results for the train direction towards Groningen show significantly better results, when compared to the results towards Leeuwarden. For the case considering both train directions, the results showed an average between the first (Leeuwarden) and the second (Groningen) case. This was not different for the cases regarding Y and Z accelerations separately.

Train velocity The average train velocities show higher values for the train directions towards Groningen, when compared to the train directions towards Leeuwarden. The results from the FDD show indistinguishable modal behaviour for lower train velocities. When the average train velocities increase, the modal behaviour becomes easier to identify, as the increased dynamic response of the bridge consists a higher contribution of this modal behaviour.

Autocorrelated case The SVPs that represent the autocorrelated case, show better performance through the more clearly distinguishable peaks for the determination of the natural frequencies. Due to the noise reduction property of the ACF, the existent noise is attenuated, therefore increasing the signal-to-noise ratio. The remaining part in the signal, after application of the ACF, includes an amplified representation of the periodic components in the dynamic response of the bridge. The location of the peaks correspond to the expected frequencies, which are derived in the original case. A significant increase in the relative amplification w.r.t. neighboring frequencies is identified, therefore making the peaks clearly visible. However, the absolute values of the power spectra are not directly representative to derive any scalar value for the accelerations, due to the magnitude altering properties of the ACF. The downside of the ACF is that the phase of the determined modes is not representative. The relative amplitudes in the singular vectors are squared, which will not present accurate absolute amplitudes for the mode shapes.

Preprocessing results For the determination of the mode shapes, the computed singular vectors do not show correspondence between the original case and the ACF case. Therefore, when regarding the mode shapes, the results of original case are compared to the results of the preprocessed case. The results displayed almost identical behaviour. The preprocessing parameters did not show great influence on the results for the derivation of the mode shapes.

RESEARCH QUESTIONS

For comfort of the reader, the research questions will be repeated, before concluding with an answer for every question.

How can the dynamic properties be obtained for an arch-railway bridge based on measurement data with appropriate stability and reliability?

1. What methods are commonly used in the analysis of vibrations?
2. How to assess the quality of the measured data?
3. What methods can be used to improve the usability of the signal?
4. Is it possible to distinguish closely spaced natural frequencies in the measured signal?

COMMON METHODS

The analysis of vibrations is a multidisciplinary field of engineering, as it brings together three fundamental areas of expertise. Namely, data science, modal analysis and signal processing. The former is related to

identifying correlations, trends and other useful properties from data (often in vast amounts). The second describes dynamic characteristics of structural elements and the latter concludes the altering of digital signals to increase accuracy and reliability. In the specific case of this research project, the subjects are combined to determine modal parameters of a dynamic system. Fundamental concepts from these fields are combined, such as the singular value decomposition and the Fourier transform, to represent the dynamic behaviour of a structure. A frequency domain method, known as the frequency domain decomposition is applied to determine the dynamic characteristics. Other procedures describe time domain methods and hybrid methods. A supplementary variation on the frequency domain decomposition is presented, where the input signals are reconstructed using an autocorrelation function, prior to the decomposition. The autocorrelation function is a common tool, which is widely applied in recurrence quantification analysis. There exist numerous additional methods, however, these methods are not included in this research project.

Overall, it is a robust method of solving for the modal parameters. The majority of the computational effort is concentrated in the SVD itself, but the FDD method gives a clear description to prepare the data for modal decomposition. This is what makes it user-friendly (Brincker et al., 2001). It is an effective solution when the data records are of significant length, and they remain to have a decent initial spectral resolution (without zero padding). Also the ability to distinguish the presence of multiple modes is very powerful.

ASSESS QUALITY OF THE MEASURED DATA

Post computational assessment on the quality of the measurements can be performed manually, by examination of the results. As operational modal analysis makes use of output-only systems, the predefined assumptions, related to the statistical properties of the system or input signals, such as ambient forces, are often inaccurate. Assumptions regarding white noise loading or stationarity of the system are never fully met in a realistic case. The characteristics of the results are dependent on the characteristics of the input signals. This property can be used to reflect on the quality of the measured data. By varying the input parameters and signals, a general understanding on the basic cases and influential parameters can be acquired. Faulty measurements can be identified. However, the process of evaluating different cases and reflecting on the results to present for preliminary interpretation requires human interaction. It will not be easily implemented into an algorithm without fundamental understanding on the data.

During the research project, the quality of the data is assessed by deriving convergence of the data. When the assumptions of OMA are met, any signs of non-convergence are related to the quality of the measured data.

IMPROVE USABILITY OF SIGNAL

To improve the usability of the signals, the adverse characteristics of the input signals, such as uncorrelated noise, should be investigated. The aim is to identify the unwanted characteristics, so a suitable solution can be applied. A selection of these characteristics of the signals can be (partially) omitted through prepossessing computations. However, there is only so much the preprocessing techniques can achieve. It is important to keep in mind that operational data will always display signs of noise, which can not be entirely separated from the signal. Then the goal is to *minimize* the contribution of such negative behaviour.

The ACF presents a clear method to attenuate noise in a periodic signal. Additionally, application of an ACF for detrending purposes is also effective. For longer discrete finite-length digital signals, the ACF can become computationally expensive. To reduce the time of computations, the considered signal can be downsampled to reduce the amount of discrete data points, without sacrificing spectral resolution through the fundamental frequency. Downsampling influences the highest measurable frequency, by the Nyquist frequency.

CLOSELY SPACED MODES

Through the FDD, closely spaced modes can be identified. When considering a discrete frequency in the first singular values plot, the corresponding singular vector can be retrieved. The singular vector represents a dominant operational deflection shape (ODS). The second singular values plot holds its own singular vector, which can be described as the second most dominant ODS for that discrete frequency. When two singular values plots are considered, the contribution of each dominant ODS is visually represented. Even if the two shapes are closely spaced, the ability to distinguish the two separate shapes remains present. However, the ODS can only be considered as structural modes if the a local amplification of a single mode is clearly visible, meanwhile the other mode will remain at its normal amplitude around the specific frequency. This brings along major advantages over a time domain method or the ordinary frequency domain representation where the multiple modes merge into a single peak.

9

Recommendations

DURING this project, predictive research is conducted to investigate the possibilities to derive modal parameters from vibrational data. A case study is investigated to extract modal parameters from a set of vibrational measurements. This chapter describes certain subjects which can be investigated further to improve on the current methods. Additional recommendations are presented regarding improved data acquisition and progressive steps which can be taken to continue research for modal analysis based on operational measurements.

9.1. PRACTICAL RECOMMENDATIONS FOR DATA ACQUISITION

Additional measurements This research argues that the measuring of dynamic properties should be performed more frequently, to gain the ability to make more accurate assumptions on the dynamic behavior of structures in the future. When working with experimental data, not all acquired data can be considered useful. A portion of the signals can be contaminated with noise or other measurement artefacts, or just not show sufficient convergence to produce reliable results. Therefore acquisition of additional measurements is recommended.

Train velocities In the literature study it is mentioned that the dynamic response of a railway bridge increases for greater train velocities. The input data, together with the results from this research project confirm that statement. Therefore, if additional tests can be performed on the bridge, it is recommended to vary the train velocities, to be able to reflect on its impact, mostly for the higher train velocities.

Length of time recordings When accurately determining natural frequencies and corresponding mode shapes, a clear distinction between the neighbouring frequencies in the estimated power spectra is desired. The spectral resolution can be increased by zero-padding, however, this will not influence the fundamental frequency of the output frequency response. It will make no difference in the ability to distinguish neighbouring frequencies, but only smoothen the output spectrum. To ensure an effective spectral resolution, recordings of significant length are recommended. If the measurement signals are of extreme length, therefore making the process computationally expensive, segmentation of the data can be applied.

Increase state space sensor density For the current case study, only the dynamic behaviour for the discrete points in space at the locations of the sensors is registered. All structural behaviour between the sensors can only be approximated and therefore, not accurately determined. Additionally, the maximum amount of distinguishable modes is dependent on the amount of applied sensors. When the fundamental modes are determined, the integer multiples of the computed modes show little to no differences, and can not be identified. An increased amount of sensors to be applied is recommended at the locations of interest, to increase accuracy on the determined mode shapes of the structure.

9.2. RECOMMENDATIONS FOR INCREASE OF RELIABILITY

Correspondence over absolute magnitude The decomposition during frequency domain decomposition (FDD) shows preference for independent absolute magnitude over level of correspondence between multiple input signals. In other words, the useful measured characteristics can easily be buried when a single noisy signal is present. The singular values plots which contain important modal information will be attenuated, but remain present in the lower singular values plots. Therefore, it is recommended to consider these lower order singular values plots as well.

Normalized frequency spectrum The frequency spectrum is obtained after applying a Fourier transform on the time domain signal. Subsequently, the individual frequency transforms will be super-positioned and form the spectral matrix. If the absolute magnitude of any individual signal before decomposition is significantly higher (exponentially larger), than the modal information of the other signals will be attenuated during the singular value decomposition (SVD). However, if the frequency transform of each time domain signal is normalized (over the total power) before adding to the spectral matrix, the absolute magnitudes do not remain relevant. The relative local peaks in the frequency spectra will remain preserved and can be identified during the SVD.

When only a small portion of the frequency spectrum is relevant to consider, such as in the case of this research project, it is recommended to apply a low-pass or band-pass filter to increase the accuracy of the

normalization process. In total, the normalization process of such frequency domain signals can be challenging. It is recommended to perform additional research in supplementary normalization methods.

Reverse mode comparison After computation of the mode shapes through FDD, the singular vector matrices can be used to reflect on the contribution of a specific mode in each of the individual measurement signals.

As mentioned in Section 7.1.1, the FDD shows its deficiency when a single *noisy* measurement contributes to the total response with a mode containing significant amplitudes w.r.t. the other measurement signals, included in the FDD. Because no normalization is applied before summation in the frequency domain, the computed singular value which corresponds to the faulty mode will be identified as the most dominantly present mode. It will present itself in the first singular values plot of the total response. Keep in mind that the first singular values plot should present the natural frequencies of the system. In Equation 9.1, the subscript s represents the modal matrices for the total response (all measurement signals included).

$$\tilde{S}_{dd,s} = U_s \Sigma_s V_s^H \tag{9.1}$$

After the FDD has computed the 3 modal matrices (based on the total response), they can be used to decompose each individual measurement signal (individual response). If only a single measurement shows great correspondence to the determined dominant mode at the alleged natural frequency, whereas the majority of the measurement signals show no correspondence to this dominant mode, than the faulty mode can be identified and the measurement signal from which the faulty mode originates, can be excluded from further computations. In Equation 9.2, the subscript i represents the case where only a single measurement signal is included. The computed matrix Σ_i includes the contributions of the system modes, to this specific measurement signal.

$$(U_s)^{-1} \tilde{S}_{dd,i} \left(V_s^H\right)^{-1} = \Sigma_i \tag{9.2}$$

This method can be used to assess the quality for each individual measurement signal.

Programming improvements In Python, the forward-backward filter can be applied using the `signal.filtfilt` command, which is included in the `scipy` package. Due to stability issues, the time signal cannot always be filtered to attenuate specific frequencies. Therefore, it is recommended that during filtering the second order sections (`output='sos'`) output type is computed, for the digital filter parameters. This way, the results will converge stability related issues can be omitted from the process.

9.3. AUTOCORRELATION FUNCTION

The autocorrelated case does present the Fourier transform of the signal without the magnitudes of noise w.r.t. the original case. Therefore, the implementation of the autocorrelation function (ACF) is recommended to be primarily used up until the decomposition (identification of dominant frequencies).

The autocorrelated case also makes use of a normalization step, so the contribution in the decomposition for every signal is about equal. The contribution of a faulty signal with relative unproportionally high magnitudes will not influence the super-positioned frequency domain and the faulty signals' frequency domain transform will be attenuated, therefore, not influencing the summed spectrum.

Phase correction When applying an ACF, the phase characteristics do not remain representative. However, the noise reduction properties are useful when in the process of determining the natural frequencies. Therefore, it is recommended to investigate the possibilities to reduce the phase distorting properties when applying an ACF.

9.4. FEM MODEL

The current research concludes on the determination of modal parameters through measurement data. For now, only a single data type is included in the determination process. However, as mentioned in the introduction, if a digital model is connected, so the computed parameters can be updated, this could be used as feedback for both the digital model and the determination of modal parameters. The connection can work

both ways, namely to calibrate the digital model, as well as include custom assumptions (boundary conditions) to ensure accurate determination of structural behaviour. Therefore, it is recommended to investigate the possibilities of connecting a digital model of the structure to the measurement data.

Train characteristics Further investigations on the dynamic characteristics of the train are recommended. The specifications of the train carriages are known and could be determined. The carriage can be tested in an experimental setup. If any natural frequency of the train carriages can be identified around the dominant frequency $f_{3.1}$, then the results can be confirmed, which can assist in the reliability quantification.

9.5. TIME DOMAIN METHODS

As mentioned in Chapter 2, the majority of the OMA methods can be considered as time domain or frequency domain methods. For the current research project, the main method which is considered is the FDD method, which is a frequency domain method. Although this method shows great strength when describing mode multiplicity for closely spaced modes, the possibility to describe structural damping is rather limited. To be able to consider structural damping, it is recommended to investigate the possibilities for the application of time domain methods.

10

References

BIBLIOGRAPHY

Ahmadian, M., & Inman, D. J. (1984). Classical normal modes in asymmetric nonconservative dynamic systems. https://doi.org/10.2514/3.48543

ANSOL. (2015). Ansys structural analysis tutorials -8: Modal analysis of an arch bridge. https://www.youtube.com/watch?v=Mxr11EeEzGY

Au, F. T., Wang, J. J., & Cheung, Y. K. (2001). Impact study of cable-stayed bridge under railway traffic using various models. *Journal of Sound and Vibration*, *240*(3), 447–465. https://doi.org/10.1006/jsvi.2000.3236

Au, S.-K., Brownjohn, J. M., Li, B., & Raby, A. (2021). Understanding and managing identification uncertainty of close modes in operational modal analysis. *Mechanical Systems and Signal Processing*, *147*, 107018. https://doi.org/10.1016/j.ymssp.2020.107018

Avci, O., Alkhamis, K., Abdeljaber, O., Alsharo, A., & Hussein, M. (2022). Operational modal analysis and finite element model updating of a 230ăm tall tower. *Structures*, *37*, 154–167. https://doi.org/10.1016/j.istruc.2021.12.078

Bao, X. X., Li, C. L., & Xiong, C. B. (2015). Noise elimination algorithm for modal analysis. *Applied Physics Letters*, *107*(4), 041901. https://doi.org/10.1063/1.4927642

Bhandary, N. P., Paudyal, Y. R., & Okamura, M. (2021). Resonance effect on shaking of tall buildings in Kathmandu Valley during the 2015 Gorkha earthquake in Nepal. *Environmental Earth Sciences*, *80*(13), 459. https://doi.org/10.1007/s12665-021-09754-9

Blok, R., Habraken, A., Pronk, A., & Teuffel, P. (2018). Resource-efficient structural design [IASS Symposium 2018 Creativity in Structural Design ; Conference date: 16-07-2018 Through 20-07-2018]. In C. Mueller & S. Adriaenssens (Eds.), *Proceedings of the iass symposium 2018* (pp. 1–10). http://iass2018.org/

Brincker, R., & Ventura, C. (2015). *Introduction to operational modal analysis*. John Wiley & Sons.

Brincker, R., Zhang, L., & Andersen, P. (2001). *Modal identification of output-only systems using frequency domain decomposition* (tech. rep.). http://iopscience.iop.org/0964-1726/10/3/303

Castellanos-Toro, S., Marmolejo, M., Marulanda, J., Cruz, A., & Thomson, P. (2018). Frequencies and damping ratios of bridges through Operational Modal Analysis using smartphones. *Construction and Building Materials*, *188*, 490–504. https://doi.org/10.1016/j.conbuildmat.2018.08.089

Cawley, P., & Adams, R. D. (1979). The location of defects in structures from measurements of natural frequencies. *The Journal of Strain Analysis for Engineering Design*, *14*(2), 49–57. https://doi.org/10.1243/03093247V142049

Chaparro, L., & Akan, A. (2018). *Signals and systems using matlab*. Academic Press.

Chen, D., Yang, Y., & Liu, P. (2015). Analysis of Deflection Problems of Large-span Continuous Rigid Frame Bridge and Prevention Measures. *MATEC Web of Conferences*, *22*, 04021. https://doi.org/10.1051/matecconf/20152204021

Chengwang, L. (2010). Singular value decomposition in active monitoring data analysis. *Handbook of Geophysical Exploration: Seismic Exploration*, *40*(100), 421–430. https://doi.org/10.1016/S0950-1401(10)04027-9

contributors, R. (n.d.). Gtw (noordelijke nevenlijnen) [Online; accessed 5-February-2022]. https://www.railwiki.nl/index.php/GTW_(Noordelijke_Nevenlijnen)

contributors, W. (2022). Stadler gtw — Wikipedia, the free encyclopedia [Online; accessed 5-February-2022]. https://en.wikipedia.org/w/index.php?title=Stadler_GTW&oldid=1105552435

Craveiro, F., Bartolo, H. M., Gale, A., Duarte, J. P., & Bartolo, P. J. (2017). A design tool for resource-efficient fabrication of 3d-graded structural building components using additive manufacturing. *Automation in Construction*, *82*, 75–83. https://doi.org/10.1016/J.AUTCON.2017.05.006

Derife, M., Atmani, A., Ait Laasri, E. H., Balil, J., & Agliz, D. (2022). Development of a low cost system for modal parameters identification under ambient vibration: A low rise building as a case study. *Journal of Building Engineering*, *54*, 104626. https://doi.org/10.1016/j.jobe.2022.104626

Erlicher, S., & Argoul, P. (2007). Modal identification of linear non-proportionally damped systems by wavelet transform. *Mechanical Systems and Signal Processing*, *21*, 1386–1421. https://doi.org/10.1016/j.ymssp.2006.03.010{\"{i}}

Frangopol, D. M., & Kim, S. (2022). Prognosis and life-cycle assessment based on SHM information. *Sensor technologies for civil infrastructures* (pp. 581–607). Elsevier. https://doi.org/10.1016/B978-0-08-102696-0.00003-8

Frýba, L. (1972). *Vibration of solids and structures under moving loads*. Springer Netherlands. https://doi.org/10.1007/978-94-011-9685-7

Fugro. (2021). *Trillingsmeting Bert Swartbrug Zuidhorn* (tech. rep.).

Gre, S., Döhler, M., Andersen, P., & Mevel, L. (2021). Uncertainty quantification for the Modal Phase Collinearity of complex mode shapes. *Mechanical Systems and Signal Processing, 152*, 107436. https://doi.org/10.1016/J.YMSSP.2020.107436

Grocel, J. (2014). Comparison of Deterministic and Stochastic Method in Operational Modal Analysis in Application for Civil Engineering Structures. *Procedia Engineering, 91*, 130–135. https://doi.org/10.1016/j.proeng.2014.12.034

Hadianfard, M. A., & Kamali, S. (2020). Analysis of Modal Frequencies Estimated from Frequency Domain Decomposition Method. *International Journal of Engineering and Technology, 12*(3), 41–47. https://doi.org/10.7763/IJET.2020.V12.1182

He, J., & Fu, Z.-F. (2001a). Mathematics for modal analysis. *Modal Analysis*, 12–48. https://doi.org/10.1016/B978-075065079-3/50002-4

He, J., & Fu, Z.-F. (2001b). *Modal Analysis*. Elsevier. https://doi.org/10.1016/B978-0-7506-5079-3.X5000-1

Hwang, E.-S., & Nowak, A. S. (1991). Simulation of Dynamic Load for Bridges. *Journal of Structural Engineering, 117*(5), 1413–1434. https://doi.org/10.1061/(ASCE)0733-9445(1991)117:5(1413)

Ingenieure, S. (2021). *Report - dynamic analysis of train passages for a design speed of v=140 km/h* [Bert Swartbrug over het Van Starkenborghkanaal].

James, J. F. (2011). *A Student's Guide to Fourier Transforms*. Cambridge University Press. https://doi.org/10.1017/CBO9780511762307

Jiang, X., Wang, L., & Zhang, H. (2019). Static and Dynamic Analysis of A through Tied Arch Bridge. *IOP Conference Series: Earth and Environmental Science, 252*(5). https://doi.org/10.1088/1755-1315/252/5/052095

Jin, S.-S., Jeong, S., Sim, S.-H., Seo, D.-W., & Park, Y.-S. (2021). Fully automated peak-picking method for an autonomous stay-cable monitoring system in cable-stayed bridges. *Automation in Construction, 126*, 103628. https://doi.org/10.1016/j.autcon.2021.103628

Juang, J. N., & Pappa, R. S. (1985). An eigensystem realization algorithm for modal parameter identification and model reduction. *Journal of Guidance, Control, and Dynamics, 8*(5), 620–627. https://doi.org/10.2514/3.20031

Khan, M. A. (2013). Seismic Bridge Design. *Earthquake-Resistant Structures*, 201–239. https://doi.org/10.1016/B978-1-85617-501-2.00008-0

Kong, M.-S., Yhim, S.-S., Son, S.-H., & Kim, D.-Y. (2006). Dynamic analysis of the multiple-arch bowstring bridge and conventional arch subjected to moving loads. *Steel Struct, 6*(3), 227–236.

Lonetti, P., Pascuzzo, A., & Davanzo, A. (2016). Dynamic Behavior of Tied-Arch Bridges under the Action of Moving Loads. *Mathematical Problems in Engineering, 2016*. https://doi.org/10.1155/2016/2749720

Lu, N., Beer, M., Noori, M., & Liu, Y. (2017). Lifetime Deflections of Long-Span Bridges under Dynamic and Growing Traffic Loads. *Journal of Bridge Engineering, 22*(11). https://doi.org/10.1061/(ASCE)BE.1943-5592.0001125

Magalhães, F., & Cunha, Á. (2011). Explaining operational modal analysis with data from an arch bridge. https://doi.org/10.1016/j.ymssp.2010.08.001

Mottershead, J. E., & Friswell, M. I. (1993). Model Updating In Structural Dynamics: A Survey. *Journal of Sound and Vibration, 167*(2), 347–375. https://doi.org/10.1006/JSVI.1993.1340

Nanga, S., Bawah, A. T., Acquaye, B. A., Billa, M.-I., Baeta, F. D., Odai, N. A., Obeng, S. K., & Nsiah, A. D. (2021). Review of Dimension Reduction Methods. *Journal of Data Analysis and Information Processing, 09*(03), 189–231. https://doi.org/10.4236/jdaip.2021.93013

Noorderbreedte. (n.d.). Bert swart-brug, zuidhorn [Online; accessed 19-August-2022]. https://www.noorderbreedte.nl/2019/11/23/bert-swart-brug-zuidhorn/

Oke, W. A., Adeyemi, O. A., Bello, K. A., & Adegbenjo, A. (2019). Approximate Mode Shape for Damped Structures. https://doi.org/10.1007/978-3-030-21894-2{_}2

Oktav, A. (2020). Identification of non-proportional structural damping using experimental modal analysis data. *Journal of Measurements in Engineering, 8*(1), 34–45. https://doi.org/10.21595/jme.2020.21259

Parker, M. (2017). Discrete and Fast Fourier Transforms (DFT, FFT). *Digital signal processing 101* (pp. 99–115). Elsevier. https://doi.org/10.1016/b978-0-12-811453-7.00010-x

Pastor, M., Binda, M., & Harařik, T. (2012). Modal Assurance Criterion. *Procedia Engineering*, *48*, 543–548. https://doi.org/10.1016/J.PROENG.2012.09.551

Pellegrino, C., Cupani, G., & Modena, C. (2010). The effect of fatigue on the arrangement of hangers in tied arch bridges. *Engineering Structures*, *32*(4), 1140–1147. https://doi.org/10.1016/j.engstruct.2009.12.040

Pioldi, F., & Rizzi, E. (2017). A refined Frequency Domain Decomposition tool for structural modal monitoring in earthquake engineering. *Earthquake Engineering and Engineering Vibration*, *16*(3), 627–648. https://doi.org/10.1007/s11803-017-0394-9

Pyoma [Online; accessed 10-August-2022]. (n.d.). https://github.com/dagghe/PyOMA.git

Rayleigh, J. (1894). *The theory of sound*. Macmillan. https://books.google.nl/books?id=zTYIAAAAIAAJ

Reynders, E., Houbrechts, J., & De Roeck, G. (2012). Fully automated (operational) modal analysis. *Mechanical Systems and Signal Processing*, *29*, 228–250. https://doi.org/10.1016/j.ymssp.2012.01.007

Saini, M. K. (n.d.). *Signals and systems properties of linear time-invariant (lti) systems*. https://www.tutorialspoint.com/signals-and-systems-properties-of-linear-time-invariant-lti-systems

Shin, K., & Hammond, J. K. (2008). *Fundamentals of signal processing for sound and vibration engineers*. John Wiley & Sons.

Smith, S. W. (2003). *Digital Signal Processing*. Elsevier. https://doi.org/10.1016/B978-0-7506-7444-7.X5036-5

Soroushian, A. (2014). A simple approach towards further accuracy in structural dynamic analysis. *Proceedings of the 4th International Conference on Computational Methods in Structural Dynamics and Earthquake Engineering (COMPDYN 2013)*, 2232–2243. https://doi.org/10.7712/120113.4661.C1413

Spijkers, J. M. J., Vrouwenvelder, A. W. C. M., & Klaver, E. C. (2005). *Structural Dynamics CT 4140 Part 1-Structural Vibrations* (tech. rep.).

Sun, M., Makki Alamdari, M., & Kalhori, H. (2017). Automated Operational Modal Analysis of a Cable-Stayed Bridge. *Journal of Bridge Engineering*, *22*(12). https://doi.org/10.1061/(ASCE)BE.1943-5592.0001141

Tarpø, M., Olsen, P., Amador, S., Juul, M., & Brincker, R. (2017). On minimizing the influence of the noise tail of correlation functions in operational modal analysis. *Procedia Engineering*, *199*, 1038–1043. https://doi.org/10.1016/j.proeng.2017.09.282

Wang, H., Zhu, Q., Li, J., Mao, J., Hu, S., & Zhao, X. (2019). Identification of moving train loads on railway bridge based on strain monitoring. *Smart Structures and Systems*, *23*(3), 263–278. https://doi.org/10.12989/sss.2019.23.3.263

Wikipedia contributors. (n.d.). Correlogram [Online; accessed 28-August-2022]. https://en.wikipedia.org/w/index.php?title=Correlogram&oldid=1101659991

Xia, H., Xu, Y. L., & Chan, T. H. (2000). Dynamic interaction of long suspension bridges with running trains. *Journal of Sound and Vibration*, *237*(2), 263–280. https://doi.org/10.1006/jsvi.2000.3027

Yang, X.-M., Yi, T.-H., Qu, C.-X., Li, H.-N., & Liu, H. (2021). Performance Assessment of a High-Speed Railway Bridge through Operational Modal Analysis. *Journal of Performance of Constructed Facilities*, *35*(6). https://doi.org/10.1061/(ASCE)CF.1943-5509.0001669

Yang, Y.-B., Yau, J.-D., & Hsu, L.-C. (1997). *Vibration of simple beams due to trains moving at high speeds* (tech. rep. No. 11).

Zbilut, J. P., & Marwan, N. (2008). The WienerKhinchin theorem and recurrence quantification. *Physics Letters A*, *372*(44), 6622–6626. https://doi.org/10.1016/j.physleta.2008.09.027

Zhang, F.-L., Ni, Y.-C., Au, S.-K., & Lam, H.-F. (2016). Fast Bayesian approach for modal identification using free vibration data, Part I Most probable value. *Mechanical Systems and Signal Processing*, *70-71*, 209–220. https://doi.org/10.1016/j.ymssp.2015.05.031

Zhu, Y.-C., & Au, S.-K. (2020). Bayesian data driven model for uncertain modal properties identified from operational modal analysis. *Mechanical Systems and Signal Processing*, *136*, 106511. https://doi.org/10.1016/j.ymssp.2019.106511

Zwingmann, B. (2010). Comparison of network arch and tied arch with vertical hangers and partial loading. https://www.researchgate.net/publication/265509151_Asymmetric_network_arch_bridges/figures?lo=1

A

Mode shapes

A.1. Z DIRECTIONS

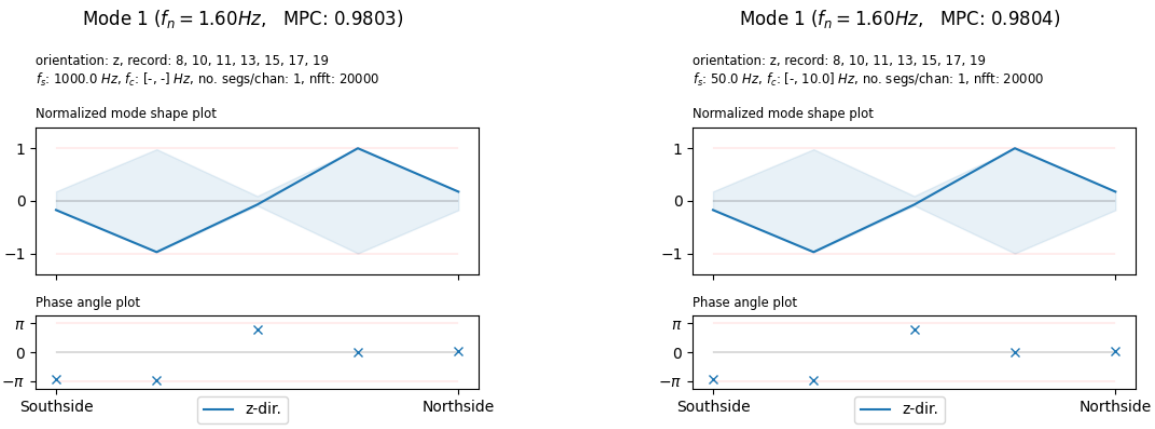

(a) Original case

(b) Preprocessed case

Figure A.1: Sensor direction Z, dominant frequency f_1

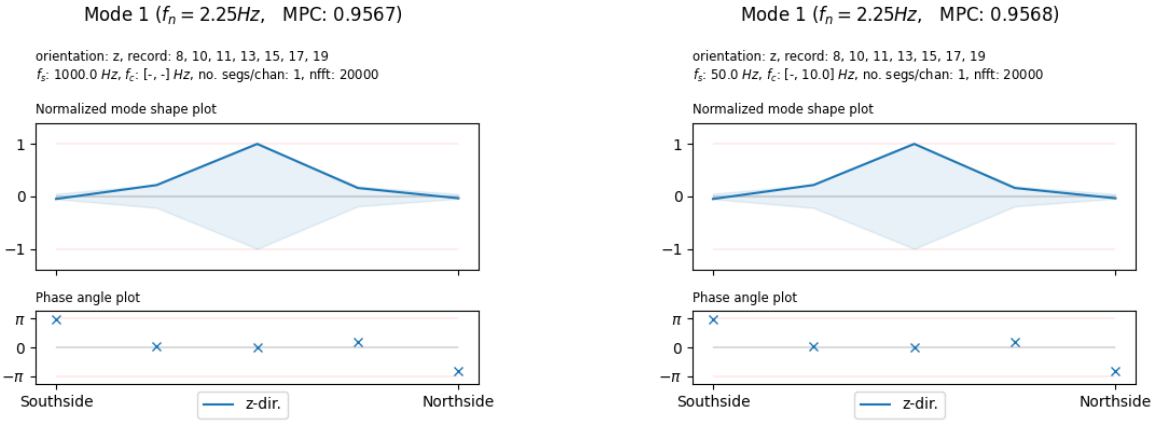

(a) Original case

(b) Preprocessed case

Figure A.2: Sensor direction Z, dominant frequency f_2

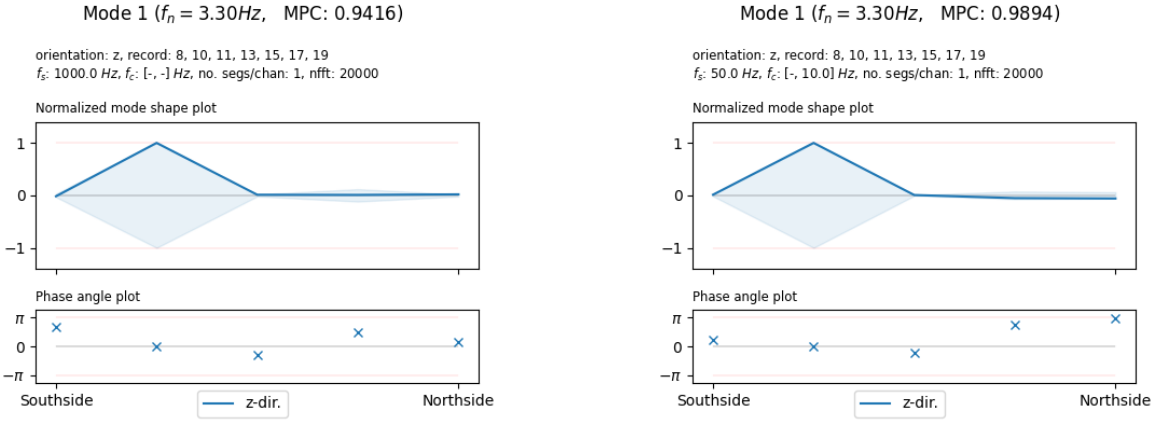

(a) Original case

(b) Preprocessed case

Figure A.3: Sensor direction Z, dominant frequency f_3

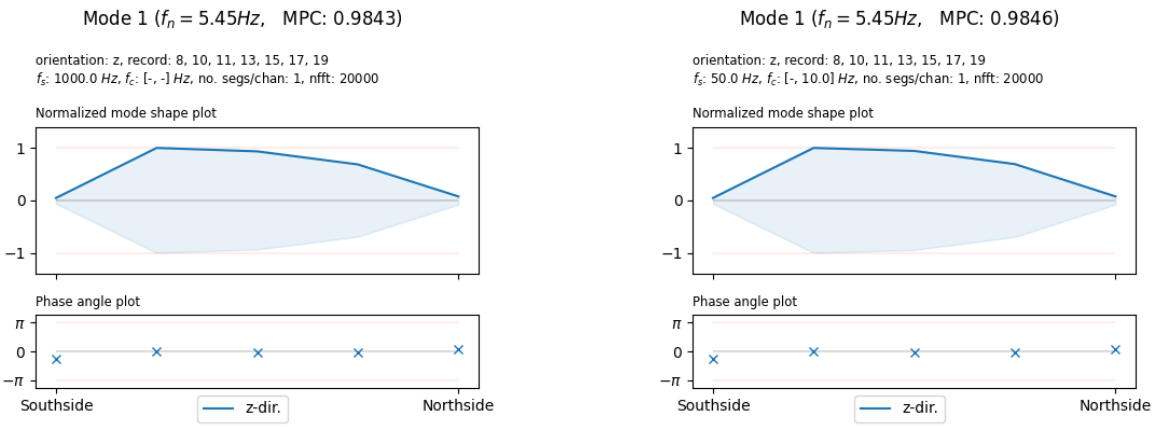

(a) Original case

(b) Preprocessed case

Figure A.4: Sensor direction Z, dominant frequency f_4

A.2. Y DIRECTIONS

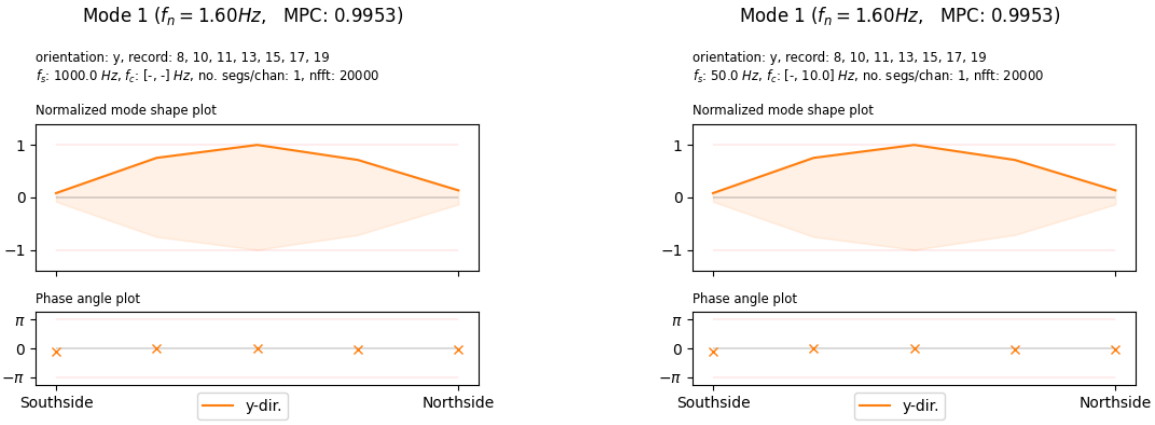

(a) Original case

(b) Preprocessed case

Figure A.5: Sensor direction Y, dominant frequency f_1

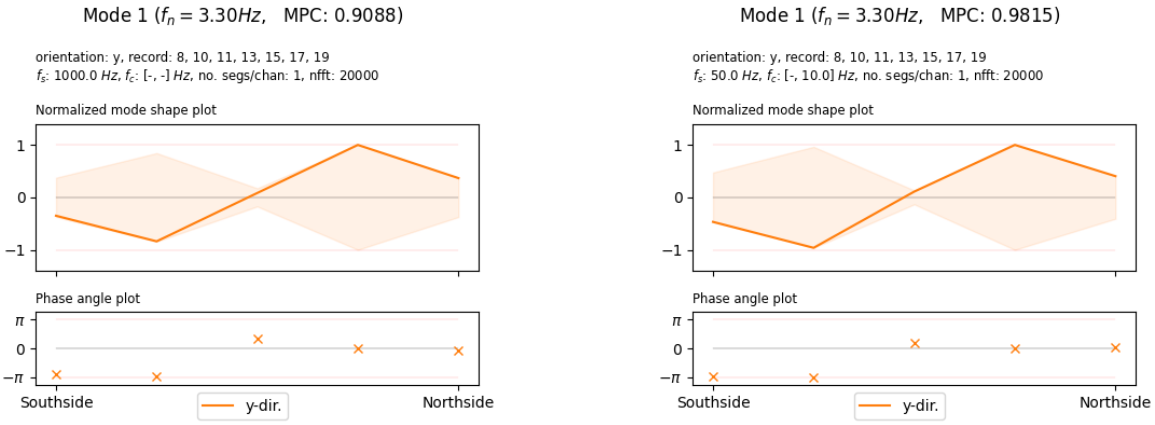

(a) Original case

(b) Preprocessed case

Figure A.6: Sensor direction Y, dominant frequency f_3

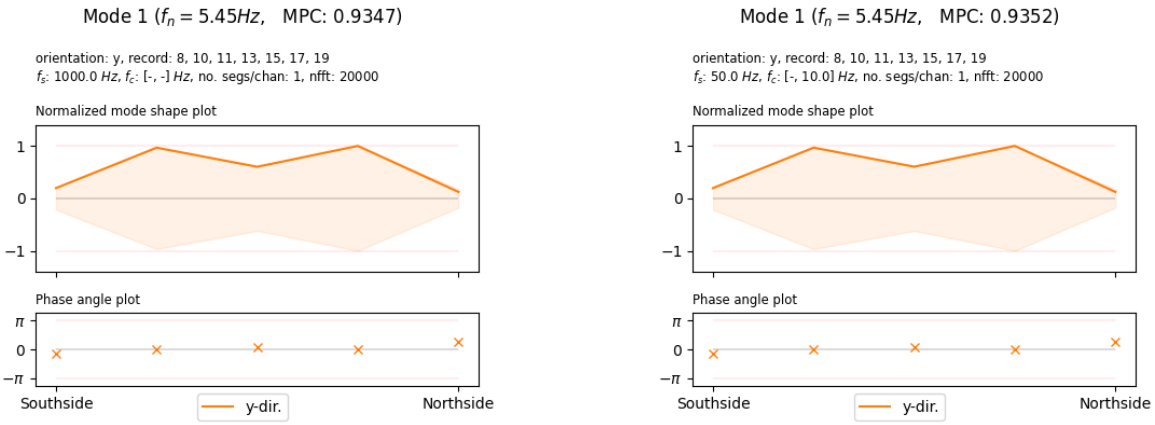

(a) Original case

(b) Preprocessed case

Figure A.7: Sensor direction Y, dominant frequency f_4

A.3. YZ DIRECTIONS

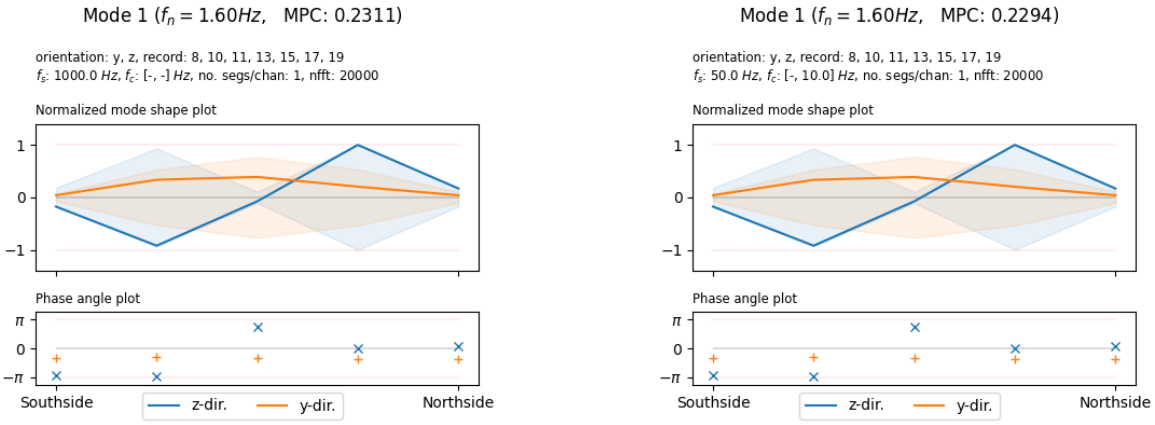

(a) Original case

(b) Preprocessed case

Figure A.8: Sensor direction YZ, dominant frequency f_1, first mode plots

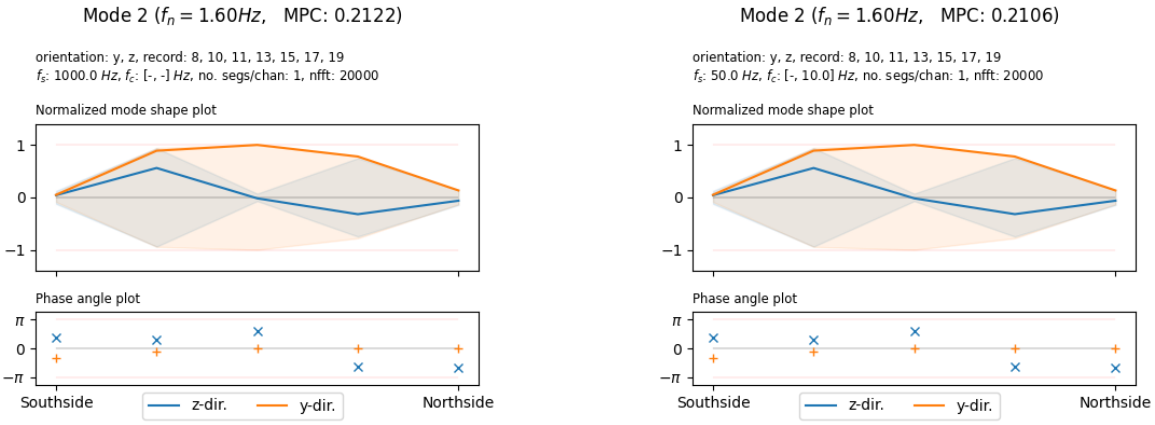

(a) Original case, sensor direction YZ, dominant frequency f_1

(b) Preprocessed case, sensor direction YZ, dominant frequency f_1

Figure A.9: Sensor direction YZ, dominant frequency f_1, second mode plots

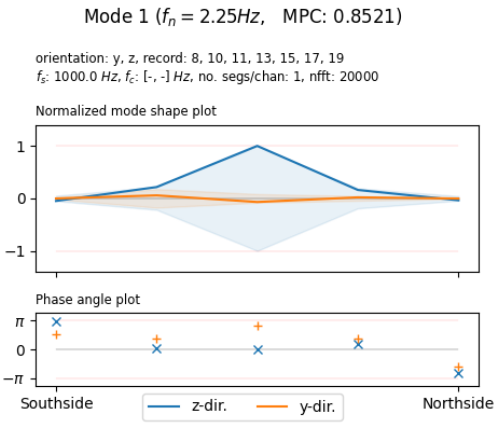

(a) Original case

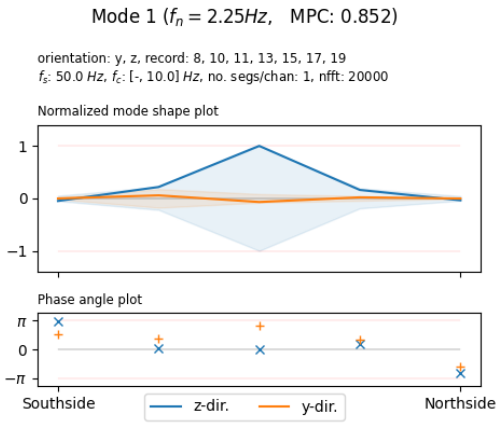

(b) Preprocessed case

Figure A.10: Sensor direction YZ, dominant frequency f_2

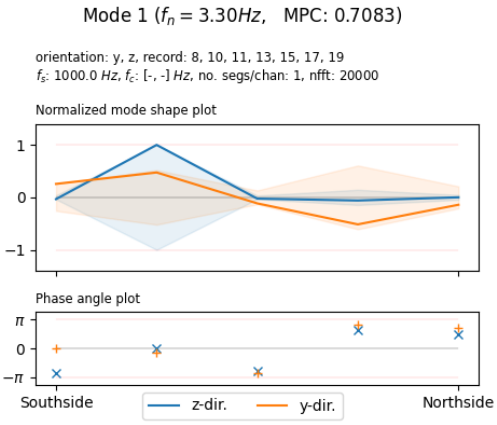

(a) Original case

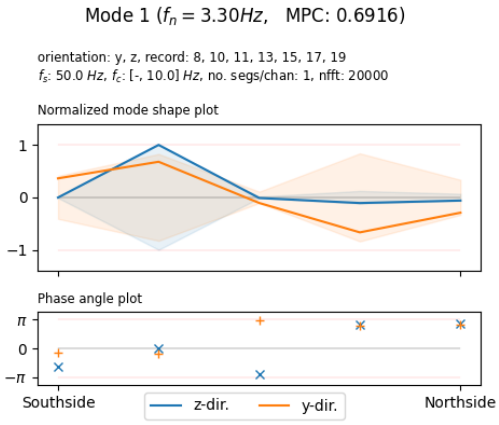

(b) Preprocessed case

Figure A.11: Sensor direction YZ, dominant frequency $f_{3.1}$

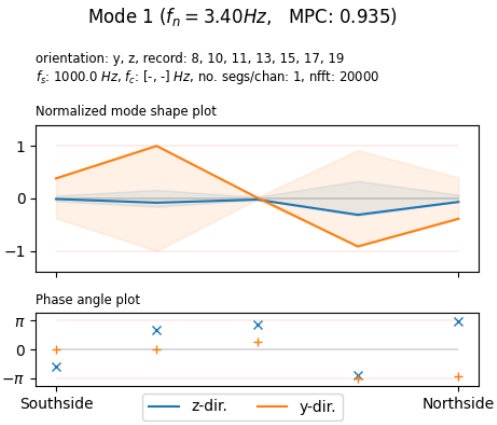

(a) Original case

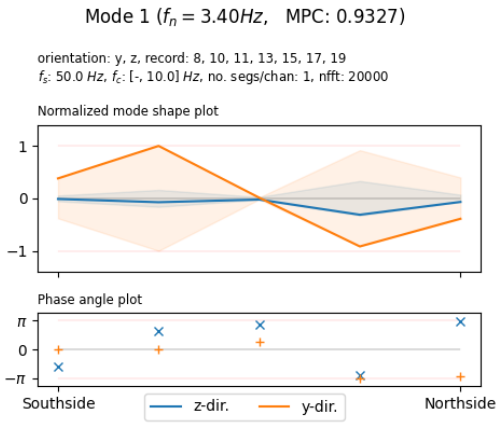

(b) Preprocessed case

Figure A.12: Sensor direction YZ, dominant frequency $f_{3.2}$

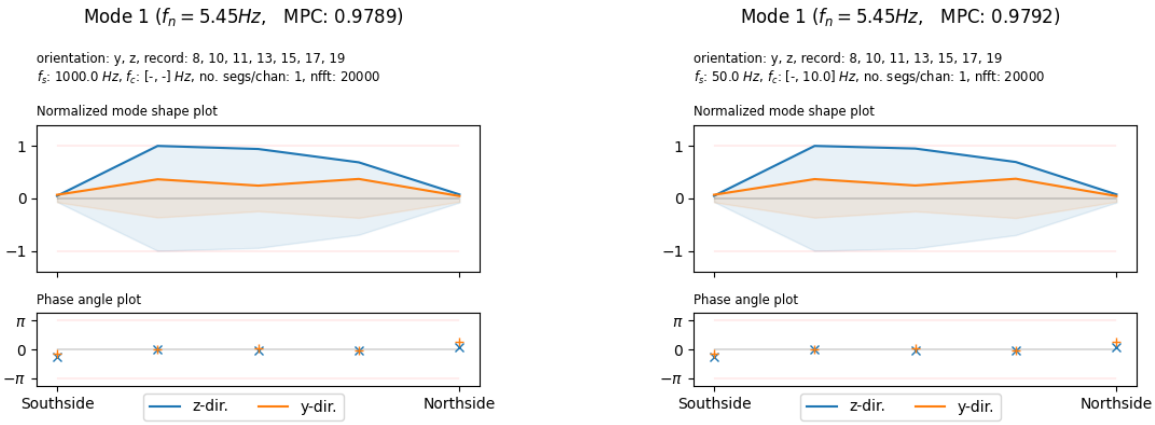

(a) Original case

(b) Preprocessed case

Figure A.13: Sensor direction YZ, dominant frequency f_4